MIT/WHOI 95-16

Massachusetts Institute of Technology
Woods Hole Oceanographic Institution

Joint Program in Oceanography/ Applied Ocean Science and Engineering

DOCTORAL DISSERTATION

Subtidal Cross-Shelf Circulation on the Northern California Shelf

by

Edward Paul Dever

June 1995

DISCLAIMER NOTICE

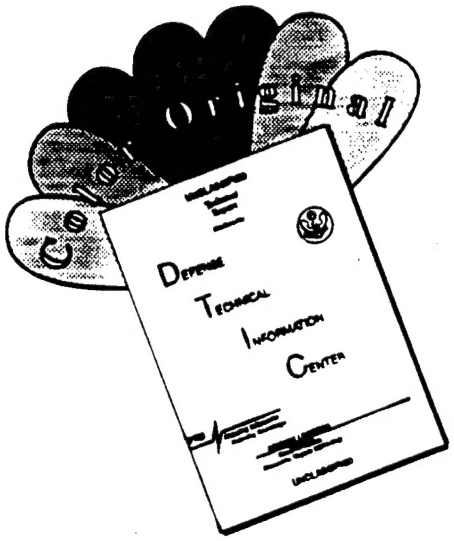

THIS DOCUMENT IS BEST QUALITY AVAILABLE. THE COPY FURNISHED TO DTIC CONTAINED A SIGNIFICANT NUMBER OF COLOR PAGES WHICH DO NOT REPRODUCE LEGIBLY ON BLACK AND WHITE MICROFICHE.

MIT/WHOI

95-16

Subtidal Cross-Shelf Circulation on the Northern California Shelf

by

Edward Paul Dever

Massachusetts Institute of Technology
Cambridge, Massachusetts 02139

and

Woods Hole Oceanographic Institution
Woods Hole, Massachusetts 02543

June 1995

DOCTORAL DISSERTATION

Funding was provided by the National Science Foundation under Grant OCE-91-15713

This thesis should be cited as: Edward Paul Dever, 1995. Subtidal Cross-Shelf Circulation on the Northern California Shelf. Ph.D. Thesis. MIT/WHOI, 95-16.

Approved for publication; distribution unlimited.

Approved for Distribution:

Philip L. Richardson, Chair
Department of Physical Oceanography

Sallie W. Chisholm
MIT Director of Joint Program

John W. Farrington
WHOI Dean of Graduate Studies

Subtidal Cross-Shelf Circulation on the Northern California Shelf

by

Edward Paul Dever

B.S., Texas A&M University (1987)
M.S., Texas A&M University (1989)

Submitted in partial fulfillment of the requirements for the degree of
Doctor of Philosophy
at the
MASSACHUSETTS INSTITUTE OF TECHNOLOGY
and the
WOODS HOLE OCEANOGRAPHIC INSTITUTION

June 1995

Author .....

Joint Program in Oceanography
Massachusetts Institute of Technology
Woods Hole Oceanographic Institution
May 26, 1995

Certified by .....

Steven J. Lentz
Associate Scientist
Thesis Supervisor

Accepted by .....

Carl Wunsch
Chairman, Joint Committee for Physical Oceanography
Massachusetts Institute of Technology
Woods Hole Oceanographic Institution

Acknowledgments

I thank Steve Lentz for advising me these last four years. Steve has always been willing to make time for visits and discussions; his willingness to give me free rein with the SMILE data made the thesis possible; his encouragement to write things up early and his careful reading of my work improved it greatly. Each of my committee members made unique contributions: Jim Price's comments and questions added to the clarity of methods sections, Paola Rizzoli emphasized a clear and complete discussion of results, and Bob Weller encouraged me to put statistical and instrumental uncertainty into context. In addition to his advice and comments on the thesis, Bob Beardsley was responsible for bringing me into coastal oceanography under SMILE and for many opportunities to go to sea. Ken Brink got me interested early on in the problems of interpreting cross-shelf velocity measurements in light of wind-forced theory.

This thesis focussed on observations from three extensive field programs on the northern California shelf; the Shelf Mixed Layer Experiment (SMILE), the Sediment Transport Events over the Shelf and Slope (STRESS) study, and the Northern California Coastal Circulation Study (NCCCS). I thank all who contributed to the success of these programs. I am particularly grateful to Brad Butman at USGS Woods Hole for making available STRESS subsurface mooring data and to John Largier (SIO, Univ. of Cape Town, South Africa), Clinton Winant (SIO), and Bruce Magnell (EG&G) for their generosity in allowing me to use NCCCS data. For SMILE, I thank Russ Davis and Lloyd Regier at SIO and Bob Beardsley and Steve Lentz at WHOI.

The people around me these years have enabled me to withstand the trials and tribulations of graduate school. I want to thank first my parents and family. You kept me going and helped me weather that first year at MIT. Later in Woods Hole, housemates John Kokinos and Alan Kuo were the source of years of good fellowship at the Lazy Pillbug. Paul Robbins provided me with a host of answers to MATLAB and other computer questions as well as many discussions about life in general and tropical fish in particular. I've lived for coffee hour in the student center; thanks to all the regulars and the irregulars for their good company and indulgence in my taste for hazelnut. Maria Hood has been a wonderful companion and generous source of strength and happiness.

Finally, I would like to thank those who funded me through graduate school. In my first year at MIT, Carl Wunsch supported me through NSF grant OCE 88-23043. At WHOI, I first started work on SMILE with Bob Beardsley under NSF grant OCE 87-16937 and continued working on it with Steve Lentz under NSF grant OCE 91-15713.

Subtidal Cross-Shelf Circulation on the Northern California Shelf

by

Edward Paul Dever

Submitted to the Joint Program in Oceanography
Massachusetts Institute of Technology
Woods Hole Oceanographic Institution
on May 19, 1995, in partial fulfillment of the
requirements for the degree of
Doctor of Philosophy

Abstract

Moored time series from the Coastal Ocean Dynamics Experiment (CODE), Shelf Mixed Layer Experiment (SMILE), Sediment Transport Events over the Shelf and Slope (STRESS) study, and Northern California Coastal Circulation Study (NCCCS) are used to study subtidal cross-shelf circulation over the northern California shelf. The northern California shelf, like much of the United States Pacific coast, is subject to strong wind forcing which exhibits characteristic seasonality. In winter and early spring, it is distinguished by poleward and equatorward fluctuations on time scales of days and by weak monthly means. In summer, it is distinguished by periods of equatorward stress lasting several weeks and by relatively strong monthly means. The intensive winter and spring SMILE and STRESS and summer CODE-2 field programs permit the examination of cross-shelf circulation under both types of wind forcing conditions at a mid-shelf site (~90 m) 6 km from the northern California coast.

The primary thesis goal is to examine the applicability of a two-dimensional conceptual model of wind-forced cross-shelf circulation. In this conceptual model, surface and bottom cross-shelf flows are forced by along-shelf wind stress and bottom stress, and interior cross-shelf flow compensates such that the depth-averaged flow is zero. A secondary thesis goal is to use the seasonal coverage of available field programs to gain insight into seasonal variability of cross-shelf circulation on the northern California shelf. To accomplish these goals, the observed subtidal cross-shelf circulation is examined in the context of the winter and spring heat and salt balances, an analytic model of wind-forced cross-shelf circulation, and the spatial scales of subtidal velocity.

Mean and fluctuating heat and salt balances estimated between December, 1988 and May, 1989 demonstrate the importance of cross-shelf fluxes and their general consistency with the simple conceptual model. Mean fluxes are consistent with the

weak mean equatorward wind stress observed during SMILE. The dominant terms in the fluctuating balances are the cross-shelf fluxes and local changes in heat and salt content. These are well correlated with each other and with the local along-shelf wind stress. The along-shelf heat flux divergence is of secondary importance to the fluctuating heat balance. It is uncorrelated with the along-shelf wind stress, and occurrences when it is strong are interpreted as effects of mesoscale features.

To examine the applicability of the wind-forced conceptual model in more detail, a simple analytic model incorporating the assumptions of the conceptual model and observed local wind forcing is compared quantitatively to estimates of surface mixed layer, interior, and bottom mixed layer cross-shelf transport for winter SMILE and STRESS and summer CODE-2 observations. This comparison suggests the model is more suited to the transient wind forcing observed during SMILE and STRESS than to the steady wind forcing observed during CODE-2. For 2–3 day wind events between December, 1988 and February, 1989, the model is well correlated with observed depth-dependent (total minus depth-averaged) transports throughout the water column and with total surface mixed layer transports. For 2–3 week wind events between April and July, 1982, the model does not work nearly as well below the surface mixed layer.

In the absence of other processes, the locally wind-forced model implies that the wind stress sets the horizontal scales of subtidal velocity. Correlation scales estimated for subtidal along-shelf velocity over the northern California shelf are for all field programs longer than the maximum mooring separation (60 km) and are similar to those of the wind stress. However, along-shelf correlation scales of cross-shelf velocity are shorter than minimum mooring separations for CODE. SMILE and NCCCS time series do resolve along-shelf correlation scales for near surface cross-shelf velocity. During this time, along-shelf correlation scales for near surface cross-shelf velocity vary on a monthly time scale. They are generally long (30 km or more) when correlation with wind stress is high and short (15 km or less) when correlation with wind stress is low. On at least one occasion, short along-shelf correlation scales coincide with the intrusion of an offshore mesoscale feature onto the shelf.

Results of the three studies show the two-dimensional model offers some insight into the observed subtidal cross-shelf circulation, particularly in winter. During this time, the heat balance, analytical transport model, and correlation scales all provide evidence that the winter wind-forced circulation is quasi-two-dimensional. Three-dimensional variability on the shelf, though important on occasion, does not appear to be wind-driven and may result from the influence of offshore mesoscale features. A quite different story emerges for summer when the simple conceptual model of cross-shelf circulation fails to describe adequately subsurface cross-shelf flow. Two useful areas of further investigation may be the non-linear response of cross-shelf velocity to wind forcing and its response to other processes such as remotely generated mesoscale features.

Thesis Supervisor: Steven J. Lentz
Title: Associate Scientist

Contents

Chapter 1

Introduction

1.1 Wind-forced shelf circulation

Subtidal circulation in the coastal ocean may be forced by a number of processes such as river outflow, tidal rectification, offshore mesoscale processes, and wind forcing. Though the relative importance and coastal ocean response to these forcings varies from region to region [*Allen et al.*, 1983], wind forcing has been recognized as dominant on many continental shelves. Based on the importance and effects of strong seasonal wind forcing, these shelves are often termed wind-driven shelves. They often occur along tectonically active continental margins. Because of this they tend to be relatively straight and narrow with adjacent coastal mountain ranges and few large estuaries and bays. These mountain ranges tend to polarize the coastal wind in the along-shelf direction. Two examples of wind-forced shelves which occur along active margins are the United States Pacific coast and the Pacific coast of South America. Though wind-forced shelves are common along active continental margins, they also occur along passive continental margins. Two examples of wind-forced shelves which do not occur along an active continental margin are the northwest African shelf [*Badan-Dangon*, 1981] and the west Florida shelf [*Allen et al.*, 1983].

In this thesis, the cross-shelf circulation over the northern California shelf (Fig. 1.1) is studied. The study region extends from Pt. Reyes in the south to Pt. Arena in the north, a distance of approximately 100 km. The topography here is typical of a

wind-forced shelf along an active continental margin. The coastline orientation remains approximately due northwest (315° T) and the shelf width, beyond the 130 m isobath, varies between 25 km offshore (in the south) to only 15 km offshore (in the north). Wind stress is strongly polarized in the along-shelf direction. The along-shelf component of wind stress has spatial scales which extend over the entire region [*Beardsley et al.*, 1987], though wind stress curl associated with the change in coastline orientation at Pt. Arena is observed for equatorward winds [*Winant et al.*, 1988].

Meteorological forcing over the northern California shelf is highly seasonal. In winter and spring, wind forcing is distinguished by the passage of low pressure systems which cause poleward and equatorward fluctuating winds on time scales of days. During this time, monthly mean surface heat fluxes are weak or even negative, becoming persistently positive (from the atmosphere to the ocean) and stronger in March [*Nelson and Husby*, 1983]. In summer, wind forcing is distinguished by the establishment of strong persistent upwelling favorable winds which are interrupted occasionally by periods of weak wind stress (relaxation events) which may last a week or longer [*Halliwell and Allen*, 1987 ; *Strub et al.*, 1987; *Beardsley et al.*, 1987]. Mean surface heat fluxes are strong and positive during the summer upwelling season. [*Nelson and Husby*, 1983; *Lentz*, 1987*a*]. The seasons are typically separated by a rapid spring transition [*Lentz*, 1987*b*] and a more gradual fall transition [*Strub and James*, 1988].

1.2 Subtidal velocities on wind-forced shelves

Many extensive field programs have described subtidal velocities on wind-forced shelves. Most of these studies have occurred when strong, persistent upwelling favorable winds prevail [*Kundu and Allen*, 1976; *Brink et al.*, 1980; *Badan-Dangon*, 1981; and *Winant et al.*, 1987]. Subtidal velocities tend to be strongly polarized in the along-shelf direction [*Smith*, 1981]. Consequently they are usually rotated into a reference frame parallel to the local topography and analyzed in terms of along-shelf and cross-shelf components. Along-shelf velocities are usually strongly correlated to local and/or remote wind forcing throughout the shelf water column [*e.g.*, *Winant*

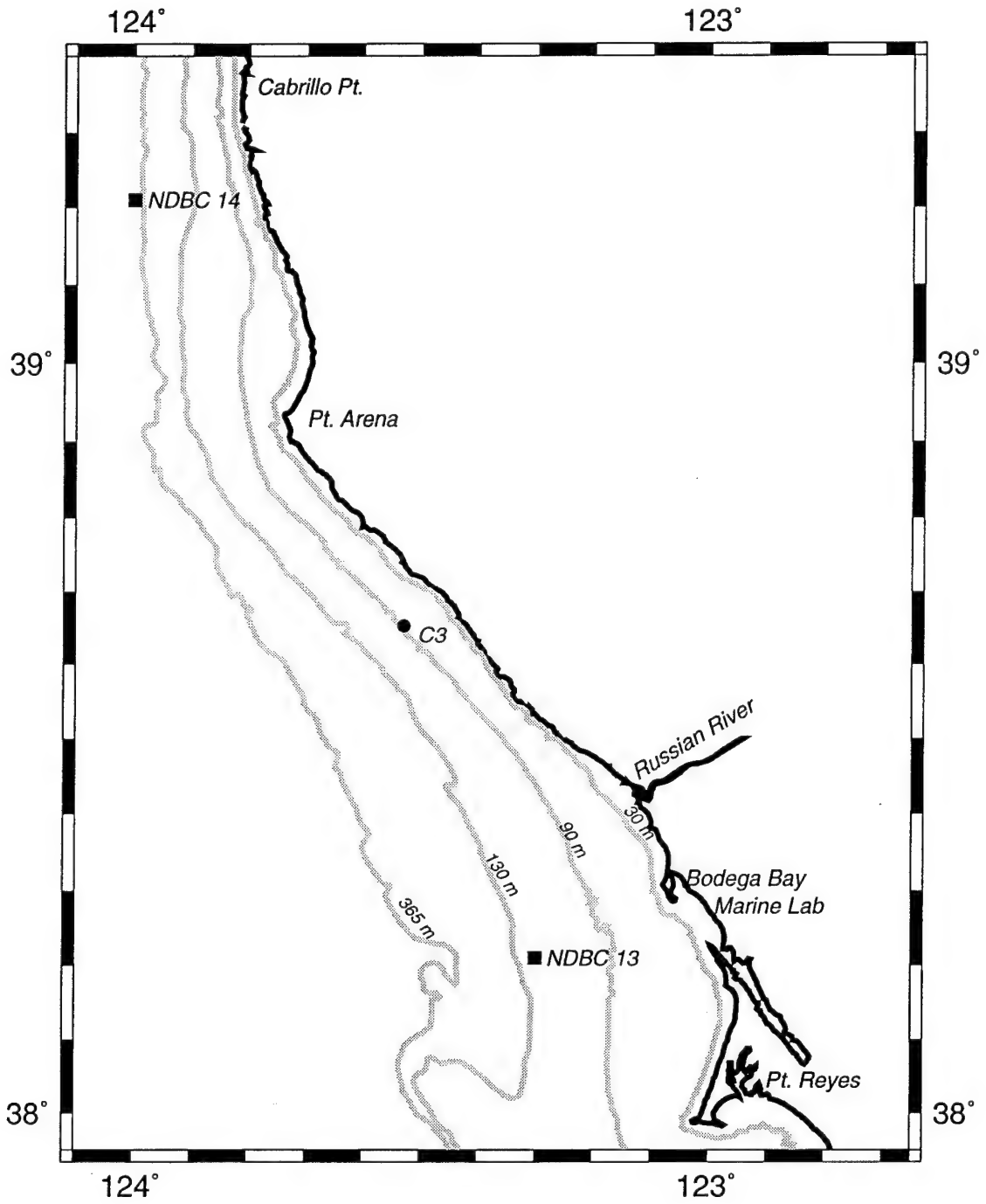

Figure 1.1. Map of the northern California shelf. For reference, National Data Buoy Center locations 46013 (NDBC 13) and 46014 (NDBC 14) and the mid-shelf C3 site occupied during the Coastal Ocean Dynamics Experiment (CODE) and Shelf Mixed Layer Experiment (SMILE) are also shown.

et al., 1987; *Chapman*, 1987]. Cross-shelf velocities are usually positively correlated to wind stress forcing near the surface [*Smith*, 1981]. Below the surface however, the picture is unclear. Though near-bottom cross-shelf velocities are correlated with interior along-shelf velocity, interior cross-shelf velocities are often uncorrelated with local wind forcing [*Winant et al.*, 1987].

1.3 Modelling velocity on wind-forced shelves

There exists a considerable body of theory concerning the dynamics which govern subtidal velocity on wind-driven (upwelling) shelves [*Allen*, 1980]. It includes surface and bottom boundary layer theory [*Brink*, 1983; *Lentz*, 1992; *Trowbridge and Lentz*, 1991], two-dimensional upwelling models [*Csanady*, 1982; *Janowitz and Pietrafesa*, 1980; *de Szoeke and Richman*, 1984; *Mitchum and Clarke*, 1986], and coastal-trapped waves (CTW) theory [*Chapman*, 1987; *Brink*, 1991].

Both locally forced models and CTW's have had reasonable success in predicting quantitatively fluctuations in the observed along-shelf velocity. *Chapman* [1987] found CTW solutions were significantly correlated to along-shelf velocity over the mid-shelf off northern California. *Lopez and Clarke* [1989] examined the linear momentum balance as forced by both remote CTW and local forcing. They found low mode CTW waves were largely responsible for determining along-shelf pressure gradients but that local wind stress was also important, especially closer to the coast. *Zamudio and López* [1994] adopted the same local plus remote approach over the northern California shelf in the context of a numerical model and found the combination of local forcing and CTW often opposed each other such that along-shelf velocity was reduced slightly relative to the purely locally forced case.

Two-dimensional conceptual models have had some success in explaining observed cross-shelf circulation and its effects, particularly in the surface boundary layer. These models would suggest interior and near-bottom cross-shelf transports compensate for wind-driven near-surface transport; a suggestion which usually agrees qualitatively with observed (over periods of several months) circulation [*Allen and Kundu*, 1978].

However when examined closely, assumptions of two-dimensionality have generally broken down for mean [*Halpern et al.*, 1977] and especially fluctuating [*Smith*, 1981] cross-shelf circulation. Therefore even sophisticated numerical models which are two-dimensional have difficulty predicting subsurface cross-shelf velocities quantitatively. *Chen and Wang* [1990] are an exception to this trend, however even this success could not be replicated [*Zamudio and López*, 1994]. Observed cross-shelf velocities also differ from the two-dimensional conceptual model in that cross-shelf velocity fluctuations have short correlation scales [*Kundu and Allen*, 1976]. *Brink et al.* [1994] examined the sensitivity of cross-shelf velocity to short-scale wind variability using a linear model and concluded that, in the context of their model, short-scale wind stress decreased correlation scales but could not account for energy levels of observed interior cross-shelf velocity.

1.4 Motivation of thesis

Cross-shelf circulation is intimately associated with wind-driven coastal upwelling which affects strongly water property distributions on wind-driven shelves. Mean and fluctuating heat and salt balances [*Lentz*, 1987*a*; *Rudnick and Davis*, 1987; *Richman and Badan-Dangon*, 1983; and *Bryden et al.*, 1980] are often dominated by cross-shelf fluxes. Understanding the processes governing cross-shelf velocity remains an issue of interest because of difficulties in modelling cross-shelf velocity quantitatively [*e.g.*, *Brink et al.*, 1994], difficulties which are especially apparent when compared to success in modelling along-shelf velocities [*e.g.*, *Chapman*, 1987 and *Zamudio and López*, 1994].

The field programs used in this study also represent a unique collection of observations. Previous studies of cross-shelf velocity on wind-driven shelves have concentrated on the coastal ocean's response to strong, persistent upwelling favorable wind stress. The winter and spring observations examined here give an opportunity to examine the ocean response to relatively brief wind-forced events. Additionally, these observations resolve surface and bottom boundary layers simultaneously at a mid-

shelf site, and closely-spaced current meter time series allow along-shelf correlation scales of near-surface cross-shelf velocity to be resolved.

1.5 Overview

This thesis has two primary goals. The first is to study the cross-shelf circulation on the northern California shelf and examine the applicability of two-dimensional upwelling theory to cross-shelf velocity throughout the water column. The second is to gain insight into seasonal variability on the northern California shelf. This includes contrasting seasonal differences in the heat balance as well as differences in the coastal ocean response to relatively brief wind-driven events observed in winter and spring and to longer wind-driven upwelling observed in summer.

The remainder of the thesis consists of three chapters which examine different aspects of the observed cross-shelf circulation on the northern California shelf and a conclusions chapter which draws together the results of chapters 2, 3, and 4. Each of the three thesis body chapters is intended as a stand-alone paper and contains its own introduction and conclusions.

The observations used here come from a number of field programs on the northern California shelf. Much of the focus is on observations from the Shelf Mixed Layer Experiment (SMILE) which took place during the winter and spring of 1988–1989 [*Alessi et al.*, 1991]. Observations from the Sediment Transport Events over the Shelf and Slope (STRESS) field programs [*Fredericks et al.*, 1993] and the Northern California Coastal Circulation Study (NCCCS) [*EG&G*, 1989, 1990*a*, and 1990*b*] are used to supplement vertical (STRESS) and horizontal (NCCCS) mooring coverage during the SMILE time period. Observations from the Coastal Ocean Dynamics Experiment (CODE) [*Rosenfeld*, 1983; *Limeburner*, 1985] are used to examine the cross-shelf circulation on the northern California shelf in summer to gain insight into seasonal and interannual variability.

1.5.1 Chapter 2

Chapter 2 is a study of the heat and salt balances on the northern California shelf in winter and spring using SMILE and STRESS observations. The fluctuating heat and salt balances are generally between changes in the heat and salt content and changes in the cross-shelf heat and salt flux. They are strongly correlated with local wind forcing and demonstrate the importance of wind-forced cross-shelf flow to temperature and salinity on the northern California shelf even when cross-shelf circulation is driven by transient rather than strong persistent wind forcing. In addition to motivating further study of the cross-shelf circulation, chapter 2 provides the most complete description of the SMILE and STRESS observations used throughout the thesis and a descriptive background in which to interpret results of later chapters.

1.5.2 Chapter 3

Chapter 3 is a study of wind-forced cross-shelf circulation. The vertical structure of cross-shelf circulation is considered at a mid-shelf mooring site over the northern California shelf in winter (SMILE and STRESS) and summer (CODE-2). Attention is first focussed on winter observations which suggest a near-surface wind-driven flow, interior return flow, and along-shelf velocity driven bottom boundary layer flow. This conceptual model of wind-driven circulation is tested by adopting an analytic two-dimensional model of cross-shelf transport. The model includes linear, barotropic dynamics, and local wind stress forcing. Modelled surface boundary layer, interior, and bottom boundary layer transports are compared quantitatively to observed cross-shelf transports within the surface mixed layer, interior, and bottom mixed layer. In winter, modelled and observed transports agree relatively well throughout the water column when the mass balance is approximately two-dimensional. In summer, the model does not perform well below the surface mixed layer, suggesting the importance of three-dimensional processes.

1.5.3 Chapter 4

Chapter 4 is a two-part study of the velocity correlation length scales on the northern California shelf. In the first part, correlation scales of along-shelf and cross-shelf velocity are estimated using observations from several field programs (CODE, NCCCS, SMILE, and STRESS). Correlation scales of along-shelf velocity are much longer than maximum mooring separation distances for all field programs and are consistent with the length scales of wind forcing. In contrast, correlation scales of cross-shelf velocity are usually shorter than minimum mooring separation distances. Minimum mooring separations from SMILE and NCCCS did resolve cross-shelf velocity correlation length scales. The second part of chapter 4 focusses on interpreting correlation scales of cross-shelf velocity in winter and spring from these observations. Correlation scales of near-surface cross-shelf velocity are shown to vary considerably on a month-to-month basis. During some months, correlation scales are longer than the maximum mooring separation (30 km), but during other months, shorter correlation scales of 10–15 km exist. Longer correlation scales coincide with predominance of wind-forcing and shorter correlation scales with the influence of mesoscale variability.

1.5.4 Conclusions

The information provided by chapters 2–4 suggests simple wind-forced models have some applicability to observed cross-shelf velocity fluctuations. The heat balance, cross-shelf transport, and correlation scales of cross-shelf velocity in winter are all often consistent with a locally wind-driven cross-shelf circulation. Even in winter factors other than wind forcing may be important. These factors are associated with a three-dimensional heat balance, failure of the two-dimensional wind-driven model, and short correlation scales of cross-shelf velocity.

The two-dimensional model appears to have considerably less applicability to the observed cross-shelf circulation in summer. Though the summer heat balance is often approximately two-dimensional, the two-dimensional model of wind-forced circulation fails below the surface mixed layer and correlation scales of cross-shelf velocity are

consistently shorter than 30 km.

The reason cross-shelf circulation is so highly three-dimensional in summer is unclear. Numerous other mechanisms which can influence cross-shelf velocity probably include: mesoscale eddies, the influence of upwelling fronts, topography, and small-scale wind stress. Dynamical processes that may be important include: nonlinear dynamics, interior shear stress, and baroclinic pressure gradients. All of these processes may act to make the cross-shelf flow three-dimensional. The success of the two-dimensional transport model and resolution of along-shelf correlation length scales in winter suggest some of these processes become more important under the steadier wind forcing conditions prevalent on the northern California shelf in summer.

Chapter 2

Heat and Salt Balances over the Northern California Shelf in Winter and Spring

Reprinted with permission from Dever, E. P., and S. J. Lentz, *J. Geophys. Res.*, *99*, 16001–16017, 1994, Copyright by the American Geophysical Union.

2.1 Abstract

Heat and salt balances are estimated over the northern California shelf from early December, 1988 through late February, 1989 (winter) and from early March through early May, 1989 (spring) from moored meteorological and oceanographic time series taken in 93 m of water 6.3 km from the coast. The winter mean offshore heat flux is 8.7×10^5 W m^{-1}, about a factor of five smaller than earlier estimates of the mean summer (upwelling season) offshore heat flux on the northern California shelf. The mean offshore heat flux is predominantly in the surface boundary layer and is balanced by an along-shelf heat flux divergence (as represented by an eddy along-shelf temperature gradient flux) and a cooling trend making the mean winter heat balance fundamentally three-dimensional. In contrast to winter, the spring mean offshore heat flux of 6.4×10^5 W m^{-1} is balanced by a positive air-sea heat flux of 8.3×10^5 W m^{-1},

which is about 80% of the mean air-sea heat flux in summer. This makes the spring mean heat budget primarily two dimensional, like the summer mean heat budget off northern California. On time scales of days, the dominant terms in the fluctuating heat budget in both winter and spring are the cross-shelf heat flux and local changes in heat content. These are well correlated with each other and with the local along-shelf wind stress. The along-shelf temperature gradient flux, uncorrelated with the along-shelf wind stress, is usually weak on time scales of days. Occurrences when it is strong are interpreted as effects of mesoscale features. Mean and fluctuating cross-shelf salt fluxes provide essentially the same information as cross-shelf heat fluxes. This is not surprising in light of the strong T-S relationship on the northern California shelf.

2.2 Introduction

The coast of northern California exhibits two distinct seasons, a summer upwelling season, and a winter/spring storm season [*Strub et al.*, 1987*a*; *Lentz and Chapman*, 1989]. These seasons are typically separated by a rapid spring transition [*Lentz*, 1987*a*] and a more gradual fall transition [*Strub and James*, 1988]. Mean meteorological conditions during the summer upwelling season are distinguished by strong positive (from the atmosphere to the ocean) sea surface heat flux [*Nelson and Husby*, 1983; *Lentz*, 1987*b*] and strong persistent equatorward winds [*Nelson*, 1977; *Strub et al.*, 1987*b*]. In response to the equatorward wind stress and a negative along-shelf pressure gradient [*Hickey and Pola*, 1983], along-shelf mean currents are equatorward near the surface and exhibit vertical shear, becoming weaker and sometimes poleward near the bottom and mean cross-shelf currents are offshore near the surface and near zero in the interior [*Winant et al.*, 1987].

Studies of the summer heat budget over the northern California shelf show the equatorward wind stress and resulting circulation produce a large mean offshore flux of heat in the surface boundary layer [*Lentz*, 1987*b*; *Rudnick and Davis*, 1988; *Send*, 1989] characteristic of coastal upwelling. The magnitude of the mean cross-shelf heat flux is similar to that found during upwelling conditions in other regions such as

Oregon and northwest Africa [*Bryden et al.*, 1980; *Richman and Badan-Dangon*, 1983] and, as in these other upwelling regions, a positive mean sea surface heat flux balances the mean offshore heat flux. Off northern California, alongshore heat transport and in-situ cooling play secondary roles in the mean heat balance for summer, and the role of onshore eddy heat flux is still unclear. In a volume heat budget, *Lentz* [1987*b*] finds only a small contribution due to cross-shelf eddy heat flux. In a study considering a single mooring at mid-shelf, *Send* [1989] finds a much stronger onshore eddy heat flux which he attributes to wind forcing. Though there have been several studies of the heat budget for the upwelling season in coastal regions, there have been few studies of the heat budget under non-upwelling conditions which exist over the northern California shelf during the winter and early spring months. From December until the spring transition in April or May, monthly mean along-shelf wind stresses on the northern California shelf are typically weak and may be poleward [*Nelson*, 1977]. And from December to February, monthly mean surface heat fluxes are weak or even negative, becoming persistently positive and stronger in March [*Nelson and Husby*, 1983]. Mean along-shelf currents are poleward and less vertically sheared than in summer, and mean cross-shelf currents are much weaker [*Lentz and Chapman*, 1989]. All this suggests the heat budget on the northern California shelf during winter and spring may be quite different from the summer upwelling season.

The mean and fluctuating heat and salt balances during winter and spring are studied using data collected at a mid-shelf mooring site off northern California from December, 1988 to May, 1989. These data are introduced in section 2.3. In section 2.4, the heat (and salt) balance equations per unit along-shelf distance are developed and the methods used to estimate the terms in these balances from the data are explained. The heat and salt balances are presented in section 2.5. Results are compared to previous studies of summer upwelling heat balances and their general applicability in light of climatological data is discussed in section 2.6.

2.3 Observations

2.3.1 Field Program

This study uses observations from the Shelf Mixed Layer Experiment (SMILE) and the Sediment Transport Events over the Shelf and Slope (STRESS) studies. These field programs took place over the northern California shelf from mid-November, 1988 to mid-May, 1989 in the same region as the previous Coastal Ocean Dynamics Experiment (CODE) [*Beardsley and Lentz*, 1987]. The central element of the SMILE array was a surface mooring, denoted C3, located at 38°38.71′ N 123°129.56′ W in 93 m of water (Figs. 2.1 and 2.2). C3 was deployed November 12, 1988 and recovered May 19, 1989. This mooring supported vector-measuring current meters (VMCMs) with temperature sensors at 12 depths from 5.5 to 49.5 m (Fig. 2.2) and a surface meteorological package. Conductivity was measured with Seabird SeaCats at 6 depths from 8.5 m to 49.5 m. A STRESS subsurface mooring, within 0.5 km of the SMILE surface mooring and also denoted C3, was deployed December 6, 1988, recovered February 27, 1989, and turned around and redeployed from March 3 to May 5, 1989 by B. Butman, USGS. The STRESS mooring had 5 vector-averaging current meters (VACMs) with temperature sensors between 30 and 6 m above the bottom (Fig. 2.2). Three VACMs were also equipped with Seabird conductivity cells. Together, the C3 SMILE and STRESS moorings provided excellent vertical resolution in temperature from 5.5 m below the surface to 6 m above the bottom. Though current observations initially had the same resolution, several VMCMs developed bearing corrosion problems which caused them to fail before the end of the six month deployment, and one VACM did not provide usable velocity data during its second deployment (Fig. 2.3).

In addition to the central SMILE and STRESS C3 moorings, some use will be made of the peripheral SMILE moorings (Fig. 2.1). The G3 and M3 moorings, approximately 15 km north and south of C3 and with similar temperature resolution, will be used to characterize along-shelf temperature gradients in the upper 49.5 m. They resembled the C4 mooring shown in Fig. 2.2. VMCM current data exists at 10

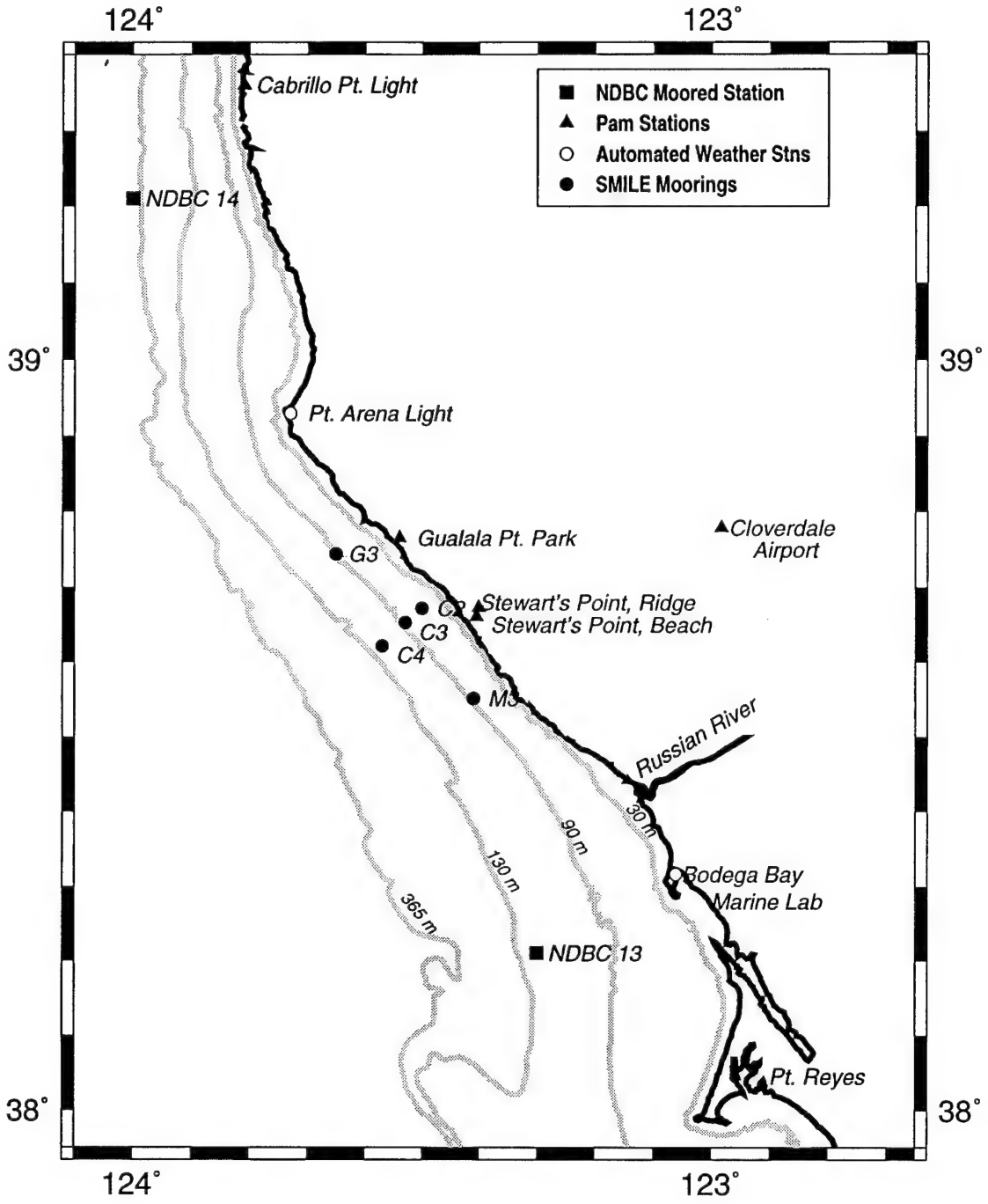

Figure 2.1 Map of SMILE region. The central mooring location was chosen to be near the CODE C3 mooring location. This chapter will primarily use data from the central C3 mooring and the along-shelf G3 and M3 moorings.

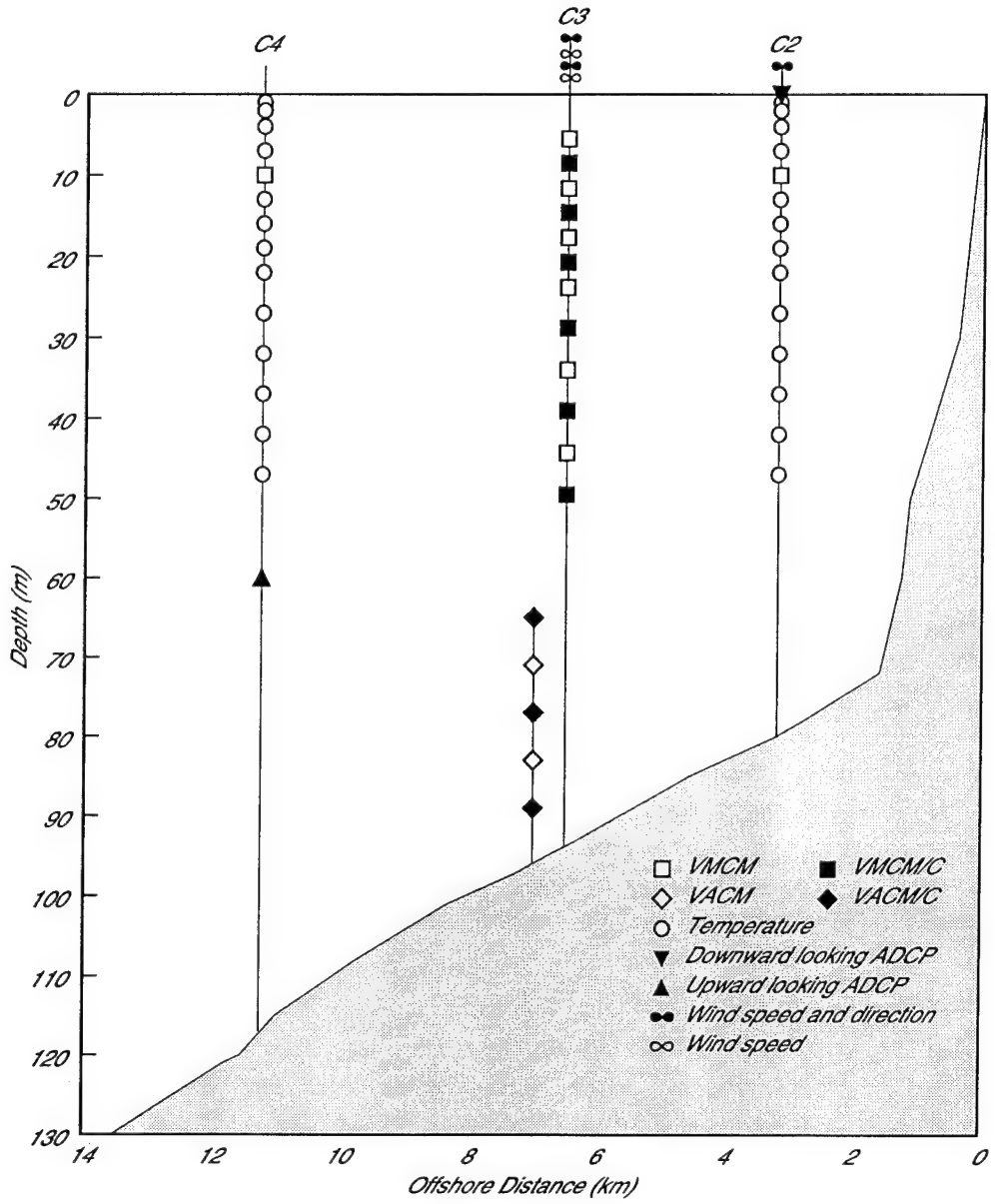

Figure 2.2 Cross section of shelf showing moorings and instrument locations. The central C3 site includes a surface mooring with instruments spanning the upper 49.5 m and a subsurface mooring with instruments spanning the lower 30 m deployed as part of STRESS. Along-shelf moorings at G3 and M3 (Fig. 2.1) had configurations similar to the C4 mooring.

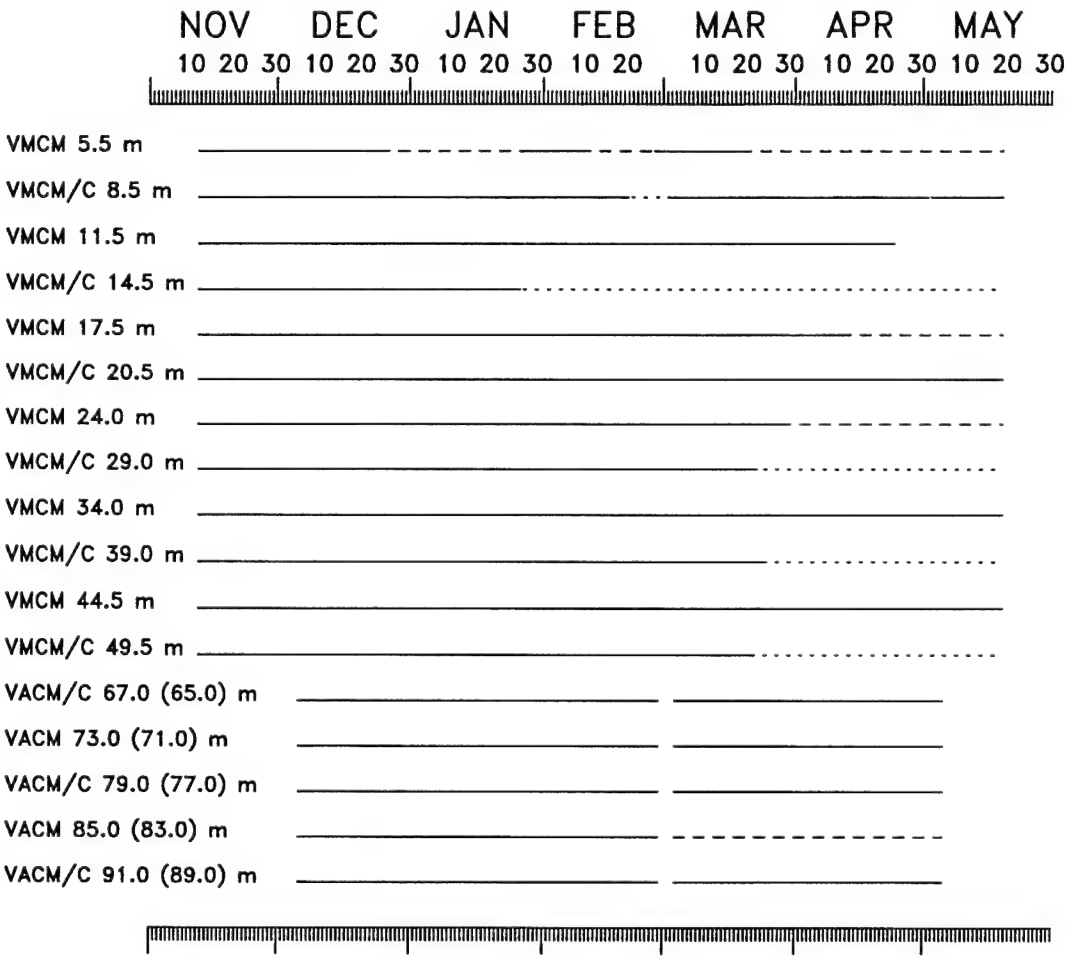

Figure 2.3 Data return for the SMILE and STRESS C3 moorings. Though many VMCM (and one VACM) velocity sensors (solid lines) failed early, almost all temperature (long dashed lines) and temperature and conductivity sensors (short dashed lines) returned complete records.

m; however upward looking acoustic doppler current profilers (ADCPs) at G3 and M3 failed shortly after deployment. Also, temperature observations at C2 (not present in winter) will be used to check estimates of heat content change in spring. Further information concerning the mooring locations, deployment times, configurations, and data return from the SMILE and STRESS experiments can be found in *Alessi et al.* [1991].

For reasons related to data coverage (Fig. 2.3) and the local air-sea heat flux (Fig. 2.4), the data were divided into two time periods: 0400 UT December 6, 1988 to 2300 UT February 20, 1989 (winter) and 2200 UT March 3 to 0400 UT May 2, 1989 (spring). The names winter and spring were chosen not on the basis of large scale meteorological patterns, such as the positions and strengths of the North Pacific subtropical high and Aleutian low [C. E. Dorman et al., Structure of the lower atmosphere over the northern California coast during winter, submitted to *Monthly Weather Review*, 1994; *Halliwell and Allen*, 1987; *Strub et al.*, 1987*b*; and *Lentz*, 1987*a*], but rather the effect of local air-sea heat flux on the mean heat budget. The winter period covers the meteorological conditions which contrast most strongly from summer upwelling conditions in that mean winds and sea surface heat flux (Fig. 2.4) are both weak. During spring, mean winds were again weak but surface heating increased, distinguishing this time period from winter. Though current meter failures began to affect severely near-surface velocity resolution during spring, this doesn't change the qualitative results.

2.3.2 Mean Winter and Spring Conditions

Before estimating the heat budgets in winter and spring, mean observations from these time periods are presented to give an overview and comparison to historical CODE data taken during the summers of 1981 and 1982 and the intervening winter. Velocity data are presented in a reference frame approximately parallel to local isobaths at C3 and identical to that of the CODE program [*Winant et al.*, 1987]. In this coordinate system, the along-shelf direction, y, is defined such that $y = 0$ at C3 and increases toward 317°T. The cross-shelf direction, x, is defined such that $x = 0$ at the coast

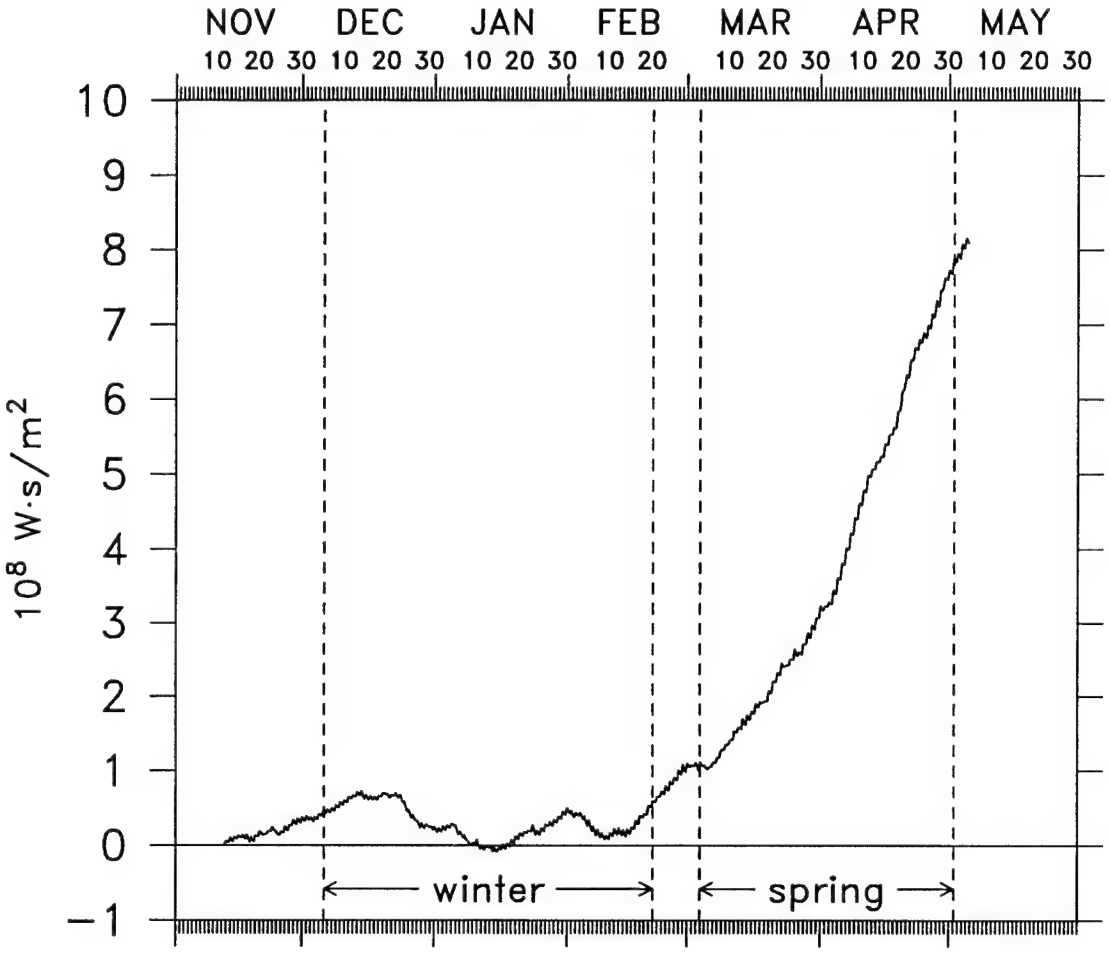

Figure 2.4 Total energy added/subtracted by net air-sea heat flux from November, 1988 to May, 1989. From November until the beginning of March, the surface heat flux is small, variable, and often from the ocean to the atmosphere. Beginning in March the surface heat flux becomes persistently positive. A change of 10^8 W s m^{-2} corresponds to a change in the depth-averaged temperature at C3 (93 m depth) of 0.26°C.

and decreases offshore. Cross-shelf and along-shelf velocities are denoted u and v respectively. The mean cross-shelf transport in this coordinate frame was nearly zero during both winter and spring. Rotations of 3.7° clockwise in winter and less than 0.3° counterclockwise in spring gave zero mean cross-shelf transport. These rotations did not qualitatively affect any of the results discussed in this chapter; therefore only results in the 317° reference frame will be presented.

In winter during both SMILE and CODE, mean along-shelf wind stress was weak (0.03 N m^{-2} in both years) and equatorward. Though upwelling favorable, it was a factor of 4–6 less than the wind stress averaged over similar record lengths during summer [*Winant et al.*, 1987]. The mean SMILE sea surface heat flux in winter was 2 W m^{-2} as compared to climatological monthly mean values of nearly 200 W m^{-2} in June, July, and August [*Nelson and Husby*, 1983]. Fig. 2.5 shows mean observations from the winter 1988–1989 (SMILE) and from a similar period during winter 1981–1982 CODE [*Lentz and Chapman*, 1989]. Mean winter cross-shelf currents were similar for CODE and SMILE, 1–3 cm s^{-1} offshore in the upper 30 m, onshore in the interior with a maximum of about 2 cm s^{-1}, and offshore from 75 m to near-bottom during SMILE (Fig. 2.5a). In contrast during the summers of 1981 (CODE-1) and 1982 (CODE-2), mean offshore currents at C3 (not shown) exceeded 6 cm s^{-1} in the upper 30 m, and mean cross-shelf currents were weak ($\sim$ 1 cm s^{-1}) below 30 m [*Winant et al.*, 1987]. During SMILE, winter mean along-shelf currents were poleward with a maximum speed of over 6 cm s^{-1} from about 50 to 75 m and weaker flow near the surface and bottom. During CODE, winter mean along-shelf currents were poleward with speeds of about 5 cm s^{-1} but were not as vertically sheared. By contrast, summer 1982 [*Winant et al.*, 1987] mean along-shelf currents were equatorward and vertically sheared with speeds of over 7 cm s^{-1} near the surface and weaker flow below 40 m at C3. Mean vertical temperature and salinity gradients were 0.01°C m^{-1} and 0.005 psu m^{-1} respectively for winter 1988–1989 (see Fig. 2.5c and d). These gradients are comparable to, but slightly smaller than, the mean temperature and salinity gradients reported for summer by *Winant et al.* [1987] and *Huyer* [1984].

In spring, the equatorward mean along-shelf wind stress was less than 0.02 N

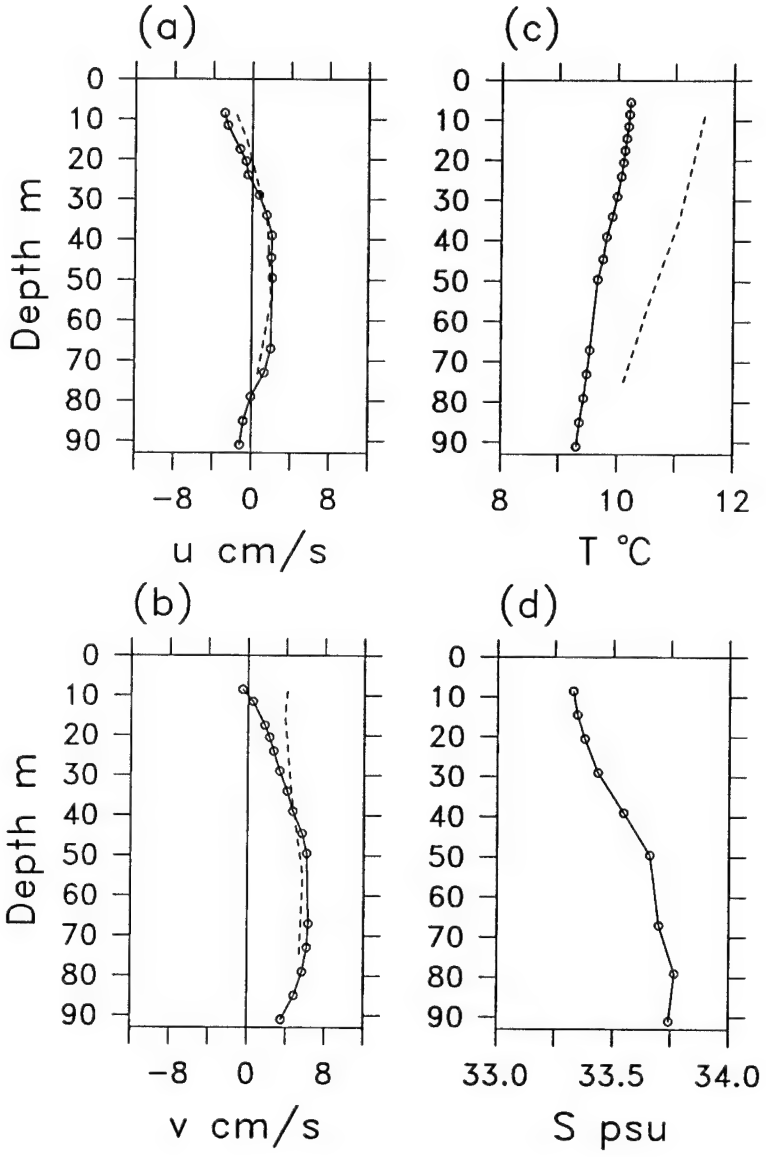

Figure 2.5 Mean winter cross-shelf (a) and along-shelf velocity profiles (b) at C3. The solid line indicates means between 0400 December 6, 1988 and 2300 February 20, 1989 (SMILE) and the dashed line indicates means between 1300 December 12, 1981 and 1200 March 22, 1982 (CODE). Mean temperature (c) and salinity profiles (d) are also shown. No salinity time series were collected during the 1981–1982 time period. Means are only shown for records lasting the entire time period. For SMILE/STRESS, these depths are indicated by circles.

m^{-2} and the mean sea surface heat flux during this time period was 133 W m^{-2}, approaching typical summer values. Mean near surface cross-shelf currents were even weaker than in winter and were offshore only at 8.5 m (Fig. 2.6a). Mean along-shelf currents (Fig. 2.6b) were more vertically sheared than in winter. Near the surface, flow was equatorward with a speed over 11 cm s^{-1}. It became weaker with depth and was poleward below 70 m. While this sheared equatorward flow is similar to the mean flow in summer, the weak equatorward mean wind stress and high temperature and low salinity at C3 suggest it was caused by a mesoscale feature over the outer shelf and slope in March and April, 1989 (see also *Largier et al.* [1993]) and not by wind-driven upwelling. Spring mean temperature and salinity profiles (Fig. 2.6c and d) were bilinear in character. Above 49.5 m, vertical gradients were 0.04°C m^{-1} in temperature and 0.013 psu m^{-1} in salinity. These gradients were about three times those observed in winter and about twice those observed in upwelling season [*Winant et al.*, 1987]. Below 49.5 m, mean vertical gradients were 0.01°C m^{-1} and 0.005 psu m^{-1}, similar to those observed in winter.

2.4 Methods

2.4.1 Developing the Heat Budget Equations

Surface to bottom vertical coverage existed only at the central C3 mooring. This constrained us to look at the heat budget over a two-dimensional cross-shelf area bounded vertically by the bottom, $z = -H(x)$, and the surface, $z = 0$, and in the cross-shelf direction by the C3 mooring, $x = -L$, and the coast, $x = 0$. The heat budget for this area is,

$$\begin{aligned} \rho c_p \int_{-L}^{0} dx \int_{-H}^{0} \frac{\partial T}{\partial t} dz &= \rho c_p \left[\int_{-H}^{0} uT|_{x=-L} dz - \int_{-L}^{0} dx \int_{-H}^{0} \left(T\frac{\partial v}{\partial y} + v\frac{\partial T}{\partial y} \right) dz \right] \\ &+ \int_{-L}^{0} Q dx \end{aligned} \tag{2.1}$$

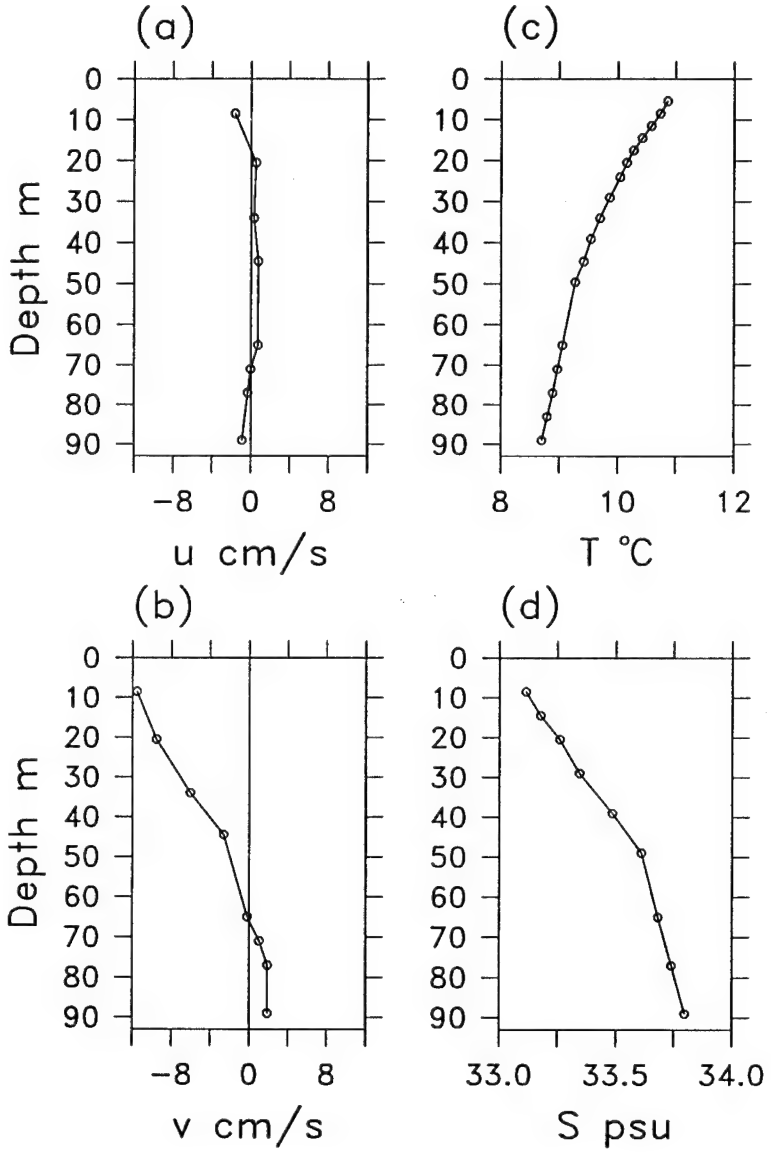

Figure 2.6 Mean cross-shelf (a) and along-shelf velocity profiles (b) at C3 between 2200 March 3, 1989 and 0400 May 2, 1989. Mean temperature (c) and salinity profiles (d) for the same time period. Means are only shown for depths (indicated by circles) with records lasting the entire time period. VMCM failures in the upper 49.5 m reduced near-surface velocity resolution during this time period.

where ρc_p is the heat capacity per unit volume (assumed constant and equal to 4.1×10^6 W s m^{-3} °C^{-1}), T is the water temperature, and Q is the net air-sea heat flux. Equation (2.1) states that changes in heat content integrated over the cross-shelf area are caused by: cross-shelf advection through the offshore side at $x = -L$; along-shelf heat flux divergence due to volume flux divergence and temperature gradient flux; and the net surface heat flux. In integrating to form (2.1), the vertical velocity is taken to be zero at the surface ($w = 0$ at $z = 0$) and given by the free slip kinematic boundary condition at the bottom ($w = -u\partial H/\partial x$ at $z = -H$), the cross-shelf heat flux is assumed to be zero at the coast (the vertical integral of $uT = 0$ at $x = 0$), and the heat flux through the seafloor is taken to be to zero. Equation (2.1) is useful because the cross-shelf integral of the cross-shelf heat flux is easily evaluated. However, as described by *Lentz* [1987*b*] and others, the addition of continuity to conservation of heat in (2.1) leads to a cross-shelf flux of temperature and along-shelf flux divergence of temperature which cancel when added together but depend on the absolute temperature scale when considered separately. In order to consider these terms separately, the velocity components, u and v, and temperature, T, in the cross-shelf and along-shelf volume flux divergence terms of (2.1) are decomposed into spatial average and perturbation quantities, e.g.

$$\langle u \rangle = \frac{1}{H} \int_{-H}^{0} u|_{x=-L} dz \tag{2.2}$$

and $u - \langle u \rangle = \tilde{u}$. The angle brackets represent depth-averaged quantities at $x = -L$ for u and T and the cross-shelf area averaged quantity for v. Tildes represent departures from these spatial averages. Hence the quantities $\langle u \rangle$, $\langle T \rangle$, and $\langle v \rangle$ are functions of time only while $\tilde{u}$, $\tilde{T}$, and $\tilde{v}$ depend on both space and time. Using this decomposition, (2.1) can be rewritten

$$\begin{aligned} \rho c_p \int_{-L}^{0} dx \int_{-H}^{0} \frac{\partial T}{\partial t} dz &= \rho c_p \left[\int_{-H}^{0} \tilde{u}\tilde{T}|_{x=-L} dz - \int_{-L}^{0} dx \int_{-H}^{0} \tilde{T} \frac{\partial v}{\partial y} dz \right. \\ &- \left. \int_{-L}^{0} dx \int_{-H}^{0} v \frac{\partial T}{\partial y} dz \right] + \int_{-L}^{0} Q dx \end{aligned} \tag{2.3}$$

where continuity has been used to eliminate the terms

$$H\langle u\rangle\langle T\rangle = \langle T\rangle \int_{-L}^{0} dx \int_{-H}^{0} \frac{\partial\langle v\rangle}{\partial y} dz. \tag{2.4}$$

Separating T, u, v, and Q in (2.3) into time mean ($\bar{}$) and fluctuating ($'$) components and time averaging gives the mean heat budget equation. Using this decomposition, the mean cross-shelf heat flux is

$$\rho c_p \int_{-L}^{0} \overline{\tilde{u}\tilde{T}} dz = \rho c_p \left[\int_{-L}^{0} \bar{\tilde{u}}\bar{\tilde{T}} dz + \int_{-L}^{0} \overline{\tilde{u}'\tilde{T}'} dz \right]. \tag{2.5}$$

The cross-shelf eddy heat flux in (2.5), $\overline{\tilde{u}'\tilde{T}'}$, is handled differently than in several previous papers [*e.g. Bryden et al.*, 1980; *Richman and Badan-Dangon*, 1983; and *Send*, 1989]. Depth-average eddy heat flux terms are often not separated from the depth-dependent flux terms and the cross-shelf eddy heat flux is often written as,

$$\int_{-H}^{0} \overline{u'T'} dz = \int_{-H}^{0} \overline{\tilde{u}'\tilde{T}'} dz + \int_{-H}^{0} \overline{\langle u\rangle'\langle T\rangle'} dz. \tag{2.6}$$

However, by (2.4) the cross-shelf, depth-averaged, eddy heat flux cancels the along-shelf, depth-averaged, eddy heat flux divergence in the same manner as the mean cross-shelf depth-averaged flux and along-shelf depth-averaged flux divergence cancel. Therefore only the depth-dependent cross-shelf eddy heat flux is considered in the mean heat budget. The vertically integrated depth-dependent fluxes in (2.3) are not a function of the absolute temperature scale. The vertical structures of the depth-dependent fluxes do depend on the temperature scale, but remain similar and have sensible interpretations provided temperature is measured relative to an average such as the depth or cross-shelf area average. The approach of separating the depth-dependent components of the heat budget is the 2-D analog to the method used to compute heat fluxes over a volume by *Lentz* [1987*b*].

2.4.2 Estimation of Terms in the Mean and Low-Passed Heat Budgets

Terms in a time mean and a 38 hour low-passed (using the PL64 filter described in *Limeburner* [1985]) version of (2.3) were estimated using time series of u, T, and v at C3, and T at G3 and M3. At deployment time, temperature and velocity observations existed at common depths at C3; however current meter failures (see Fig. 2.3) necessitated interpolation of velocity components at about half the temperature sensor depths for at least a portion of the time series. It was also necessary to extrapolate above and below the shallowest and deepest observations to the surface and bottom. Because vertical length scales of variability were much greater than the instrument separations, interpolated values were insensitive to the particular interpolation scheme and linear interpolation was chosen. Extrapolation of current and temperature information from the shallowest VMCM (at 8.5 m or 5.5 m) to the surface was more problematic. I chose to extrapolate above and below the shallowest and deepest functioning sensor depths assuming a vertically uniform profile.

In winter, uniform extrapolation of u between 5.5 m and the surface and between 91 m and the bottom yielded similar results as more complicated extrapolation schemes, despite winter near-surface and near-bottom current data during SMILE and STRESS [*Santala*, 1991 and *Gross et al.*, 1992] which suggest this is an oversimplification. For example, linear extrapolation above the shallowest and below the deepest observations, changed mean winter values of the cross-shelf heat flux by only 10%. Uniform extrapolation probably did well because the surface boundary layer, as indicated by mean and median surface mixed layer (SML) depths of 16 and 14.5 m (estimated following *Lentz* [1992]), was resolved by several current meters; hence it was not solely dependent on transport above 5.5 m. This is supported by a comparison of the low-passed SML to surface Ekman transport, $\tau_y/\rho f$, which shows they are correlated at the 99.9% level (correlation coefficient 0.71) with a regression coefficient of SML transport on Ekman transport of 0.78.

In spring, uniform extrapolation of current and temperature above the shallowest

observations almost certainly resulted in some underestimate of the cross-shelf heat flux. The mean SML depth in spring was 6 m and over half the SML depth estimates were 0 m suggesting the surface boundary layer was not well resolved by functioning current meters. This is also indicated by a comparison of low-passed SML transport to the low-passed surface Ekman transport which shows that though they are still correlated at the 99.9% level (correlation coefficient 0.78), the regression coefficient of SML transport on Ekman transport is 1.45 in spring. Inclusion of a transition layer below the SML, as suggested by *Lentz* [1992], did not account for this discrepancy. Though linear extrapolation above 8.5 m increased the spring mean offshore heat flux by almost a factor of two, only uniform extrapolation results are presented because uniform extrapolation was consistent with the winter analysis, and because the absence of current measurements above 8.5 m during most of spring made all extrapolation schemes untestable.

After interpolating and extrapolating current observations to the C3 temperature depths, components of the mean and fluctuating heat budgets were calculated. The depth-dependent cross-shelf velocity, $\tilde{u}$, was calculated by subtracting the depth-averaged cross-shelf velocity, $\langle u \rangle$, (found by trapezoidally integrating u and dividing by the depth, 93 m) from u at each observation depth. Depth-dependent temperature time series, $\tilde{T}$, were estimated in the same way. The low-passed time series of cross-shelf heat flux was calculated by multiplying the hourly time series of the $\tilde{u}$ and $\tilde{T}$ together, vertically integrating them, and low-pass filtering the result. The mean cross-shelf heat flux was estimated from the unfiltered cross-shelf heat flux time series, and the cross-shelf eddy heat flux was calculated by vertically integrating the covariance of $\tilde{u}$ and $\tilde{T}$.

To estimate the change in heat content over the cross-shelf area, time series of $\partial T/\partial t$ were computed at each C3 depth using centered differences of hourly observations. Because there were no temperature measurements between C3 and the coast in winter, heat content was assumed to be uniform from C3 to the coast. To estimate heat gain or loss over the cross-shelf area, the time derivatives of temperature at each depth were multiplied by the estimated cross-shelf distance from C3 to the isobath

equal to each measurement depth and vertically integrated. Time-averaged and low-pass filtered changes in heat content were derived from the hourly time series. The assumption that heat content changes were uniform in the cross-shelf direction was checked for the upper 49.5 m in spring using the C2 mooring. C2 was deployed just prior to the beginning of the spring time period and was halfway between the C3 mooring and the coast (Fig. 2.2). Due to near shore warming, inclusion of the C2 mooring increased the estimate of mean heat content change in spring by about one third, but did not alter the fundamental balances of the spring mean and fluctuating heat budgets discussed in section 5. For this reason, and because cross-shelf temperature information was unavailable below 49.5 m in spring, estimates for cross-shelf integrated heat content change are based on the C3 mooring alone for both winter and spring.

The net surface heat flux at C3 was estimated from bulk formulas using hourly meteorological measurements at C3 and nearby locations. It was assumed spatially uniform and was multiplied by the distance to the coast, 6.3 km, to get the cross-shelf integrated sea surface flux. The hourly time series was then averaged and low-pass filtered to give mean and fluctuating air-sea heat fluxes. Procedures for estimating the sea surface flux and discussions of uncertainties are given in Appendices A and C.

Lack of information about spatial variability of along-shelf velocity and temperature made estimates of along-shelf heat flux divergence subject to strong assumptions. The along-shelf heat flux divergence in (2.3) is given by:

$$-\rho c_p \int_{-L}^{0} dx \int_{-H}^{0} v \frac{\partial T}{\partial y} dz, \tag{2.7}$$

the heat flux divergence caused by along-shelf advection of an along-shelf temperature gradient, and

$$-\rho c_p \int_{-L}^{0} dx \int_{-H}^{0} \tilde{T} \frac{\partial v}{\partial y} dz, \tag{2.8}$$

the heat flux divergence caused by the along-shelf volume transport divergence. Following *Richman and Badan-Dangon* [1983], (2.7) is called the along-shelf temperature

gradient flux. It was estimated from temperature observations at G3 and M3 and velocity measurements at C3. The along-shelf temperature gradient in the upper 49.5 m at C3 was estimated by differencing G3 and M3 temperatures and dividing by the along-shelf distance, 29.2 km. G3 and M3 temperatures were linearly interpolated to the same depths as the C3 observations where necessary. To estimate the along-shelf temperature gradient flux, the along-shelf temperature gradient was multiplied by the along-shelf velocity at C3. Gaps in along-shelf velocity observations were filled following the same interpolation/extrapolation procedure used on the cross-shelf velocity. In the absence of other information, the along-shelf temperature gradient flux was assumed to be uniform in x so that the integral of $v\partial T/\partial y$ in the cross-shelf direction was estimated by multiplying by the distance to the coast at each depth. This was vertically integrated from 49.5 m to the surface. Mean, eddy, and fluctuating components of the along-shelf temperature gradient flux were estimated as for the cross-shelf heat flux. Observations of along-shelf velocity at C2 in spring and of the cross-shelf structure of temperature, along-shelf velocity, and along-shelf heat flux in summer [*Winant et al.*, 1987, and *Lentz*, 1987*b*] indicate the assumption of uniformity in x is an oversimplification. However, the sign and magnitude of the along-shelf temperature gradient flux as estimated above are consistent with other information in both the time mean and fluctuating heat budgets.

Unfortunately, the depth-dependent along-shelf heat flux divergence in (2.8) cannot even be crudely estimated because $\partial v/\partial y$ is unknown. It is unlikely that (2.8) dominates the winter heat budget given its near closure. However, (2.8) may play a significant role in spring when the heat balance does not close as well and circumstantial evidence indicates the presence of mesoscale features.

2.4.3 Estimating the Mean and Low-passed Salt Budgets

Conductivity time series measured at the central SMILE and STRESS moorings allowed some terms in the salt budget to be estimated and compared to the heat budget. The salt balance used was analogous to (2.3) and terms in the salt budget were estimated in the same manner as those in the heat budget. To gauge qualita-

tively the effects of the reduced vertical resolution of salinity measurements relative to temperature measurements, the heat budget was recalculated at the same reduced resolution as the salt budget. Vertically integrated values for cross-shelf fluxes and heat content changed by roughly 10%, but the basic balances did not. The lack of along-shelf salinity time series measurements meant along-shelf salinity fluxes could not be estimated. The mean net freshwater surface flux was estimated from evaporation based on the latent heat flux at C3 and precipitation from a coastal rain gauge at Stewart's Point (see Fig. 2.1). Other rainfall measurements taken during SMILE show this rain gauge is representative of rainfall extending northward approximately 90 km to Cabrillo Point (see Fig. 32, *Alessi et al.* [1991]).

2.5 Results

2.5.1 Mean Winter and Spring Heat Budgets

Using the methods developed in section 2.4.2 the vertically integrated winter and spring heat balances per unit along-shelf distance are estimated and presented in Tables 2.1 and 2.2. In both winter and spring, the mean cross-shelf heat flux, though about a factor of five smaller than in summer, is a dominant term in the mean heat budget. Tables 2.1 and 2.2 show it is largely the result of the mean advection of the mean temperature field (Figs. 2.5 and 2.6). Mean cross-shelf velocities are highest in the surface and bottom boundary layers. This leads to the vertical structures in Figs. 2.7 and 2.8 which show a near-surface offshore maxima caused by the offshore flow of the warmest water on the shelf and a near-bottom onshore maxima caused by the offshore flow of the coldest water on the shelf. Though the general character of the vertical structures of the winter and spring cross-shelf heat flux is similar, they differ in detail. In winter, the near-surface offshore heat flux extends to 25 m. In spring near-surface offshore heat flux values are larger than in winter but are confined to the top 10 m. This is due to a stronger spring near-surface stratification and near-surface offshore mean flow only above 10 m in spring. The highly surface intensified

	Mean	Eddy Contribution to Mean	Standard Error	Standard Deviation
Heat content change	−2.8	—	5.0	33.8
Cross-shelf heat flux	−8.7	1.5	3.7	25.3
Along-shelf temp. gradient flux	5.1	5.2	1.9	10.6
Air-sea heat flux	0.1	—	0.5	3.6
Heat balance residual	−0.6	—	4.6	25.5
Salt content change	7.9	—	44.1	299.4
Cross-shelf salt flux	147.9	3.0	45.5	308.9

Table 2.1: Mean winter 1988–1989 heat and salt balances. Heat balance units are in 10^5 W m^{-1} and salt balance units are in 10^{-3} m^2 psu s^{-1}. Standard error estimates are calculated from low-passed data with the number of independent observations found from the record hours divided by an integral time scale of 60 hrs for the along-shelf temperature gradient flux and heat balance residual and 40 hrs for all other terms.

structure of the spring mean cross-shelf flux is a further suggestion that it may be underestimated, since the top velocity sensor (at 8.5 m during most of this time) is only barely within the near-surface region. The near-bottom offshore heat transport is consistent with Ekman bottom boundary layer dynamics in that observed interior poleward flow is associated with offshore near-bottom flow (the correlation between v at 67 m and u at 91 m, −0.45, is significant at the 99% level).

The other advective contribution to the mean heat budgets, the along-shelf temperature gradient flux, is the second largest component of the winter mean heat budget and the third largest component of the spring mean heat budget. Tables 2.1 and 2.2 show this term (especially in winter) is largely the result of an eddy along-shelf temperature gradient flux and not a mean advective flux. Though the magnitude of the along-shelf temperature gradient flux should be viewed skeptically, since its estimation is subject to strong assumptions, the negative correlation coefficients associated with the eddy along-shelf temperature gradient flux in winter were greater than −0.30 (the 95% significance level) suggesting stronger than average poleward flow was associated with equatorward temperature gradients and vice versa at C3. During spring, this correlation coefficient is weaker and the mean advection of the

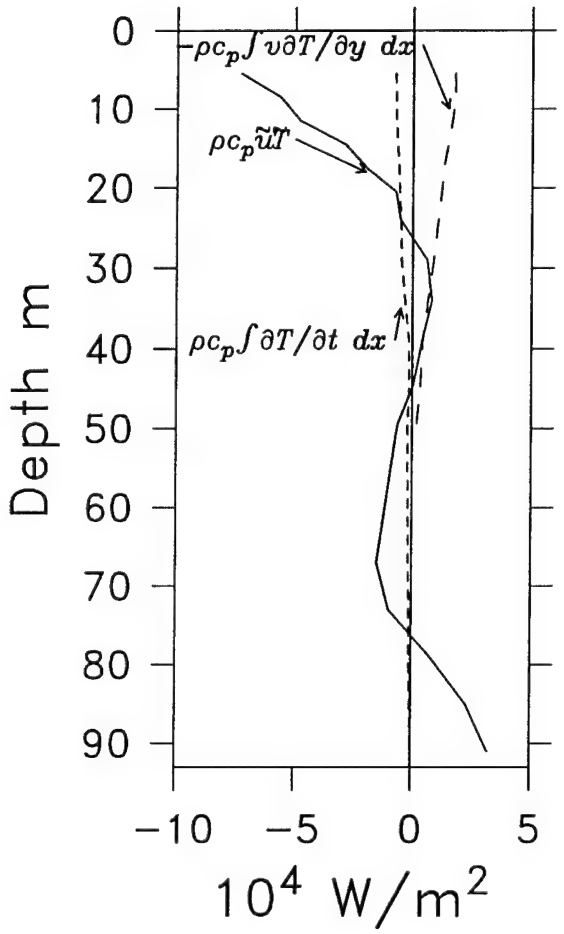

Figure 2.7 Vertical profiles of the largest 3 terms in the 1988–1989 mean winter heat budget. The mean cross-shelf heat flux is indicated by the solid line, the local heat content change by the short dashed line, and the along-shelf temperature gradient flux by the long dashed line. The mean cross-shelf heat flux is almost entirely the result of the mean advection of the mean temperature field. In contrast, the mean along-shelf temperature gradient flux is almost entirely due to eddy along-shelf temperature gradient flux.

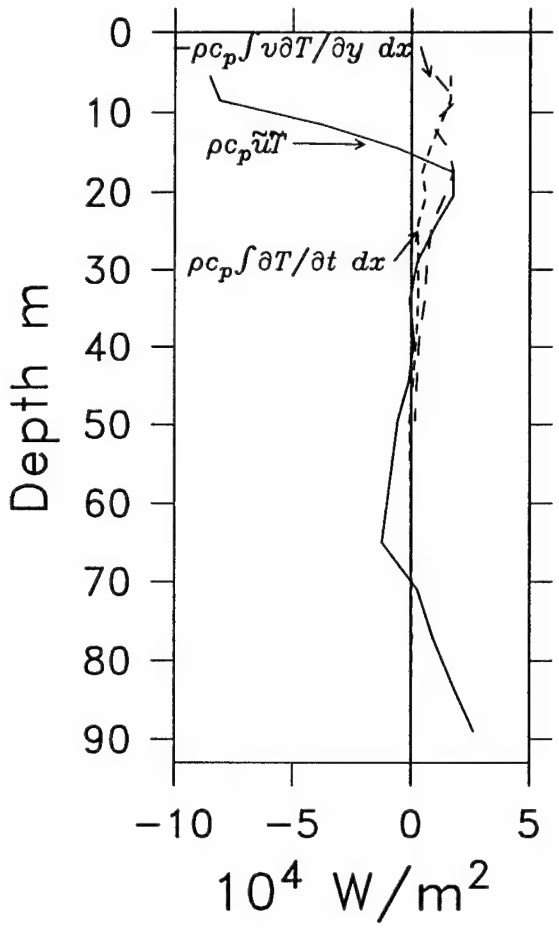

Figure 2.8 Profiles of terms in the mean spring heat budget. The mean cross-shelf heat flux is indicated by the solid line, the local heat content change by the short dashed line, and the along-shelf temperature gradient flux by the long dashed line. The largest single component of the mean spring heat flux is the mean surface heat flux (not shown).

	Mean	Eddy Contribution to Mean	Standard Error	Standard Deviation
Heat content change	3.1	—	6.4	38.0
Cross-shelf heat flux	−6.4	1.1	7.2	42.7
Along-shelf temp. gradient flux	4.3	2.9	2.8	13.7
Air-sea heat flux	8.3	—	0.9	5.2
Heat balance residual	3.2	—	8.7	42.2
Salt content change	−32.4	—	60.4	360.1
Cross-shelf salt flux	41.7	−13.9	60.0	357.9

Table 2.2: Mean spring 1989 heat and salt balances. Heat balance units are in 10^5 W m^{-1} and salt balance units are in 10^{-3} m^2 psu s^{-1}. Standard error estimates calculated as in Table 2.1.

mean temperature gradient became about half as large as the eddy along-shelf temperature gradient flux. The mean along-shelf temperature gradient flux is greatest near the surface and decreases monotonically with depth. This decrease is primarily due to larger near-surface values of along-shelf temperature gradient flux rather than the smaller cross-shelf area represented by deeper observations.

It is in the air-sea heat flux that winter and spring show the greatest difference. In winter, its contribution to the mean heat budget is an order of magnitude smaller than the largest estimated terms (Table 2.1), but in spring it becomes the single largest term in the mean heat budget (Table 2.2). This was due to an increase in incoming short-wave radiation from an average of 104 W m^{-2} in winter to a 190 W m^{-2} in spring and a decrease in the latent heat flux from an average of −39 W m^{-2} in winter to −18 W m^{-2} in spring.

As a result of the above processes, the local heat content decreases in winter and increases in spring. Winter in-situ cooling corresponded to a depth-averaged temperature drop at C3 of about 1.0°C over a 77 day period. The winter change in mean heat content is largest near the surface and decreases with depth. Above 60 m, this decrease was due primarily to larger near-surface mean values of in-situ cooling and below 60 m was due to the smaller cross-shelf area represented by near-bottom observations. Spring in-situ heating would correspond to a depth-averaged

temperature increase at C3 of about 1.1°C over a 59 day period but this increase occurred primarily in the upper 20 m with little change in heat content below this depth.

Our analysis has shown the mean winter and spring balances are qualitatively different. In winter, the absence of surface heating leads to a three-dimensional balance between the negative cross-shelf heat flux and positive along-shelf temperature gradient flux. In spring, surface heating is a major term in the mean heat balance, which is primarily between surface heating and a negative cross-shelf heat flux. In both winter and spring, the mean cross-shelf heat flux is due to the mean advection of the mean temperature field and has a vertical structure consistent with a wind forced surface boundary layer and an along-shelf velocity forced bottom boundary layer. In contrast, the along-shelf temperature gradient flux is due to an eddy gradient flux rather than to mean along-shelf advection.

2.5.2 Fluctuating Heat Budgets

Fluctuations in the low-pass filtered heat budget (Figs. 2.9 and 2.10) are one to two orders of magnitude larger than means (in Tables 2.1 and 2.2). In contrast to the mean heat budgets, the dominant balance in the fluctuating heat budgets at periods of days to weeks was

$$\int_{-L}^{0} dx \int_{-H}^{0} \frac{\partial T}{\partial t} dz = \int_{-H}^{0} \tilde{u}\tilde{T} dz. \tag{2.9}$$

The along-shelf temperature gradient flux was only occasionally important at these time scales and air-sea heat flux only became appreciable on time scales of one month or longer in spring (Figs. 2.11 and 2.12). The correlations of terms in (2.9) with each other and with the low-passed along-shelf wind stress at C3 (Tables 2.3 and 2.4) indicate the likely physical process accounting for the balance represented in (2.9) was the response of the cross-shelf heat transport and temperature to local along-shelf wind forcing. The lower spring correlation coefficients may be caused by a lack of velocity information above 8.5 m, weak wind forcing in April, and/or the presence of a mesoscale feature over the northern California shelf during this time

	Along-Shelf Wind Stress	Heat Content	Cross-Shelf Heat Flux	Along-Shelf Temp. Gradient Flux	Salt Content	Cross-Shelf Salt Flux
Along-shelf wind stress	1	0.68	0.64	0.14	−0.69	−0.60
Heat content		1	0.59	0.21	−0.71	−0.53
Cross-shelf heat flux			1	−0.08	−0.57	−0.80
Along-shelf temp. gradient flux				1	−0.18	0.27
Salt content					1	0.53
Cross-shelf salt flux						1

Table 2.3: Correlation coefficients for low-passed winter 1988–1989 heat and salt balances. Zero lagged correlation coefficients were very near maximum lagged correlations. For a 40 hour integral time scale (used for wind stress, heat (salt) content changes and cross-shelf heat (salt) fluxes), correlations of 0.20, 0.30, and 0.39 are significant at the 80%, 95%, and 99% levels respectively. For a 60 hour integral time scale (used for correlations involving along-shelf temperature gradient fluxes), correlations of 0.24, 0.36, and 0.46 are significant at the 80%, 95%, and 99% levels respectively.

[*Largier et al.* 1993]. On an event basis, examination of Figs. 2.9 through 2.12 shows: episodic removal of heat from the shelf occurring on five occasions (December 7 and 24, January 11, January 24, and April 10) following equatorward wind stresses of 0.2 N m^{-2} or greater, several shortlived increases in heat content associated with poleward winds immediately preceding winter upwelling events, and a longer increase in heat content during poleward wind stresses for several weeks in March. This last increase in heat appears similar in character to the removal of heat caused by upwelling events in winter. It does not show upwelling and downwelling are symmetric, though it does indicate the shortlived upwelling/downwelling events prior to the transition to upwelling season may have similar effects on the fluctuating heat budget.

To examine the vertical structure of the low-passed heat balance, covariance em-

	Along-Shelf Wind Stress	Heat Content	Cross-Shelf Heat Flux	Along-Shelf Temp. Gradient Flux	Salt Content	Cross-Shelf Salt Flux
Along-shelf wind stress	1	0.65	0.60	0.00	−0.57	−0.61
Heat content		1	0.35	0.06	−0.74	−0.39
Cross-shelf heat flux			1	−0.36	−0.15	−0.95
Along-shelf temp. gradient flux				1	−0.36	0.33
Salt content					1	0.24
Cross-shelf salt flux						1

Table 2.4: Correlation coefficients for low-passed spring 1989 heat and salt balances. Zero lagged correlation coefficients were very near maximum lagged correlations. Integral time scales are as in Table 2.3. Correlations of 0.23, 0.35, and 0.45 are significant at the 80%, 95%, and 99% levels respectively for correlations between wind stress, heat (salt) content change, and cross-shelf heat (salt) flux. Correlations of 0.28, 0.41, and 0.53 involving along-shelf temperature gradient flux are significant at the 80%, 95%, and 99% levels respectively.

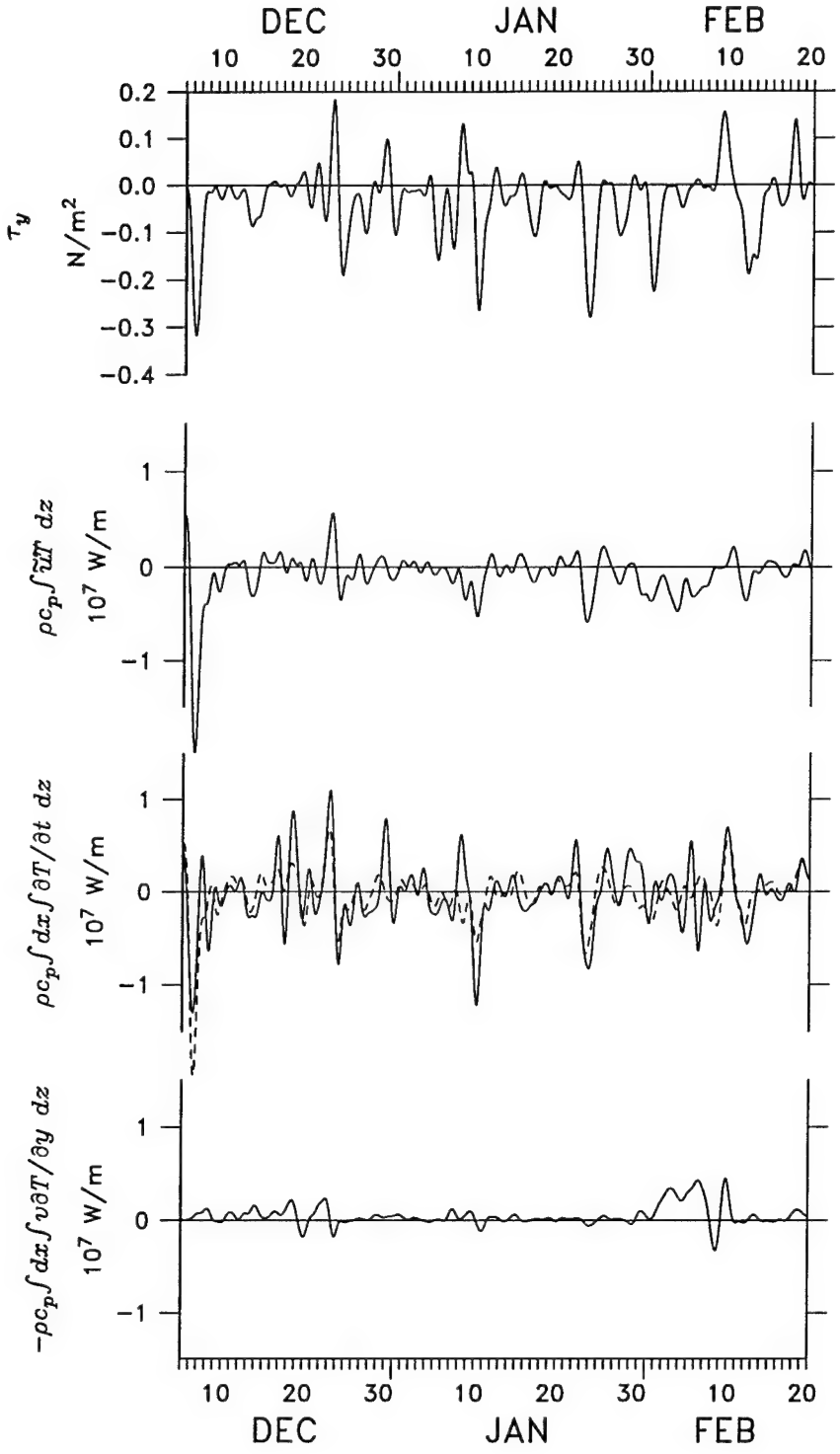

Figure 2.9 Low passed time series of along-shelf wind stress and terms in the depth-integrated winter heat budget. Zero lag correlations of terms are given in Table 2.3. The dashed line in the third plot is the sum of the cross-shelf heat flux, along-shelf temperature gradient flux, and net air-sea heat flux. The correlation between this sum and the estimated heat content change is 0.67.

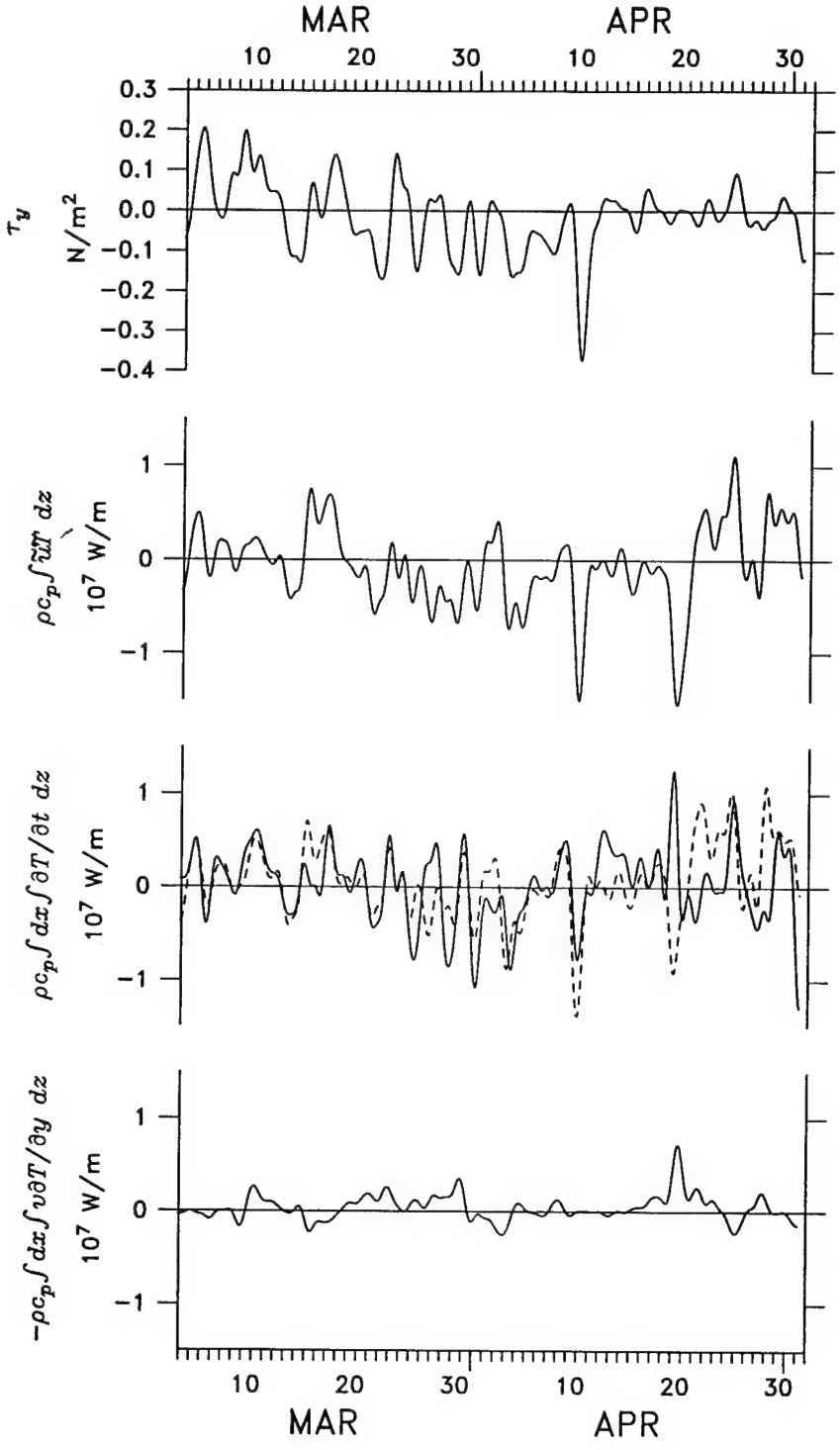

Figure 2.10 Low passed time series of along-shelf wind stress and terms in the depth integrated spring heat budget. The dashed line in the third plot is the sum of the cross-shelf heat flux, along-shelf temperature gradient flux, and net air-sea heat flux. The correlation between this sum and the estimated heat content change is 0.39. Other zero lag correlations are given in Table 2.4.

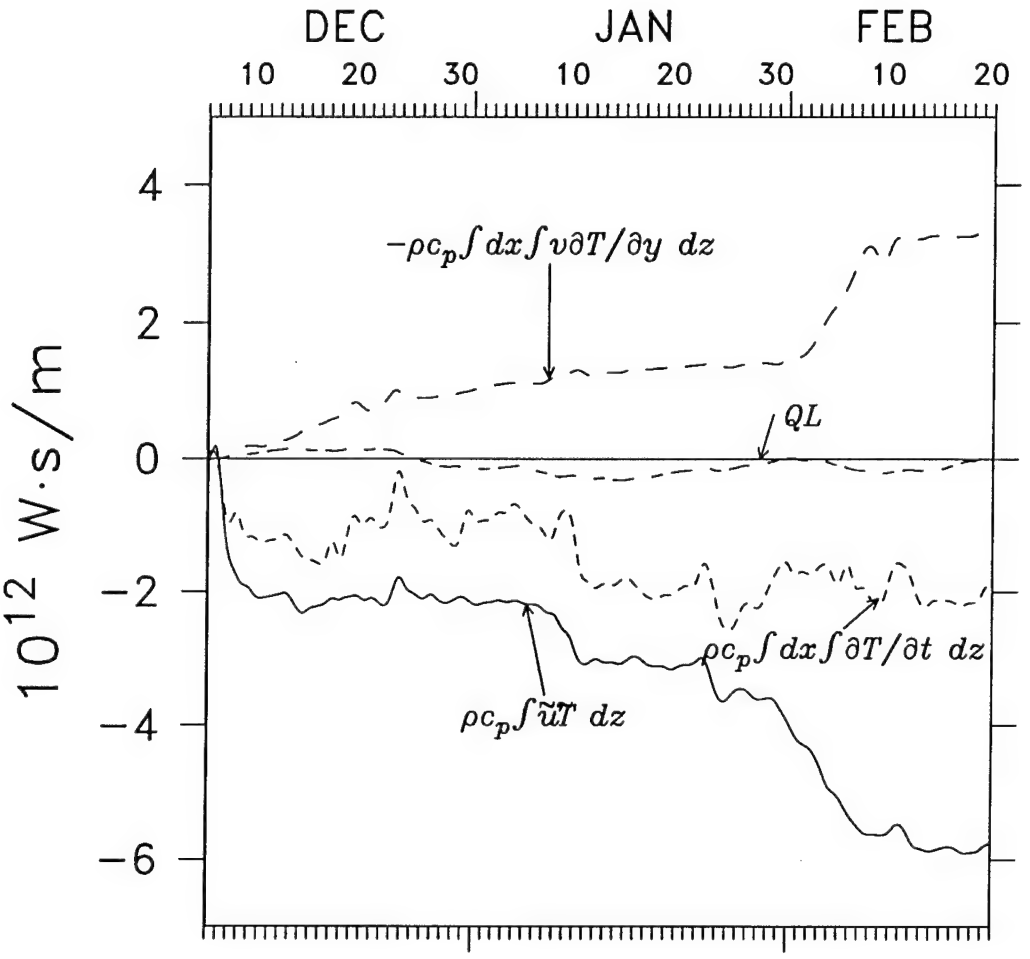

Figure 2.11 Time integrated change in heat content at C3 through the winter. The heat content change is indicated by the short dashed line, the change due to cross-shelf advection by the solid line, that due to along-shelf advection by the long dashed line, and that due to surface heating by the alternate dashed line. A change of 10^{12} W s m^{-1} corresponds to a change in the depth-averaged temperature of 0.54°C.

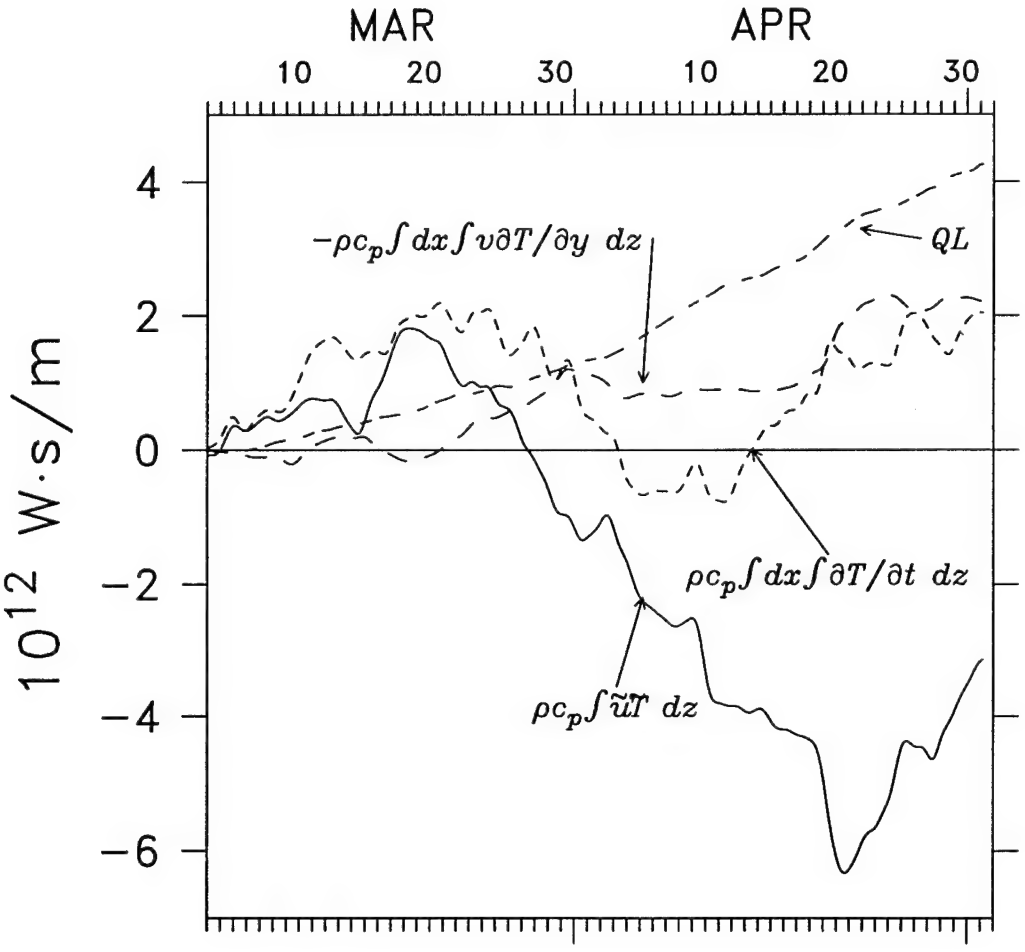

Figure 2.12 Time integrated change in heat content at C3 through the spring. The heat content change is indicated by the short dashed line, the change due to cross-shelf advection by the solid line, that due to along-shelf advection by the long dashed line, and that due to surface heating by the alternate dashed line. A change of 10^{12} W s m^{-1} corresponds to a change in the depth-averaged temperature of 0.54°C.

pirical orthogonal functions (EOFs) were formed from the low-passed time series of heat content change, along-shelf temperature gradient flux, and cross-shelf heat flux. The vertical structure of the lowest EOF of the fluctuating cross-shelf heat flux (Figs. 2.13 and 2.14) has near-surface and near-bottom maxima in the same direction, unlike the mean cross-shelf heat flux (Figs. 2.7 and 2.8) which has offshore flow of cool water in the bottom boundary layer caused by the mean poleward flow. Figs. 2.13 and 2.14 suggest a 2-D conceptual model with offshore flow of relatively warm water in a wind driven surface boundary layer and onshore return flow of cooler water in the interior and in the bottom boundary layer. Like the depth-integrated time series, the lowest EOF amplitude time series of heat content change are correlated with the cross-shelf heat fluxes above the 99% level (correlation coefficient of 0.56 (0.49) in winter (spring)) and both are correlated with the wind stress (0.64 (0.61) for heat content change and 0.63 (0.69) for cross-shelf heat flux).

Along-shelf temperature gradient flux usually made a secondary contribution to the fluctuating heat budgets. It was not correlated with the along-shelf wind stress and became evident during several events lasting two to three weeks in December, early February, March, and late April (Figs. 2.9 and 2.10); factors which suggest it may be due to mesoscale features. The lowest EOF (Figs. 2.13 and 2.14) of the along-shelf temperature gradient flux is surface intensified, and its amplitude time series shows all instances of large along-shelf temperature gradient flux are surface intensified. In at least two events (February and April), the positive contribution of the along-shelf temperature gradient flux acts to balance a simultaneous negative cross-shelf heat flux. However in the spring event of April 20–26, estimates of heat content change do not agree well with the sum of cross-shelf heat flux, along-shelf temperature gradient flux, and air-sea heat flux, which may indicate the along-shelf heat flux divergence contained in (2.8) is important during this time.

The fluctuating balances in both winter and spring are predominantly between heat content change and cross-shelf heat fluxes. These are well correlated with the wind, and the fluctuating cross-shelf heat flux has a vertical structure determined by wind-driven surface and bottom boundary layers. The along-shelf temperature

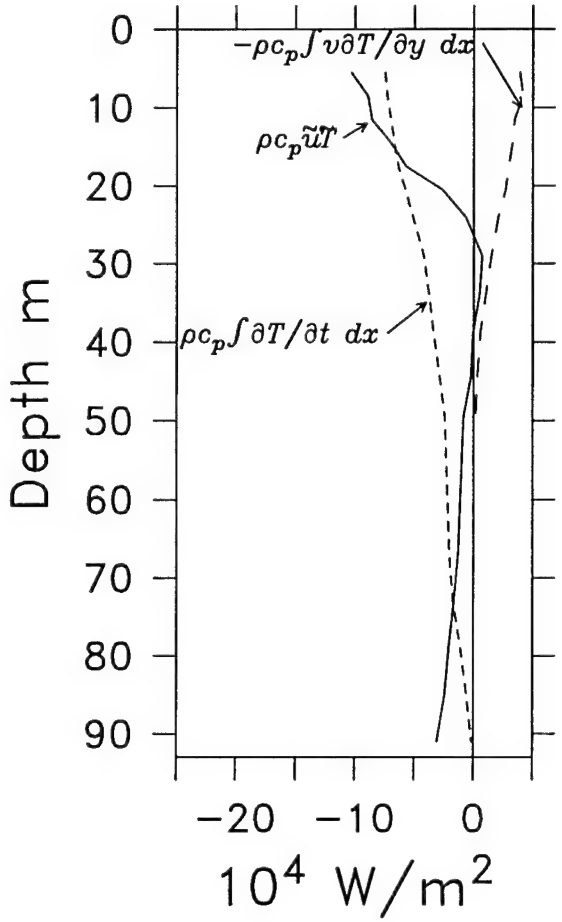

Figure 2.13 Lowest EOFs of terms in the low-passed winter heat budget. These account for 79%, 77%, and 86% of the cross-shelf heat flux (solid line), local heat content (short dashed line), and along-shelf temperature gradient flux (long dashed line), variance respectively.

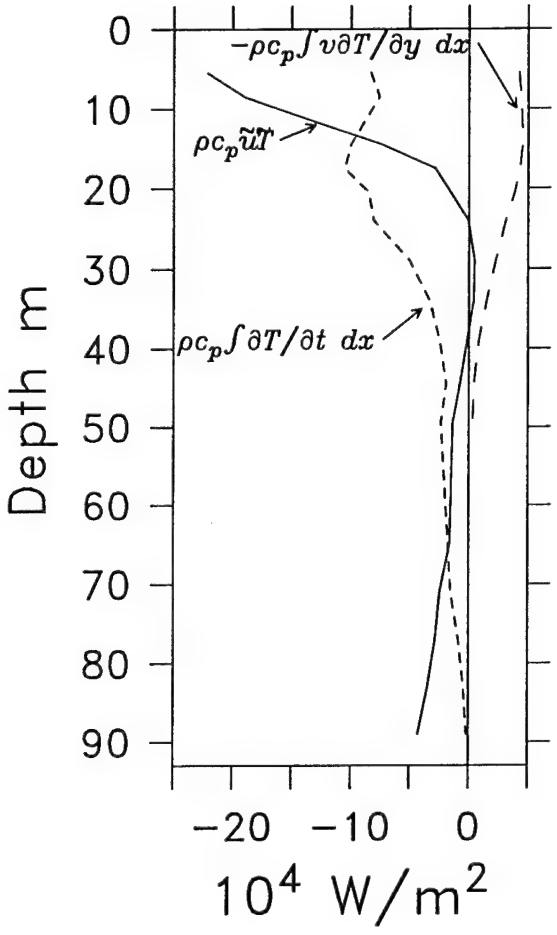

Figure 2.14 Lowest EOFs of terms in the low-passed spring heat budget. These account for 77%, 62%, and 81% of the cross-shelf heat flux (solid line), local heat content (short dashed line), and along-shelf temperature gradient flux (long dashed line), variance respectively.

gradient flux is only secondarily important. It is not correlated to the wind, may result from poleward advection of an equatorward temperature gradient or vice versa, and is probably due to mesoscale features. The air-sea heat flux is not important to the fluctuating winter heat budget and becomes important on time scales of one month to the spring heat balance.

2.5.3 Salt Budget

In general, the salt balance was similar to the heat balance. The largest term in the mean salt balances (Tables 2.1 and 2.2) was the onshore salt flux. Its vertical structure (shown only for winter in Fig. 2.15) was essentially a mirror image of the vertical structure of the mean cross-shelf heat flux (Figs. 2.7 and 2.8) suggesting it was caused by a mean offshore advection of low salinity water near the surface. Other estimated terms in the mean salt balance were much smaller than the mean cross-shelf salt flux which, in the absence of other processes, would increase salinity about +2.18 psu in winter and +0.47 psu in spring. In winter, the observed mean salinity change was much less, about +0.12 psu, and in spring the mean salinity change was actually −0.37 psu. The net surface freshwater flux could have offset the cross-shelf flux by only 0.04 (0.11) psu in winter (spring). This imbalance suggests an along-shelf salt flux divergence closed the mean salt budgets. It's possible this along-shelf salt divergence was a result of river runoff from the Russian River south of C3 (Fig. 2.1), but even in the absence of river runoff, the mean T-S relationship (Fig. 2.16) suggests the mean along-shelf temperature gradient flux at C3 would be associated with a negative contribution to the salt balance.

To gauge qualitatively whether along-shelf salinity gradients were associated with along-shelf temperature gradients, observations from three SMILE CTD cruises [*Limeburner and Beardsley*, 1989*a*, *b*, and *c*] in November, 1988, February through March, 1989, and May, 1989 were compared with simultaneous C3 mooring temperatures and salinities. The cruises included repeated surveys and along-shelf sections with a total of 92 stations along the 93 m isobath with roughly 15 km resolution. Along-shelf temperature and salinity differences were negatively correlated with a correlation co-

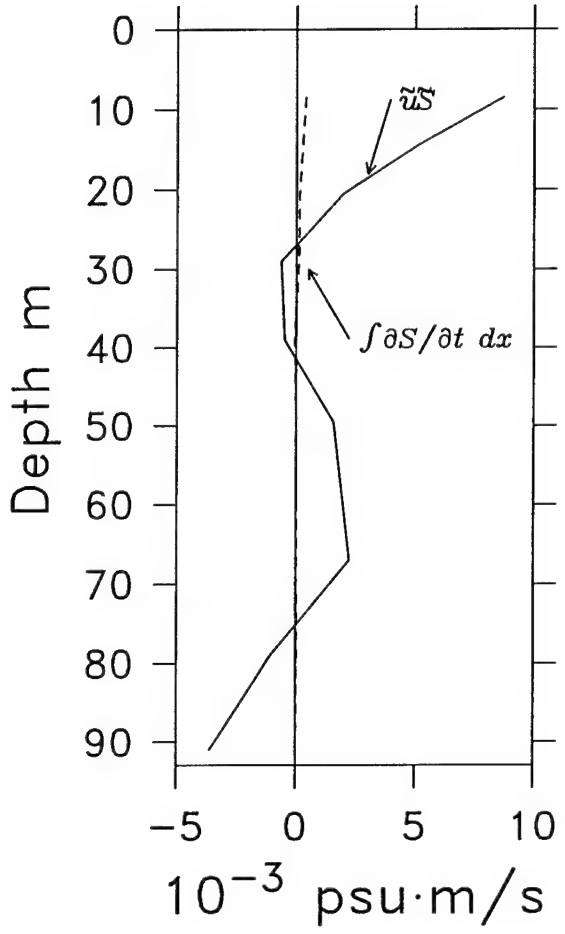

Figure 2.15 Salt flux profiles of terms in the mean winter salt budget. The mean cross-shelf salt flux is indicated by the solid line and the local salt content change by the dotted line.

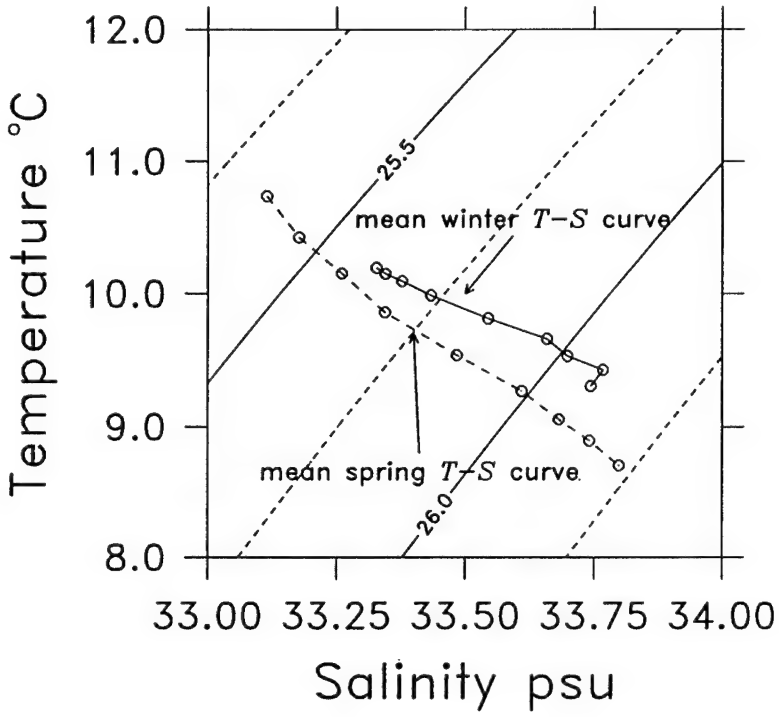

Figure 2.16 Mean T-S relation at C3 in winter (solid) and spring (dashed). Surface mooring observation depths were at 8.5, 14.5, 20.5, 29.0, 39.0, and 49.5 m. Subsurface mooring observation depths were at 67, 79, and 91 m in winter and 65, 77, and 89 m in spring.

efficient of -0.59. Assuming each CTD survey or along-shelf section represented an independent observation (time evolution was rapid enough that individual surveys lasting one or two days could not be considered synoptic), this correlation coefficient is significant at the 95% level. The negative correlation coefficient indicates that a poleward transport of low salinity water would be associated with a poleward transport of heat and vice versa.

Like the mean salt balance, the low-passed fluctuating salt balance provided essentially the same information as the low-passed heat balance. Cross-shelf heat and salt fluxes are negatively correlated (Tables 2.3 and 2.4), as are changes in heat and salt content. Changes in salinity and the cross-shelf salt flux are well correlated to each other and to the along-shelf wind stress. The lowest EOF modes of vertical structure for salt content and cross-shelf salt flux are very similar to, and negatively correlated with, those of heat content (correlation coefficients -0.70 and -0.60 in winter and spring) and cross-shelf heat flux (correlation coefficients -0.79 and -0.93 in winter and spring). The periods when cross-shelf salt flux and changes in salt content agree least correspond to the periods when the along-shelf temperature gradient flux was important, a further indication that the along-shelf salt flux divergence is related to the along-shelf temperature gradient flux.

2.6 Discussion and Summary

Mean and fluctuating heat and salt budgets per unit along-shelf distance have been estimated using measurements from the 1988–1989 SMILE/STRESS field programs for the northern California shelf. Based on data coverage and the absence or presence of persistent surface heating, these time series have been analyzed as two distinct periods: a winter period characterized by weak surface heating, and a spring period during which surface heating is important. Both winter and spring were subject to weak mean winds, making meteorological conditions different from summer upwelling season, which began immediately after the end of the spring time period in 1989. The goals of this discussion are: to contrast the winter and spring heat budgets with

those observed in the summer upwelling season on the northern California shelf and elsewhere, and to put the results in the context of climatological forcing conditions.

One of several points which stand out in comparing the mean winter, spring, and summer-upwelling heat balances is the relative magnitudes of terms in the balances. To compare the winter and spring heat budgets per unit along-shelf distance to the volume heat budget of *Lentz* [1987*b*], the heat content change and along-shelf heat flux divergence values reported by Lentz were divided by his study volume of 79.1 km^3 and multiplied by the cross-shelf area between CODE C3 and the coast, 0.39 km^2. Similarly, the cross-shelf heat flux values were divided by the along-shelf distance, 56 km; and the net air-sea heat flux was divided by the surface area of 936 km^2 and multiplied by the distance between CODE C3 and the coast, 5.8 km. The mean cross-shelf heat flux and net air-sea heat flux are directly dependent on the persistence of upwelling favorable winds and seasonal variation in solar insolation. Therefore they show the greatest variations in magnitude between winter, spring, and summer. The mean cross-shelf heat fluxes per unit along-shelf distance in winter and spring (Tables 2.1 and 2.2) are about a factor of five smaller than the estimated summer value on the northern California shelf of -42.3×10^5 W m^{-1}. The mean net air-sea heat flux also shows large variability; it increases from winter and spring values (Tables 2.1 and 2.2) to 10.0×10^5 W m^{-1} in summer. By contrast, the summer mean along-shelf temperature gradient flux (a portion of the total heat flux divergence) and heat content change (-2.7×10^5 W m^{-1} and -2.4×10^5 W m^{-1} respectively) have similar magnitudes to those in winter and spring (Tables 2.1 and 2.2).

These changes in relative magnitude lead to differences in the character of winter, spring, and summer mean heat balances. The winter heat balance is between the negative mean cross-shelf heat flux and positive along-shelf temperature gradient flux, making it three dimensional to the lowest order. The mean spring and summer heat balances are between the negative cross-shelf heat flux and positive net air-sea heat flux, making them more two-dimensional in character. However, the cross-shelf heat flux is much weaker in spring than in summer, so that a mean increase in heat content occurs in spring, rather than the slight decrease observed in summer upwelling

season.

Regardless of the season, the mean cross-shelf heat flux is of importance to the mean heat balance. The most prominent characteristic of its vertical structure in winter and spring, a near-surface offshore heat flux, is similar to that observed in upwelling systems off Oregon [*Bryden et al.*, 1980], northwest Africa [*Richman and Badan-Dangon*, 1983], and northern California [*Lentz*, 1987*b*]. Below the surface, the winter and spring mean cross-shelf heat fluxes decrease in magnitude and have a sign which varies with depth. Near the bottom, the winter and spring cross-shelf heat fluxes are stronger and onshore due to the offshore flow of the coldest water on the shelf. *Richman and Badan-Dangon* [1983] also observed a near-bottom increase in cross-shelf heat transport magnitude on the northwest African shelf, though it was offshore due to onshore transport of cold water. The directions of near-bottom cross-shelf heat transport found by *Richman and Badan-Dangon* [1983] and this study can be explained by a near-bottom Ekman transport driven by a mean interior along-shelf flow. *Bryden et al.* [1980] and *Lentz* [1987*b*] find no near-bottom increase in cross-shelf heat transport, possibly because the bottom boundary layer, expected to be thin during active upwelling events [*Weatherly and Martin*, 1978, and *Trowbridge and Lentz*, 1991], was not resolved with available measurements. The mean winter and spring cross-shelf heat flux vertical structures are consistent with the notion that mean winds, though weak, drive an offshore flow of relatively warm water in the surface boundary layer and poleward along-shelf currents set up an offshore flow of the coldest water in the bottom boundary layer.

Though mean heat budgets observed in winter, spring, and summer are quite different, fluctuating heat budgets are similar. The magnitude of the fluctuations in winter and spring are within a factor of two of fluctuations in the summer upwelling budget [*Lentz*, 1987*b*]. In all three cases, the dominant balance is between the cross-shelf heat flux and local changes in heat content. These terms are highly correlated with the local along-shelf wind stress and each other (this is true to a lesser degree in spring). The vertical structure of the fluctuating cross-shelf heat flux, as represented by the lowest EOF mode, suggests wind driven surface and bottom boundary layers.

Thus it appears short time scale variability is dominated by a wind driven cross-shelf heat flux with a resulting change in heat content in winter, spring, and summer [*Lentz*, 1987*b* and *Lentz and Chapman*, 1989]. It is interesting to note that poleward winds associated with downwelling can result in a shoreward flux of heat and an increase in heat content. In this respect at least, downwelling events appear to be similar to upwelling events in winter and spring.

This two-dimensional picture of the fluctuating heat budget is upset in February, March, and late April when the along-shelf temperature gradient flux becomes important on time scales of weeks. During these times, the along-shelf temperature gradient flux tends to be offset by the cross-shelf heat flux, reducing the net change in heat content. *Lentz* [1987*b*] found a similar event in the 1982 summer upwelling heat budget which he attributed to the presence of an offshore mesoscale feature seen in satellite infrared images. The events in February, March, and April, 1989 do not appear to be locally wind driven and may also be due to mesoscale features. *Largier et al.* [1993] also observed mesoscale features over the northern California shelf and slope in March and April, 1989 during the Northern California Coastal Circulation Study (NCCCS), a field program designed to study large scale circulation.

The mean heat balances in winter 1988–1989 and spring 1989 differ to varying degrees from summer upwelling balances which are thought to be relatively robust. However, even the largest terms in the mean balances (Tables 2.1 and 2.2), with the exception of the spring air-sea heat flux, are scarcely larger than their standard errors. One question which then arises is: how general are the 1988–1989 mean balances? To help answer this question, a heat balance is constructed from more limited data taken in the winter of 1981–1982 (Appendix B). This analysis yielded very similar mean (and fluctuating) balances as those in the winter of 1988–1989; hence it provided some confidence in the generality of 1988–1989 results. However, the along-shelf wind stress, the net air-sea heat flux, and the along-shelf velocity, all important factors in determining the winter and spring heat balances, are likely to vary significantly over the course of a single season as well as between seasons and geographically. Because the dominant terms in the mean winter and spring heat

balances have small magnitudes compared to their fluctuations, variation in these forcing factors may alter the magnitude or even the sign of individual terms in the mean winter and spring heat balances.

The most important factor in determining the cross-shelf heat flux, the along-shelf wind stress, is less uniform in time and space than in summer when winds are generally upwelling favorable. *Nelson* [1977] and *Strub et al.* [1987*a*] show seasonal along-shelf winds to be equatorward all along the Washington, Oregon and California coasts during summer months but spatially variable in winter months, becoming poleward north of 39° N, remaining equatorward south of this latitude, and weak and variable off northern California. The locations of both the SMILE and CODE field programs are near this latitude where the sign and magnitude of a mean winter or spring along-shelf wind stress may be expected to vary. Fig. 2.17, the thirty day low-pass filtered along-shelf (in the 317°T reference frame) component of wind stress observed from December through May during CODE and SMILE at NDBC 13 and the monthly mean climatological wind stress calculated by *Nelson* [1977] at a one degree square centered at 38° N 123° W, shows year to year variability in winter and spring wind fields near the SMILE and CODE locations. From December through February, climatological monthly mean winds are near zero but equatorward. Winds during this time in 1988–1989 are equatorward (within approximately one standard deviation) of this climatological mean, and winds during 1981–1982 are also equatorward within a standard deviation of the climatological mean. C. E. Dorman et al. (Structure of the lower atmosphere over the northern California coast during winter, submitted to *Monthly Weather Review*, 1994) found the number of equatorward, poleward, and weak wind events during winter of 1988–1989 was fairly typical based on an examination of ten years of wind records at NDBC 13. Monthly mean winds during spring, prior to the spring transition to upwelling season, are probably also generally equatorward and weak as in Fig. 2.17. All this indicates a weak mean upwelling may generally be present near 39° N in winter and spring suggesting a resulting mean offshore heat flux.

The net air-sea heat flux was not a dominant factor in the winter mean heat

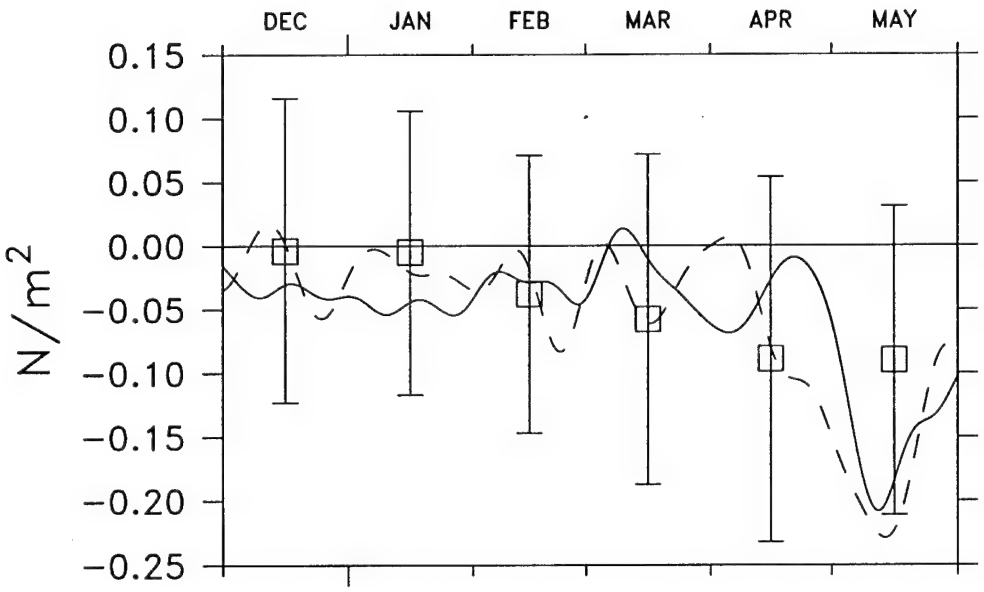

Figure 2.17 Along-shelf (317°T) wind stress component for the months of December through May. The monthly climatological winds from *Nelson* [1977] are indicated by the squares. As in indication of the variability in observations used by Nelson, approximate standard deviations were found by taking the square root of the sum of the squares of standard deviations for east and north wind stress components (calculated from standard error and observation numbers presented in *Nelson* [1977]). The 1988–1989 30 day low-pass filtered winds are indicated by the solid line, and the 1981–1982 30 day low-pass filtered winds by the dashed line.

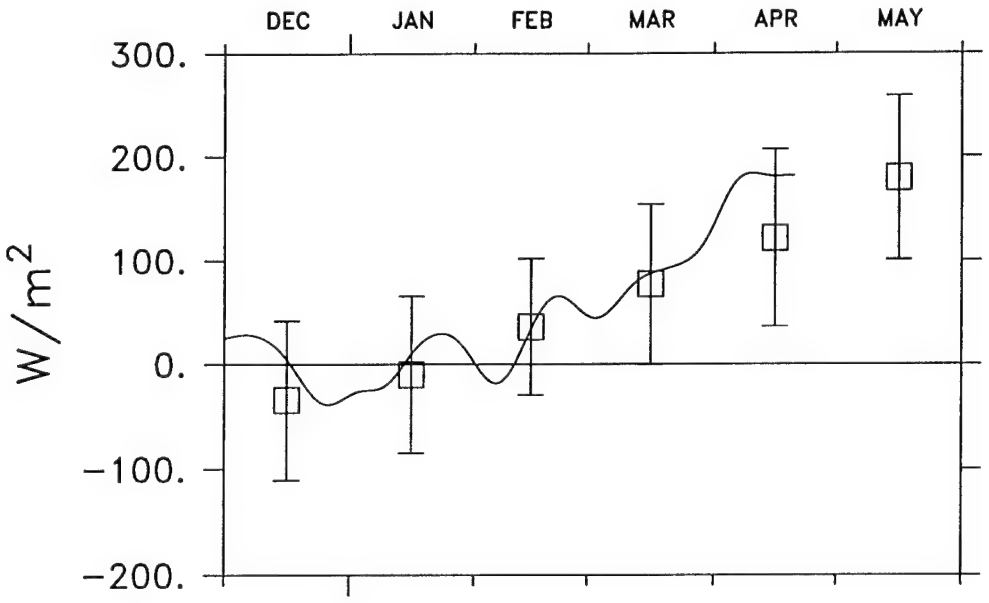

Figure 2.18 Net surface heat flux for the months of December through May. The monthly climatological air-sea heat flux from *Nelson and Husby* [1983] is indicated by the squares with standard deviations calculated from standard errors and observation numbers presented in Nelson and Husby, 1983. The 1988–1989 30 day low-pass filtered surface heat flux is indicated by the solid line.

balance, but became so in the spring heat balance. The separation into winter and spring in 1988–1989 is dependent on the mean winter air-sea heat flux being small, and a relatively rapid change to mean spring surface heating prior to the transition to upwelling. Fig. 2.18 shows the thirty day low passed air-sea heat flux at C3 in 1988–1989 with the climatological heat flux at a one degree square centered at 38° N 123° W from *Nelson and Husby* [1983]. This shows monthly mean air-sea heat fluxes are indeed small relative to summer values, and may be negative during winter months, and that they increase rapidly in March and April. The spring transition in 1988–1989 occurred in early May, 1989, which allowed for two months of surface heating prior to the spring transition to upwelling. However, the spring transition is generally thought to occur earlier, in March or April [*Strub and James*, 1988]. This would cut short the spring period of surface heating prior to strong upwelling so 1988–1989 may be anomalous in this respect. Fig. 2.17 shows the 1988–1989 wind stress plotted with that in 1982 when the spring transition occured in mid April [*Lentz*, 1987*a*].

Another factor which may influence the heat balance is the along-shelf velocity.

Through bottom boundary layer dynamics, this may affect the near-bottom cross-shelf heat flux as well as the along-shelf heat flux divergence. Year to year variability is evident in a comparison of 1988–1989 SMILE mean along-shelf currents to those during a similar time of year in 1981–1982 at the same location (see Fig. 2.4 and *Lentz and Chapman* [1989]). However, mean interior along-shelf currents are poleward in both years. If poleward interior currents are a regular part of the seasonal cycle, as *Strub et al.* [1987] find, they would set up a mean offshore Ekman flow in the bottom boundary layer. The near-bottom onshore heat flux associated with this Ekman flow could be a persistent feature in winter and spring.

Along-shelf velocity is also important in determining the along-shelf temperature gradient flux. It's important to note the along-shelf temperature gradient flux observed in winter and spring 1988–1989 and winter 1981–1982 was not the result of a mean advection of a mean temperature gradient, but rather was an eddy flux. The physical mechanisms behind the along-shelf temperature gradient flux deserve further study. In winter and spring, it is not significantly correlated to the local along-shelf wind, but appears to be associated with mesoscale features. Winter 1981–1982 results at CODE C3 and R3 suggest the contribution of this term to the heat balance may vary over along-shelf separation scales of 30 km. In summer, *Lentz* [1987*b*] found an along-shelf heat flux divergence of approximately the same magnitude on the northern California shelf; however the mean summer along-shelf heat flux divergence was primarily the result of the mean along-shelf advection of a mean temperature field rather than an eddy heat flux divergence. Fluctuations in the summer along-shelf heat flux divergence were attributed to wind related occurrences such as relaxation from upwelling [*Send et al.*, 1987] as well as an offshore mesoscale feature. Because the along-shelf temperature gradient flux seems to be associated with mesoscale features and because only a few were observed during this study, their effects on a climatological winter heat budget are uncertain.

2.7 Appendix A: Estimation of the Net Sea Surface Heat Flux

The net surface heat flux was estimated at C3 as

$$Q = Q_i + Q_b + Q_l + Q_s \tag{2.10}$$

where Q_i is the net solar radiation, Q_b is the net longwave radiation, Q_l is the latent heat flux, and Q_s is the sensible heat flux. These four terms were estimated using formulas very similar to those employed by *Lentz* [1987*b*]. The explanation below is taken from that paper with modifications as necessary: $Q_i = I(1 - Ab)$ where I is the measured insolation and Ab is the ocean albedo given by *Payne* [1972]. The insolation was measured at C3 using two types of Eppley pyranometers, a model 8-48, and a model PSP. Because the 8-48 returned a nearly complete record (the PSP failed in early February), this instrument was used to estimate net surface heat flux. However a comparison of the 8-48 data with other available insolation data at C3 and on the coast showed the 8-48 suffered a gain problem, consistently reading low by about 20%. To account for this, the 8-48 was regressed onto available C3 PSP data and this regression coefficient was used to obtain a more accurate estimate of insolation. $Q_b = Q_{cs} - R$, where the Efimova formula of *Simpson and Paulson* [1979] was used to compute the clear sky upward long wave radiation, Q_{cs}, from the water temperature at 5.5 m, and R is the downward measured long wave radiation reflected from the atmosphere. $Q_s = \rho_a C_P C_h u_w (T_a - T_s)$, where ρ_a is the density of air, C_P is the heat capacity of air, C_h is the sensible heat flux coefficient given by *Friehe and Schmitt* [1976], u_w is the wind speed, T_a is the air temperature 52 km south of C3 at NDBC 13, and T_s is the water temperature at 5.5 m. $Q_l = LC_e u_w (q - q_s)$, where L is the heat of evaporation, C_e is the latent heat flux coefficient given by *Friehe and Schmitt* [1976], q is the absolute humidity given by multiplying the measured relative humidity by the saturation humidity at T_a, and q_s is the absolute humidity at the ocean surface taken to be $0.98 q_{sat}$ at the temperature T_s, where q_{sat} is the saturation humidity. The

necessity of using the air temperature at NDBC 13 and the water temperature at 5.5 m causes some uncertainty in longwave, latent and sensible heat flux estimates. The air temperature at NDBC 13 was used because air temperature records at C3 were lost due to a leak in the vector averaging wind recorder (VAWR). Comparisons of NDBC 13 to NDBC 14 (located 76 km north of C3) air temperature observations suggest the temperature difference is at most 3°C over 127 km, the distance between NDBC 13 and 14,so that C3 air temperatures are approximately those at NDBC 13. The water temperature at 5.5 m was used because water temperature records at 1 m below the surface were lost due to leakage in the VAWR at C3.

The net surface heat flux at C3 was assumed to be uniform from C3 to the coast. From shore measurements and the C2 buoy (present in spring), some components of the net sea surface heat flux can be checked for cross-shelf variation. All meteorological variables measured at C3 were also measured on the coast at the Stewart's Point Beach location shown on Fig. 2.1. Stewarts Point and C3 data presented in *Alessi et al.* [1991] show that averages of relative humidity and incoming long wave radiation were within 5% and their standard deviations within 15%. Wind speed averages and standard deviation do decrease by about a factor of two between C3 and the coast. Spring measurements of wind speed at C2 indicate most of this decrease occurs between C2 and the coast. Neglecting the cross-shelf variation in wind speed probably resulted in an overestimate of the cross-shelf integrated latent heat flux and sensible heat flux. However, sensible and latent heat fluxes were not the largest components of the mean winter and spring net air-sea heat fluxes. These were the mean incoming short-wave radiation and outgoing long wave radiation.

2.8 Appendix B: The Winter Heat Budget in 1981–1982

For comparison with the 1988–1989 results, the heat balance from 1300 December 12, 1981 to 1200 March 22, 1982 is examined using two moorings deployed on the northern

California shelf as part of the Coastal Ocean Dynamics Experiment (CODE). One mooring, denoted CODE C3, was 6 km southeast of the SMILE C3 location. The second mooring was 34 km southeast of the CODE C3 location and was denoted R3. Both moorings were in 90 m of water and had temperature and (VACM) velocity sensors at 9, 35, 55, and 75 m. The C3 mooring had an additional VACM sensor at 15 m. Wind stress data were also acquired at NDBC 13 (located 43 km from C3 and 16 km from R3). The winter CODE data are presented and analyzed by *Lentz and Chapman* [1989]. Though the vertical resolution of the winter CODE data is poorer than that of the SMILE data and the air-sea heat flux cannot be estimated, the winter CODE data appear to be sufficient to resolve the simple vertical structures found in the winter SMILE heat balance (Fig. 2.7). Additionally, historical data [*Nelson and Husby*, 1983] and the winter SMILE results suggest the surface heat flux is negligible during winter.

The heat budgets at CODE C3 and R3 were estimated using essentially the same methods presented in section 3 except for the along-shelf temperature gradient flux. Because only two moorings were present, the along-shelf temperature gradient at both C3 and R3 was represented by the temperature difference divided by the along-shelf distance between C3 and R3; hence differences in the along-shelf temperature gradient flux between C3 and R3 were entirely due to spatial variations in v. The CODE reference frames [*Winant et al.*, 1987] of 317°T and 329°T at C3 and R3 were used. Rotation to the reference frame required to make the mean cross-shelf transport at C3 zero (325°T) affected mean heat flux results by only about 10%. The actual local isobath orientation at R3 is not clear and rotation to other plausible reference frames showed mean cross-shelf heat flux values at R3 varied from 50% to 200% of the values in the 329°T coordinate frame, though the fluctuating balance was less sensitive.

Both mean and fluctuating heat balances at C3 for 1981–1982 are qualitatively similar to those in 1988–1989 both in the magnitude of the vertically integrated budget (Table 2.5) and in vertical structure. The mean offshore heat flux in the upper 30 m is approximately balanced by mean cooling and an eddy along-shelf

	Mean	Eddy Contribution to Mean	Standard Error	Standard Deviation
C3 heat content change	−4.1	—	6.7	52.3
C3 cross-shelf heat flux	−15.5	−3.8	6.5	50.3
C3 along-shelf temp. gradient flux	7.0	7.3	3.1	19.9
C3 heat balance residual	−4.4	—	7.7	49.0
R3 heat content change	−6.0	—	10.2	78.8
R3 cross-shelf heat flux	−8.5	−1.4	7.8	60.2
R3 along-shelf temp. gradient flux	−3.6	−3.2	4.0	25.0
R3 heat balance residual	−6.9	—	10.1	63.6

Table 2.5: Mean winter 1981–1982 heat and salt balances at C3 and R3. Heat balance units are in 10^5 W m^{-1}. Standard error estimates calculated as in Table 2.1.

temperature gradient flux. The low-passed fluctuating heat balance in 1981–1982 is again an approximate balance, (2.9), between changes in heat content and cross-shelf heat flux which are well correlated (Table 2.6) with the wind stress. The along-shelf temperature gradient flux is uncorrelated with the wind and becomes important only during several events. Though the 1981–1982 heat balance at C3 is similar to that in 1988–1989, spatial differences between C3 and R3 did exist. The offshore heat flux at C3 is larger than at R3 and the mean along-shelf temperature gradient flux, which adds heat at C3, removes it at R3. These qualitative results are not sensitive to changes in the R3 coordinate frame.

2.9 Appendix C: Effects of Measurement Uncertainty on Heat and Salt Balances

The purpose of this appendix is to estimate the uncertainties of the measurements which went into estimating the heat and salt balances and to consider their effects on the mean and fluctuating heat and salt balances.

	Along-Shelf Wind Stress	C3			R3		
		Heat Content	Cross-Shelf Heat Flux	Along-Shelf Temp. Gradient Flux	Heat Content	Cross-Shelf Heat Flux	Along-Shelf Temp. Gradient Flux
Along-shelf wind stress	1	0.73	0.54	0.25	0.70	0.67	0.08
C3 heat content		1	0.56	0.33	0.57	0.52	0.17
C3 cross-shelf heat flux			1	0.19	0.38	0.38	0.24
C3 along-shelf temperature gradient flux				1	0.27	0.07	0.52
R3 heat content					1	0.65	0.10
R3 cross-shelf heat flux						1	0.04
R3 along-shelf temperature gradient flux							1

Table 2.6: Correlation coefficients for low-passed winter 1988–1989 heat and salt balances. Zero lagged correlation coefficients were very near maximum lagged correlations. Integral time scales are as in Table 2.3. Correlations of 0.17, 0.25, and 0.33 are significant at the 80%, 95%, and 99% levels respectively for wind stress, heat content change, and cross-shelf heat flux. Correlations of 0.20, 0.30, and 0.39 involving along-shelf temperature gradient flux are significant at the 80%, 95%, and 99% levels respectively.

2.9.1 Surface heat flux uncertainty

The surface heat flux becomes important to the winter and spring heat balances on time scales of months. Therefore the interest here is in estimating the effects of persistent biases introduced into the net surface heat flux rather than random errors. Several sources of biases undoubtedly exist in the estimates of surface heat fluxes used in chapter 2. Some of these biases, such as over-estimation of wind speed, are instrumental, and some, such as an underestimate of the albedo in winter, are introduced in calculation. The probable biases and their effects on the total uncertainty of the net winter and spring surface heat fluxes are detailed here.

As mentioned in Appendix A, leakage of the VAWR at C3 caused loss of all air temperature (T_a) data. As a result, T_a at NDBC 13 was used to represent that at C3. To gauge spatial differences, T_a at NDBC 13 was compared to that at NDBC 14 located north of Pt. Arena. Instantaneous differences were at most 3° and the mean temperature difference over the common record period was 0.18°; within the uncertainty of the NDBC temperature sensors (±1°). Because I consider it unlikely that both temperature sensors would be biased by 1°, I'm going to consider ±0.2° as a bound for a mean bias in T_a. This uncertainty affects both latent and sensible heat fluxes.

The leakage of the VAWR at C3 also caused the loss of surface water temperature (T_w) at C3 so the water temperature at the 5.5 m VMCM was used instead. In winter, comparison of 5 m temperature sensors with near-surface (1–4 m) temperature sensors at the G3 and M3 SMILE moorings showed mean temperature differences in winter were at the same level as instrument accuracy (about 0.05°). In spring, surface heating became appreciable and on some occasions, instantaneous temperature differences in the upper 5 m exceeded 1°. However, mean temperature differences in the upper 5 m remained less than 0.15° during spring, and I consider the mean 5.5 m temperature at C3 to be within 0.15° of the surface temperature.

The relative humidity sensor at C3 used in the latent heat flux calculations returned a complete time series. Comparison of relative humidity at C3 with that

measured at Stewart's Point indicates an uncertainty of approximately 5%, in line with previous [*Weller et al.*, 1990] estimates of uncertainty for this type of sensor.

Wind speed was measured with a VAWR mounting a Gill 3-cup wind speed sensor. This sensor is known to overestimate wind speed. Following *Weller et al.* [1990], this overspeeding is taken as 6%.

The shortwave radiation measured at C3 was off by a constant gain factor (Appendix A). This was compensated for by regressing the longer Eppley 8-48 time series on a truncated Eppley PSP time series also taken at C3. Depending on the exact procedures followed, this regression coefficient is between 1.15 and 1.18, an uncertainty of about 3% and within the manufacturer's stated uncertainty of 5%. An additional bias enters into the calculations in that the albedo is taken as a constant 0.07. In fact, the albedo varies with season and could be up to 0.10 in the winter months [*Payne*, 1972]. The resulting uncertainty in net shortwave radiation at C3 is about 8% in winter and 5% in spring.

Incoming longwave radiation was also measured at C3. The Eppley PIR sensor used in these calculations functioned well for almost the entire winter and spring time periods. Comparisons with other longwave sensors at C3 and Stewart's Point indicate its uncertainty was approximately 5%. However, a persistent bias of 3% was introduced by neglecting to account for reflected downward longwave radiation in the net longwave heat flux, Q_b.

Applying all the likely uncertainties and biases listed above, the total estimated bias is about ± 22 W/m^2 for the mean winter surface heat flux and ± 24 W/m^2 for the mean spring surface heat flux. To compare these with the values listed in Tables 2.1 and 2.2, they must be multiplied by the cross-shelf distance to C3, 6.3 km, to get cross-shelf integrated uncertainties of 1.4×10^5 W/m and 1.5×10^5 W/m. Though not big enough to affect the qualitative winter and spring balances, they are larger than the statistical uncertainty listed in Tables 2.1 and 2.2.

2.9.2 Velocity time series uncertainty

Uncertainty in velocity time series affects both mean and fluctuating advective heat fluxes. Vertical structure EOF's of velocity time series revealed no obvious directional or speed errors beyond those noted in section 2.3.1. In particular, comparison between the bottom surface moored VMCM (49.5 m) and the top subsurface moored VACM (67 or 65 m) showed no persistent offset in direction as measured current speed increased. The effects of uncertainty in cross-shelf direction were considered by calculating the heat balances in a rotated coordinate frame. Results were qualitatively very similar for both mean and fluctuating heat balances and differed quantitatively by only about 10% during SMILE.

2.9.3 Temperature and salinity time series uncertainty

Uncertainty in temperature (T) and salinity (S) time series also affects mean and fluctuating heat and salt balances. The vertical resolution of SMILE and STRESS ensures T and S fluctuations are always reflected at more than one sensor (with similar amplitudes) giving confidence that they are real. Uncertainty in temperature sensors is taken to be about 0.05° based on comparisons between adjacent temperature sensors in the surface and bottom boundary layers, however the conductivity sensors tp estimate salinity are particularly sensitive to biofouling. To attempt to quantify surface moored T and S uncertainty, shipboard yoyo CTD stations were occupied near the C3 moorings on three SMILE hydrographic cruises in November, 1988, February–March, 1989, and May, 1989. Fewer stations are available to assess the accuracy of the subsurface moored STRESS conductivity sensors as only the February–March cruise occurred when the STRESS mooring was in the water. A breakdown of the average temperature and salinity differences by cruise shows that though differences are present on all three cruises, average salinity differences remain small (around 0.01 psu) until the May cruise. During this May cruise, salinity differences jump to around 0.04 psu. This suggests some drift in the conductivity cells between March and May, 1989. Therefore the uncertainty in the trend of S is taken to be 0.01 psu in winter

and 0.04 psu in spring. Trends in T and S were much bigger than their uncertainties. Temperature trends were from 0.4° to 2° in winter and ranged up to 3.3° (for near-surface sensors) in spring. Salinity trends were about 0.1 psu in winter and -0.4 psu in spring.

Chapter 3

Wind-forced cross-shelf circulation on the northern California shelf

3.1 Abstract

Velocity time series have been used to study cross-shelf circulation on the northern California shelf and to examine the applicability of classical ideas of locally wind-forced cross-shelf circulation to the relatively brief, episodic wind-driven events observed in winter and to the persistent upwelling events observed in summer. A simple linear two-dimensional model of cross-shelf transport was applied and compared quantitatively to estimates of cross-shelf transport in the surface mixed layer, interior, and bottom mixed layer. In winter, model transports were highly correlated to the total surface flow and showed some skill in predicting subsurface cross-shelf flow. The observed depth-dependent cross-shelf flow (cross-shelf flow with the depth-averaged cross-shelf flow subtracted out) was surprisingly well correlated to the model with regression coefficients near one. Though this simple model described the depth structure of the wind-forced cross-shelf transport fairly well in winter, the same model did not work as well below the surface mixed layer when compared to summer observations. This implies a two-dimensional wind-forced model of cross-shelf circulation may have more applicability to the brief wind events observed in winter than to the persistent wind events observed in summer. The reason for this is unclear. Numer-

ous factors not included in the simple linear wind-forced model such as mesoscale features, upwelling fronts, topography, baroclinic pressure gradients, remote forcing, and small-scale wind stress all affect cross-shelf circulation. It's possible some of these processes are more pronounced on the northern California shelf in summer.

3.2 Introduction

Understanding the processes which govern cross-shelf circulation on wind-driven shelves remains an issue of both practical and theoretical interest. It is of practical interest because cross-shelf circulation is intimately associated with wind-driven coastal upwelling which affects strongly water property distributions on wind-driven shelves. Both mean and fluctuating heat and salt balances [see chapter 2 and *Lentz*, 1987*a*; *Rudnick and Davis*, 1987; *Richman and Badan-Dangon*, 1983; and *Bryden et al.*, 1980] are often dominated by cross-shelf transport. Understanding the processes governing cross-shelf velocity also remains an issue of theoretical interest because of difficulties in modelling cross-shelf velocity quantitatively, difficulties which are especially apparent when compared to success in modelling along-shelf velocities [*e.g. Chapman*, 1987 and *Zamudio and López*, 1994].

Many observational studies of cross-shelf velocity on wind-driven shelves have focussed on actively upwelling shelves and have revealed a number of common features of mean and subinertial fluctuating velocities (throughout this chapter the term mean will refer to time averages over record lengths of one to several months and the term subinertial will refer to records which have been filtered to pass periods longer than $\sim$ 36 hrs and suppress both tidal and inertial oscillations). At mid-shelf, cross-shelf velocity has a vertical structure consistent with turbulent surface and bottom boundary layers, separated by a possibly stable interior [*Badan-Dangon et al.*, 1986, *Kundu and Beardsley*, 1991]. In the surface boundary layer (SBL), cross-shelf velocity is significantly correlated with the along-shelf wind stress component [*Smith*, 1981, and *Winant et al.*, 1987] in the sense expected from Ekman dynamics, and transport within the SBL agrees quantitatively with the wind stress estimates of surface Ek-

man transport [*Lentz*, 1992 and *Lentz*, in preparation]. Similarly, Ekman dynamics strongly influence near-bottom cross-shelf velocities. The structure of near bottom velocity suggests veering in an Ekman sense and forcing by along-shelf interior flow [*Kundu*, 1976; *Dickey and Van Leer*, 1984; *Lentz and Trowbridge*, 1991].

Interior cross-shelf velocities have been more difficult to interpret in light of simple conceptual models. Classical upwelling theory would suggest interior and near-bottom cross-shelf transports compensate for wind-driven near-surface transport such that the mass balance is two-dimensional in the sense that the total cross-shelf transport is zero. Observations do show a tendency for this in a mean as well as fluctuating sense [*Allen and Kundu*, 1978], and *Davis and Bogden* [1989] find evidence of an along-shelf pressure gradient consistent with an interior geostrophic cross-shelf velocity which would act to balance surface Ekman transport. However a closer examination of the data has revealed the mass balance for both mean [*Halpern et al.*, 1977] and fluctuating [*Smith*, 1981] cross-shelf flow is often three-dimensional in the sense that the depth-averaged cross-shelf flow is not zero. Therefore even sophisticated numerical models which are two-dimensional have difficulty predicting subsurface cross-shelf velocities quantitatively. *Chen and Wang* [1990] are an exception to this trend, however even this success could not be replicated [*Zamudio and López*, 1994]. Observed cross-shelf velocities also differ in other ways from the classic two-dimensional upwelling model in that cross-shelf velocity fluctuations can have short correlation scales [*Kundu and Allen*, 1976] and be more energetic than predicted by linear wind-forced models [*Brink et al.*, 1994]. A variety of explanations for this have been suggested including short scale turbulence [*Kundu and Allen*, 1976], instrument noise, and sensitivity of cross-shelf velocity to short scale wind variability. *Brink et al.* [1994] examined the latter possibility using a linear model and concluded that, in the context of their model, short scale wind stress shortened correlation scales but could not account for energy levels of observed interior cross-shelf velocity.

The purpose of this study is to examine mean and subinertial velocities on a wind-driven shelf and use these observations to test quantitatively the ability of two-dimensional upwelling theory to model cross-shelf circulation in the surface boundary

layer, interior, and bottom boundary layer. Though it will focus on observations taken on the northern California shelf in winter when along-shelf wind forcing was intermittent and variable in direction, comparison will be made to observations from previous studies which occurred in summer when winds were strong, relatively steady, and upwelling favorable.

The remaining structure of this chapter is as follows. Section 3.3 introduces the observations used in the study. The mean and fluctuating cross-shelf velocity data for December, 1988 – February, 1989 are presented in section 3.4 in order to gain insight into the response of cross-shelf circulation to wind stress conditions which prevail on the northern California shelf in winter. In section 3.5, I apply a simple analytical model of wind-forced cross-shelf transport and compare it quantitatively with estimates of cross-shelf transport in the surface, interior, and bottom boundary layers. To highlight seasonal differences in cross-shelf circulation and make clear the limits of a two-dimensional model, I apply the simple transport model to cross-shelf circulation on the northern California shelf in both winter and summer in section 3.5. Results are summarized in section 3.6.

3.3 Observations

Observations used in this study were taken at a mid-shelf site approximately 6 km off the northern California coast (Fig. 3.1). Cross-shelf circulation was observed in the summer 1982 upwelling season during the Coastal Ocean Dynamics Experiment (CODE-2) and in the winter 1988–1989 during the Shelf Mixed Layer Experiment (SMILE) and Sediment Transport Events on Shelves and Slopes (STRESS) study. Both CODE-2 and the combination of SMILE and STRESS included wind measurements and velocity and temperature measurements throughout the water column at C3.

During CODE-2 the C3 site was instrumented with surface and subsurface moorings. The surface mooring included a Vector Averaging Wind Recorder (VAWR) and 3 Vector Measuring Current Meters (VMCMs) at depths from 5 m to 15 m. The

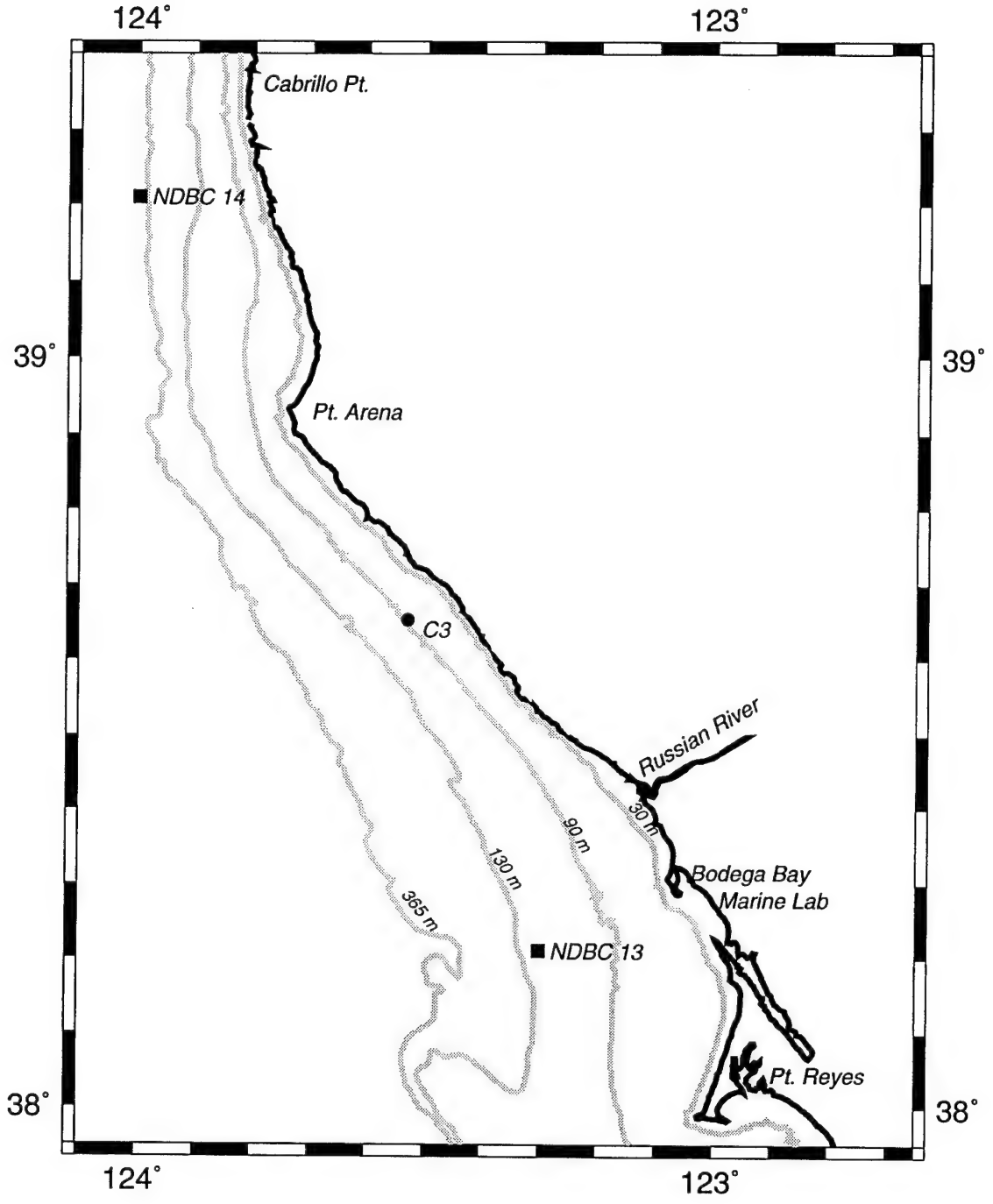

Figure 3.1. Map of the northern California shelf showing the nominal location of the central C3 site occupied in 1982 during CODE-2 and in 1988–1989 during SMILE and STRESS. Exact locations varied several km between experiments. Total water depth at the CODE-2 C3 site was 90 m, while that at the STRESS C3 site was 97 m. For reference, National Data Buoy Center locations 46013 (NDBC 13) and 46014 (NDBC 14) are also shown.

subsurface mooring included 8 VMCMs from 10 to 83 m depth. All current meters also recorded temperature. For the purposes of this study, the velocity record at C3 was examined from 0400 UT April 5, 1982 to 1800 UT July 25, 1982. This time period begins just prior to the 1982 spring transition to upwelling [*Lentz*, 1987*b*] and includes the CODE-2 common analysis period [*Winant et al.*, 1987] which ran from April 13, 1982 to July 25, 1982. The CODE observations have been extensively studied [*Beardsley and Lentz*, 1987]; two of the most complete descriptions of the CODE-2 moored velocity time series are found in *Limeburner* [1985] and *Winant et al.* [1987].

SMILE and STRESS also used surface and subsurface moorings to obtain complete vertical coverage at C3, though the mooring configurations were somewhat different. The C3 SMILE surface mooring included a VAWR and 12 VMCMs at depths from 5.5 m to 49.5 m. The STRESS subsurface mooring included 5 Vector Averaging Current Meters (VACMs) from 67 to 91 m depth. Both the VMCMs and VACMs also recorded temperature. As part of STRESS a bottom tripod supporting 6 Bottom Acoustic Shear Sensors (BASS) was also deployed near the STRESS subsurface mooring. Further information concerning the SMILE and STRESS field programs is found in chapter 2 section 3.1, *Alessi et al.* [1991], *Gross et al.* [1992], and *Fredericks et al.* [1993].

Though the SMILE deployment lasted from mid-November, 1988 to mid-May, 1989, VMCM bearing failures reduced vertical coverage of velocities as the experiment progressed. There were two separate deployments of the STRESS subsurface mooring in early December, 1988 and early March, 1989. Therefore, the time period selected here for study extends from 0400 UT December 6, 1988 to 2300 UT February 20, 1989. This time period covers the period of most complete vertical coverage and coincides with the winter time period examined in chapter 2.

3.4 Description of cross-shelf velocities during the winter 1988–1989

Mean and subinertial cross-shelf velocities observed during SMILE and STRESS in the winter 1988–1989 are described in this section. Particular attention is focussed on the vertical structure of cross-shelf velocity and the role of wind forcing. The description is here confined to the cross-shelf velocity under winter conditions because aspects of cross-shelf velocity under upwelling conditions have been extensively examined on the northern California shelf using the summer 1982 CODE-2 velocity time series [*Winant et al.*, 1987; *Rudnick and Davis*, 1987; *Send et al.*, 1987; *Davis and Bogden*, 1989; *Lentz and Trowbridge*, 1991; and *Lentz*, 1992] as well as elsewhere [*e.g. Smith*, 1981].

3.4.1 Definition of cross-shelf direction

Two common reference frames employed in interpreting cross-shelf velocity data are: the approximate local isobath orientation determined from a chart, and the principal axis of low-passed depth-averaged velocity [*Smith*, 1981]. At the C3 location, the local isobath direction has historically been taken as 317°T [see *e.g.*, *Winant et al.*, 1987], and the principal axis of depth-averaged velocity in CODE-2 was approximately 5° to the right of this [*Winant et al.*, 1987]. As explained by *Smith* [1981], both choices of coordinate frames have their shortcomings. Determination of the local isobath direction from charts is imprecise, and the spatial scales which define the local isobath in terms of its effects on mean and subinertial cross-shelf velocities are unclear. Adopting the principal axis of the depth-averaged velocity causes depth-averaged cross-shelf velocity fluctuations to be minimized and uncorrelated with the much stronger along-shelf velocity fluctuations; hence it would seem the best reference frame in which to apply a two-dimensional model. However, if the vertical structure of velocity is not adequately resolved by measurements, the principal axis reference frame determined from these measurements may differ from that of the true depth-

averaged velocity. Though there is some ambiguity in the definition of cross-shelf direction, rotation from the local isobath frame (317°T) to the principal axis reference frame (323°T from December, 1988 to February, 1989) causes little qualitative change. Results in this chapter will generally be presented in the 317°T reference frame; results for which there is an appreciable difference in the principal axis frame will be noted.

3.4.2 Mean cross-shelf velocities

The most basic features of the winter mean cross-shelf velocity profile (Fig. 3.2, Table 3.1) are: offshore near-surface flow consistent with the mean equatorward wind stress (0.03 N m^{-2}), offshore near-bottom flow consistent with the mean interior poleward along-shelf flow, and a vertically uniform flow in the interior between 34 and 67 m (extending over both surface and subsurface moorings). Note that wind forcing does not determine the poleward mean interior along-shelf flow and resulting offshore near-bottom flow as both are in opposition to the weak mean equatorward wind stress. The mean balance between offshore boundary layer flow and interior onshore flow is nearly perfect. The depth-averaged cross-shelf velocity, as determined by trapezoidally integrating the mean flow from the surface to 97 m and dividing by this depth, is only 0.20 cm s^{-1}. Rotation to the principal axis estimate of the cross-isobath direction changes the mean cross-shelf velocity to -0.22 cm s^{-1}, an indication that the mean depth-averaged cross-shelf flow between December, 1988 and February, 1989 is zero to within our ability to define a cross-shelf direction.

The depths of the mean offshore near-surface and near-bottom velocities are also qualitatively consistent with the mean surface mixed layer (SML) and bottom mixed layer (BML) thicknesses (calculated following *Lentz* [1992] and *Lentz and Trowbridge* [1991]). The mean SML depth for the winter time period is 16.5 m and the mean BML height is 11.1 m above bottom. This suggests that, in a mean sense, the near-surface and near-bottom flows are resolved by several current meters and that the SML and BML provide a reasonable indication of the SBL and BBL thicknesses as defined by velocity, though the SBL and BBL may include some transition layer below and above the SML and BML respectively [*Lentz*, 1992, and *Lentz*, in preparation].

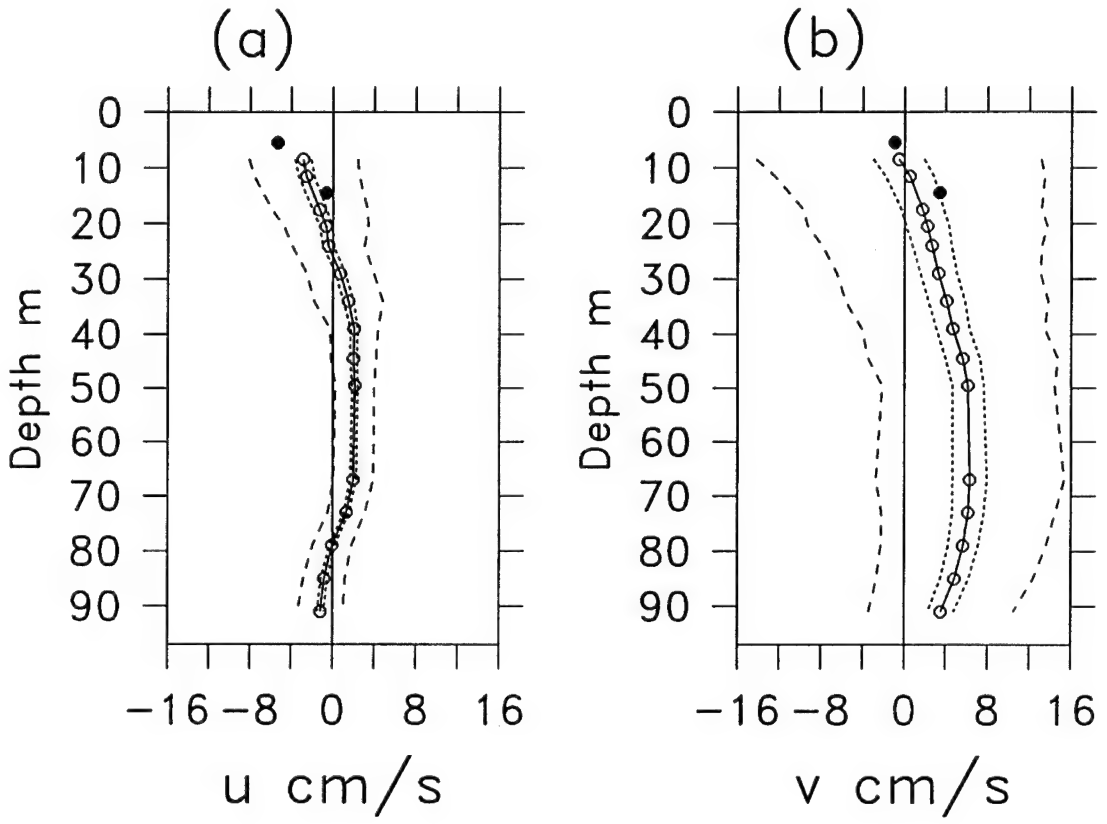

Figure 3.2. Mean cross-shelf (a) and along-shelf (b) currents (solid lines) between 0400 December 6, 1988 and 2300 February 20, 1989. Means were calculated from hourly time series which, except as indicated, cover the entire time period. Instrument depths are indicated by open circles. Velocity records which lasted the entire time period are connected; truncated velocity records at 5.5 and 14.5 m (shown with solid symbols) are unconnected. Standard deviations (dashed line) and standard errors (dotted line) of low-passed filtered fluctuations of velocity records are also indicated. Standard error estimates are calculated with an integral time scale of 40 h for low-passed cross-shelf velocity fluctuations and 60 h for low-passed along-shelf velocity fluctuations.

depth m	u mean cm/s	u standard deviation cm/s	u correlation to τ_y	lag hrs	v mean cm/s	v standard deviation cm/s	v correlation to τ_y	lag hrs
5.5^{+}	−5.35	6.59	0.50	2	−0.96	17.62	0.41	12
8.5	−2.86	5.25	0.51	1	−0.55	13.68	0.43	13
11.5	−2.55	5.09	0.53	2	0.51	12.95	0.41	15
14.5^{++}	−0.65	3.63	0.73	1	3.40	11.26	0.47	16
17.5	−1.28	4.61	0.47	4	1.73	11.43	0.42	18
20.5	−0.65	4.06	0.36	1	2.22	11.50	0.45	18
24.0	−0.43	3.47	0.26*	2	2.66	10.54	0.47	17
29.0	0.72	3.22	−0.19*	−41	3.30	9.77	0.50	18
34.0	1.51	3.30	0.23*	23	4.09	9.73	0.55	17
39.0	2.06	2.30	−0.15*	0	4.69	8.79	0.56	16
44.5	2.00	2.18	−0.31	0	5.64	9.12	0.58	15
49.5	2.13	1.87	−0.42	2	6.14	8.30	0.58	15
67.0	1.99	1.92	−0.31	−6	6.31	9.06	0.64	14
73.0	1.33	1.78	−0.37	−5	6.16	8.36	0.66	14
79.0	−0.04	1.87	−0.46	0	5.68	7.95	0.68	14
85.0	−0.80	1.99	−0.53	3	4.85	7.53	0.69	13
91.0	−1.16	2.18	−0.62	5	3.53	6.95	0.69	13
$< u, v >$	0.20	2.08	−0.17*	−40	4.01	9.00	0.58	15

Table 3.1: Statistics of mean and low-passed velocity. * insignificant at 95 % level. All record lengths 1844 hrs except $^{+}$ (811 hrs) and $^{++}$ (1238 hrs)

3.4.3 Fluctuating cross-shelf velocities

Like the vertical structure of the mean cross-shelf flow, the vertical structure of the subinertial (38 h low-pass filter described in *Limeburner* [1985]) fluctuating flow often suggests a wind-forced SBL, an along-shelf velocity forced BBL and an interior flow which tends to compensate the boundary layer flows. Offshore flow in the SBL is intermittent in strength, reflecting the nature of winter wind forcing. It is strongly sheared, especially near the bottom of the SML, though the SML appears roughly to describe the vertical extent of near-surface flow. Return flow in the interior is generally over a greater range of depths than near-surface flow, weaker in magnitude, and less vertically sheared. As with the mean interior cross-shelf velocity, there is little evidence of a break in vertical structure at the transition from the surface to subsurface mooring. Offshore flow in the SBL coupled with interior return flow is common, and is most notable on December 24, January 11, and January 24 following equatorward wind stresses of 0.2 N m^{-2} or greater. Near-bottom offshore flow is common below 75 m, presumably due to the generally poleward along-shelf interior velocity. The BML doesn't describe the vertical extent of near-bottom offshore flow as well as the SML describes the near-surface flow, though it still provides a rough guide.

The basic three layer vertical structure of cross-shelf velocity, as indicated by the SML and BML depth estimates plotted on Fig. 3.3, is also demonstrated in Table 3.1. Current meters within the top 20 m are generally within the SML and within this region cross-shelf velocities are significantly positively correlated at near zero lags to local along-shelf wind stress. Though SML depths occasionally extend to near 40 m during strong wind events, current meters between 24 and 39 m are often below the SML. Because of variability in the SML depth, correlation coefficients of cross-shelf velocity with along-shelf wind stress are not significant in this region. The SML seldom extends below 40 m, and current meters between 44 and 73 m are generally within the stratified interior region. Correlation coefficients between cross-shelf velocity and wind stress are here negative with near zero lag, though not as high

as near-surface correlation coefficients. Correlation coefficients of cross-shelf velocity with wind stress are most strongly affected by the choice of reference frame between 44 and 73 m. In this portion of the water column, correlation coefficients of cross-shelf velocity with wind stress increase from -0.3 to -0.4 in the isobath reference frame (317° T) to -0.4 to -0.5 in the principal axis reference frame (323° T). These correlations contrast with those reported for summer conditions by *Winant et al.* [1987], who found insignificant correlation of interior u with wind stress. Current meters between 79 to 91 m are often within the BML. At these depths the correlations between cross-shelf velocity and along-shelf wind stress are still negative but at a positive non-zero lag, in contrast to those near the surface and in the interior. Because near-bottom cross-shelf lags are small compared to along-shelf velocity, cross-shelf velocities here may represent a combination of the interior response (which has near zero lag) and the bottom Ekman response (which would be expected to have the same lag as the interior along-shelf velocity). The correlations of along-shelf velocity and near-bottom cross-shelf velocity with along-shelf wind stress imply their variability is dominated by wind forcing, unlike their means.

Though wind forcing is important to cross-shelf velocity, it cannot explain all cross-shelf velocity variability. Fig. 3.3 reveals that, unlike the mean cross-shelf flow, significant depth-averaged cross-shelf velocity fluctuations occur. The depth-averaged cross-shelf velocity magnitude and the lack of a simple relationship between it and local wind forcing is also indicated in Table 3.1. The depth-averaged cross-shelf velocity is uncorrelated with the local wind stress, and its standard deviation is roughly equal to that of the cross-shelf velocity below 34 m. Fluctuations in depth-averaged cross-shelf velocity are most notable in late January and in February. During this period the depth-averaged cross-shelf velocity is large relative to even near-surface velocities. In chapter 2, three-dimensional fluctuations were also found in the heat balance during this period. Because these fluctuations were uncorrelated with local wind forcing and had longer time scales than winter wind stress variability, they may be associated with unresolved mesoscale features.

The analysis of mean and low-passed cross-shelf velocities here reveals two ma-

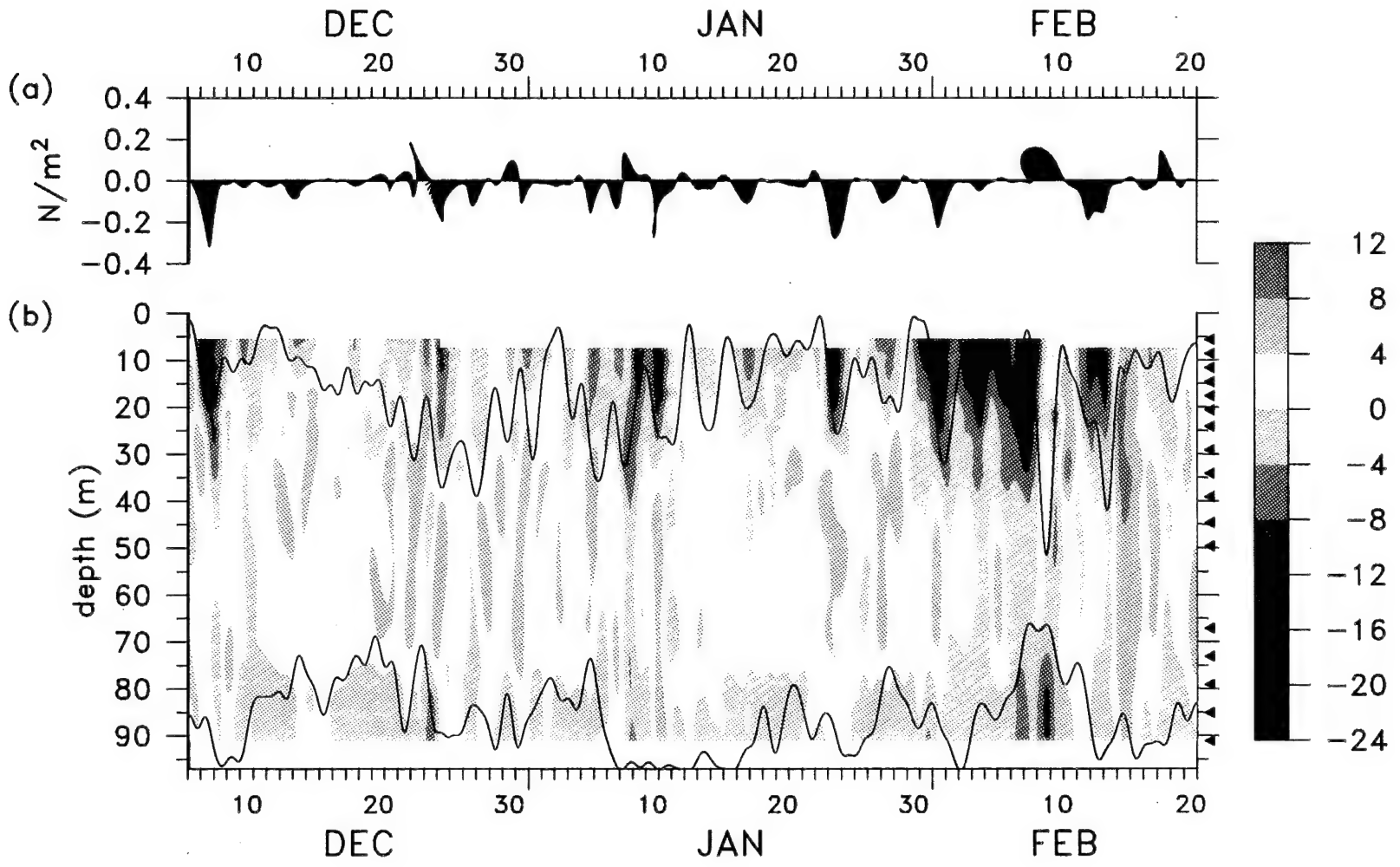

Figure 3.3. Stick vectors of low-passed wind stress at C3 (a) and contour plot of subinertial cross-shelf velocities (b). Low-passed SML and BML depths are indicated by the solid black lines superimposed on the contour plot.

jor aspects of the cross-shelf circulation observed in winter 1988–1989. The first is that the vertical structure of the cross-shelf circulation is often consistent with a wind-forced SBL, an along-shelf velocity forced BBL, and an interior return flow. The thicknesses of these three dynamic regions can be roughly estimated from temperature-defined surface and bottom mixed layers. The second major aspect of cross-shelf circulation described here is that the depth-averaged cross-shelf velocity may be as strong as the depth-dependent cross-shelf circulation. This depth-averaged flow is uncorrelated with local wind stress forcing.

3.5 Interpreting the cross-shelf circulation in terms of vertically integrated transports

3.5.1 Estimating observed cross-shelf transports

To further examine the cross-shelf circulation, I will estimate transports within the SML, interior, and BML. This approach is adopted because it simplifies interpretation of current meter records which are at fixed depths when dynamical flow regions vary in depth. Though *Lentz* [1992] provides evidence that boundary layers include a transition layer which extends beyond the mixed layer thicknesses, the SML and BML are here adopted as proxies for boundary layer depths in the absence of any clear scale for these transition layers. In any event, the inclusion of a transition layer will not prove crucial to any of the results discussed in this chapter. The concept of examining cross-shelf transport within dynamic regions has been treated before [*e.g. Badan-Dangon et al.*, 1986]; however the vertical resolution of the CODE-2, and SMILE and STRESS time series allows the use of empirical estimates of boundary and interior layer thicknesses throughout the water column rather than the indirect subsurface theoretical scales utilized by *Badan-Dangon et al.* [1986]. Both the total and the depth-dependent transports (transports relative to the depth-averaged flow) will be estimated to understand better the vertical structure of the cross-shelf flow and the importance of depth-averaged cross-shelf velocity to total cross-shelf velocity

in the SML, interior and BBL.

SML and BML thicknesses are estimated (following *Lentz* [1992] and *Lentz and Trowbridge* [1991]) from the deepest and shallowest instrument depths with a temperature difference less than 0.05°C from the measurements nearest the surface and bottom boundary. To calculate transports within the SML, interior, and BML, hourly cross-shelf velocity records are trapezoidally integrated from the surface to the SML depth, from the SML depth to the BML depth, and from the BML depth to the bottom. Similarly, the top to bottom integrated transport is calculated by trapezoidally integrating from the surface to the bottom depth. For CODE-2, the bottom depth is estimated to be 90 m. For SMILE and STRESS, the bottom depth at the STRESS subsurface mooring, 97 m, is used rather than the 93 m nominal depth of the SMILE C3 surface mooring, because of interest in near bottom transports, and for the sake of consistency with *Lentz and Trowbridge* [in preparation]. Interpolation of current meter gaps and extrapolation above and below the shallowest and deepest current meters is handled as in chapter 2. Uniform extrapolation is used above and below the shallowest and deepest current meters and linear interpolation is used to bridge any gaps in interior current meter records.

Both the CODE-2 and SMILE and STRESS velocity records resolve near-surface and interior flow, however it's possible that the reduced (relative to SMILE and STRESS) vertical resolution of the CODE-2 C3 mooring, may affect transport estimates in the BML which was most often resolved by only one current meter [*Lentz and Trowbridge*, 1991].

3.5.2 Application of a two-dimensional cross-shelf transport model

In winter, the correlation of cross-shelf velocity with the local along-shelf wind stress throughout the water column (Table 3.1) suggests we may be able to apply a wind-forced model quantitatively to interpret cross-shelf transports during this time. Aside from Table 3.1, a number of factors suggest we should be able to gain some insight

into cross-shelf circulation during winter on the northern California shelf with a simple two-dimensional conceptual model. The fluctuating heat balance (chapter 2) is also well correlated with the local wind stress and is often nearly two-dimensional. Though the top to bottom integrated cross-shelf transport is occasionally very large, it is uncorrelated with the local wind stress, suggesting wind-forced dynamics do not directly govern it, and there is a tendency for subsurface transport to balance wind forced surface transport, so that it's useful to test this balance quantitatively. Finally, despite the successful application of remotely forced coastal-trapped waves (CTW) theory to along-shelf flow on the northern California shelf [*e.g. Chapman*, 1987], there is also evidence to suggest local wind forcing, which may not be adequately represented by the lower modes typically calculated with CTW, is very important, especially nearer to shore [*Lopez and Clarke*, 1989].

There is reason to believe a two-dimensional model will be less applicable in summer CODE-2 observations. Though *Lentz* [1992] established cross-shelf transport within the SML is both well correlated to, and similar in magnitude to, wind stress derived estimates of surface Ekman transport in summer, and the correlation of along-shelf wind stress with cross-shelf velocities on the northern California shelf during the summer of 1982 [*Winant et al.*, 1987] suggests wind forcing is important in the SBL and BBL, previous results of applying a two-dimensional numerical model to interior cross-shelf velocities in summer are mixed (see *Chen and Wang* [1990] and *Zamudio and López* [1994]). Though there is reason to expect the transport model to fail in summer, a comparison to its relative success in winter may highlight which aspects of cross-shelf circulation can be understood in terms of a simple wind-forced model and what forcing conditions must be present for a two-dimensional model to have applicability.

The analytic two-dimensional model adopted to test the dynamics of wind forced cross-shelf circulation follows directly from the transport models developed in *Csanady* [1982] and, except for the parameterization of bottom friction, is a transport analog of the velocity model examined by *Janowitz and Pietrafesa* [1980]. The model development given here is very similar to that in *Janowitz and Pietrafesa* [1980] but

is included in the interest of completeness. Despite the model's simplicity, it can simulate the response of distinct surface boundary, interior, and bottom boundary layers to surface wind forcing and an along-shelf pressure gradient. Here it is applied and checked quantitatively with observed cross-shelf transport estimates. The model includes a large number of simplifying assumptions, the most important of which is two-dimensional volume conservation. Other assumptions include: a rigid lid, an implicit three layer structure of flow (distinct and separate boundary layers), no dynamical role for density gradients, linear dynamics including linear bottom friction, and boundary layers which are at steady state with surface and bottom stresses. The vertically integrated along-shelf momentum equation under these assumptions is:

$$\frac{\partial V}{\partial t} + fU = -gh\zeta_y + \frac{\tau_s^y}{\rho} - \frac{\tau_b^y}{\rho} \tag{3.1}$$

where U and V are the vertically integrated cross-shelf and along-shelf transports respectively, f is the Coriolis parameter, $gh\zeta_y$ is the shallow water along-shelf pressure gradient assuming no density contribution, τ_s^y is the along-shelf component of wind stress, and τ_b^y is the along-shelf component of bottom stress, and ρ is a constant density set equal to 1026 kg m^{-3}.

The coastal boundary condition of $U = 0$ and the vertically integrated two dimensional continuity equation imply

$$U = 0 \tag{3.2}$$

for all x. To solve (3.1), U is decomposed into surface, interior, and bottom boundary components, *i.e.*,

$$0 = U = U_{SE} + U_I + U_{BE} \tag{3.3}$$

where, for time scales long compared to f, the cross-shelf surface Ekman solution is $U_{SE} = \tau_s^y/\rho f$ and the cross-shelf bottom Ekman solution is $U_{BE} = -\tau_b^y/\rho f$. U_{SE} is estimated from measured wind velocity using the *Large and Pond* [1981] neutral stability bulk formula. U_{BE} is estimated from a linear drag law using modelled interior

velocities. The exact form of the linear drag law is not crucial; but because the BASS bottom stress estimate directions are approximately 45° from the interior flow direction, the choice is here made to estimate τ_b by solving the equations for a bottom Ekman layer rather than using the common linear drag law which assumes bottom stress is in the direction of interior velocity. The bottom Ekman layer equations with a constant eddy viscosity A, and boundary conditions far from the bottom given by interior velocity components u_I and v_I leads to (see *e.g. Pedlosky*, [1979]):

$$\tau_b^y = \frac{\rho A}{\delta}(u_I + v_I) = \frac{\rho \delta f}{2}(u_I + v_I) \tag{3.4}$$

where $\delta = (2A/f)^{0.5}$ is the bottom Ekman layer thickness. Assuming interior velocities are constant with respect to depth, $u_I = U_I/h$ and $v_I = V_I/h$, where h is the total water depth, the bottom Ekman transport is:

$$U_{BE} = -\frac{\tau_b^y}{\rho f} = -\frac{\delta}{2h}(U_I + V_I) \tag{3.5}$$

This formulation of bottom Ekman transport is consistent with the tensor formulation [*Jenter and Madsen*, 1989] of bottom stress for a constant eddy viscosity model. It differs from the common linear drag law which would lead to $\tau_b^y = rV_I/h$ but because $V_I \gg U_I$, the choice of the tensor or traditional linear drag law has little effect on τ_b^y.

Assuming an inviscid interior, the interior transports are governed by:

$$\frac{\partial V_I}{\partial t} + fU_I = -gh\zeta_y \tag{3.6}$$

Together (3.3), (3.5), and (3.6) form a set of coupled first order linear ordinary differential equations in time for U_I, U_{BE}, and V_I. Eqs. (3.5) and (3.6) contain two unknown variables; ζ_y, and δ. No systematic attempt was made to choose these variables in a best fit sense, rather physically reasonable values were chosen *a priori* and rationalized in terms of what is known about them.

A mean ζ_y is chosen as a mechanism to account for the tendency for poleward along-shelf flow in the absence of a strong equatorward wind stress. Based on observed

mean along-shelf flows, this value is set at -5×10^{-8} in winter and -1.2×10^{-7} in summer. These values agree in magnitude with the along-shelf gradients found for the northern California shelf by *Hickey and Pola* [1983], though the winter ζ_y must be of the opposite sign in order to account for the observed mean poleward flow. The mean along-shelf pressure gradient affects only the mean transports, all variability in the model is locally wind forced with no fluctuating pressure gradient. It would be possible to include fluctuating pressure gradients resulting from coastal-trapped waves as *Zamudio and López* [1994] do, however, they found the cross-shelf velocity response to pressure gradients resulting from coastal-trapped waves was secondary to that of local wind forcing for the primitive equation model they used, and the emphasis here is on identifying and interpreting the response of cross-shelf flow to local wind forcing.

The parameter δ sets the strength of the linear bottom friction. It is chosen to be 6 m based on the BASS estimates of bottom shear velocity taken during the STRESS and CODE-2 field programs. This friction parameter corresponds to a linear drag coefficient of about 3×10^{-4}m s^{-1} or a quadratic drag coefficient of about 3×10^{-3} and yields bottom shear velocities of 0.5–1.0 cm s^{-1}, in agreement with typical BASS sensor estimates of bottom shear velocity in the STRESS experiment [*Gross et al.*, 1992] as well as in the earlier CODE experiment [*Grant et al.*, 1984].

Given ζ_y and δ, (3.3), (3.5), and (3.6) a solution can be easily found by using (3.5) to solve for U_I in (3.3);

$$U_I = \frac{-U_{SE} + \epsilon V_I}{1 - \epsilon} \tag{3.7}$$

where $\epsilon = \delta/2h$. Equation (3.7) in turn can be substituted into (3.6) to give a first order differential equation in terms of V_I:

$$\frac{\partial V_I}{\partial t} + \beta V_I = \frac{\beta U_{SE}}{\epsilon} - gh\zeta_y = F(t) \tag{3.8}$$

where β is $\epsilon f/(1-\epsilon)$. The solution to (3.8) is:

$$V_I = e^{-\beta t}\left[\int_0^t e^{\beta t'} F(t')dt' + C\right] \tag{3.9}$$

The constant of integration, C, is given by the interior transport specified at $t = 0$.

As a simple example of the behavior of (3.9), assume $\zeta_y = 0$, τ_s^y = constant, and $V_I = 0$ at $t = 0$. Then the solution to (3.9) is:

$$V_I = \frac{1}{\epsilon} U_{SE}(1 - e^{-\beta t}) \tag{3.10}$$

with U_I and U_{BE} given by (3.7) and (3.3) for this set of forcing conditions as:

$$U_I = -U_{SE}\frac{e^{-\beta t}}{1-\epsilon} \tag{3.11}$$

and

$$U_{BE} = U_{SE}\left(\frac{e^{-\beta t}}{1-\epsilon} - 1\right) \tag{3.12}$$

The factor β gives the frictional time scale of the model. For $\delta = 6$ m, $1/\beta$ is about 4 days. The cross-shelf transport below the SBL for times short compared to β is primarily in the interior rather than BBL. For times longer than β, U_{BE} becomes larger than U_I and at steady state, the subsurface cross-shelf transport is entirely in the BBL.

The frictional time scale $1/\beta$ suggests seasonal differences in wind stress on the northern California shelf could cause seasonal differences in the model response to wind forcing. In winter, the dominant time scales of wind forcing are set by the passage of low pressure systems through the region and are generally three days or less; hence the subsurface winter model response is primarily in the interior. In summer, persistent upwelling favorable winds lasting several weeks are common and would lead to a subsurface model response primarily in the BBL. This seasonal difference is indicated by spectra of along-shelf wind stress (Fig. 3.4) which show variability at frequencies lower than β is greater in the summer of 1982 than in the winter of 1988–1989.

In practice, all variability in the model was forced with the 38 h low-passed τ_s^y. Equation (3.9) is integrated numerically from time $t = 0$ to get V_I. U_I and U_{BE} are then determined from (3.3) and (3.7). Beyond the frictional time scale (4 days) the

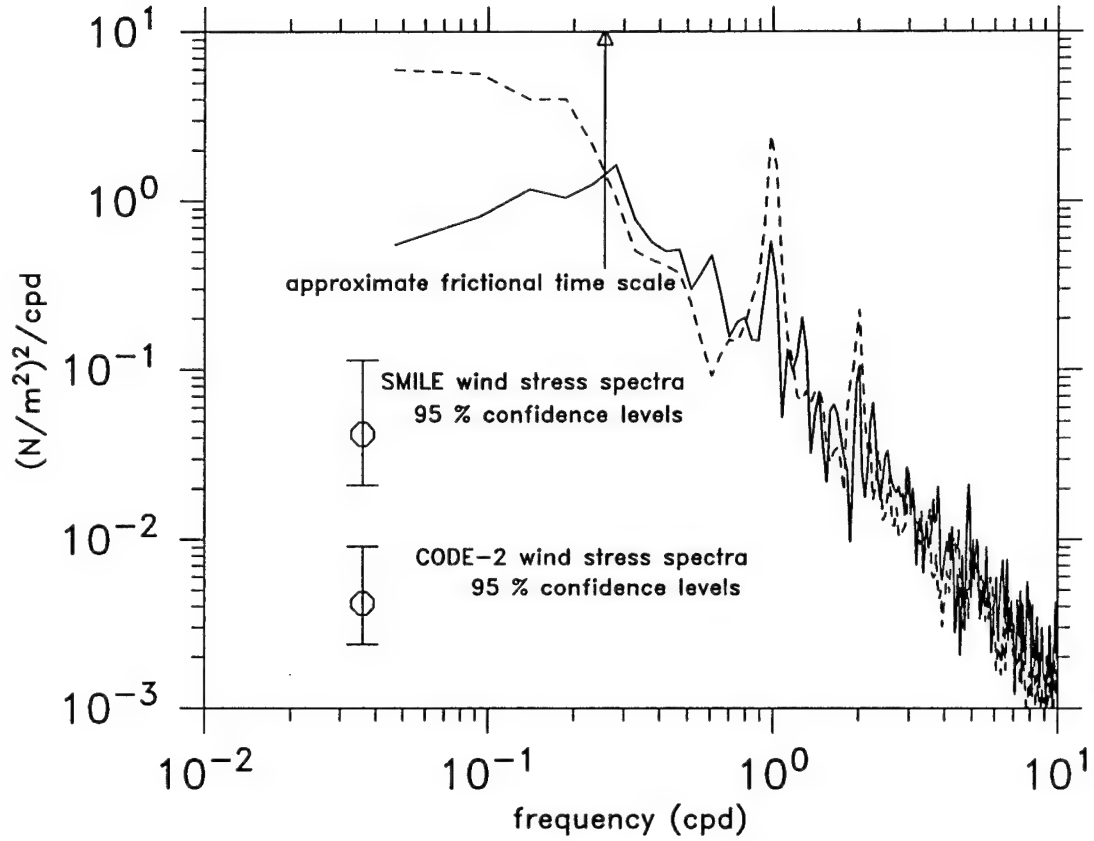

Figure 3.4. Along-shelf wind stress spectra. SMILE (solid) and CODE-2 (dashed) spectra show similar variability for periods between 1 and 4 days. The CODE-2 wind spectrum is affected by persistent upwelling favorable winds which last up to three weeks and shorter relaxation events which can last a week or more; hence it shows more variability for periods longer than 4 days than SMILE.

model is insensitive to the initial condition; here the initial condition was chosen as the observed V at $t = 0$. For comparison with the observed transports, the surface model transports are calculated from U_{SE} plus that portion of U_I within an observed SML. The interior transport is assumed to be uniform with depth so that the total surface transport from the model is:

$$U_S = U_{SE} + \frac{\delta_{SM} U_I}{h} \tag{3.13}$$

where δ_{SM} is the SML depth and h is the total depth. The modelled U_I and U_B are similarly represented as:

$$U_I' = U_I \left(1 - \frac{\delta_{SM} + \delta_{BM}}{h}\right) \tag{3.14}$$

and

$$U_B = U_{BE} + \frac{\delta_{BM} U_I}{h} \tag{3.15}$$

The total along-shelf transport, V, was also calculated from $V = V_{SE} + V_I + V_{BE}$, where V_{SE} and V_{BE} were estimated from the the cross-shelf component of wind stress and the appropriate analog of (3.5) respectively.

3.5.3 Comparison of observed and modelled cross-shelf transports for winter 1988–1989

Modelled cross-shelf transports were compared to total (Fig. 3.5 and Table 3.2) and depth-dependent (Fig. 3.6 and Table 3.2) transports. The depth-dependent transports were calculated by subtracting the depth-averaged cross-shelf velocity from the total cross-shelf velocity. This procedure was adopted to focus the model comparison to the depth structure of the observed flow, which the model is capable of representing, rather than the depth-averaged cross-shelf flow which the model is incapable of representing. Comparisons of modelled to depth-dependent transports should be viewed with caution. If, for example, the SML transport was highly correlated with local wind forcing, but the interior and BML transport were uncorrelated with local

	mean	σ	total transport			depth-dependent transport		
	m^2/s	m^2/s	r_{max}	r_0	a	r_{max}	r_0	a
U_S:	−0.25	0.63	0.70 +2	0.70	0.87	0.85 +1	0.85	0.84
U_I:	0.33	0.51	0.20 +0	0.20	0.58	0.72 +3	0.71	0.72
U_B:	−0.09	0.26	0.43 −7	0.39	0.57	0.46−6	0.43	0.57
V:	4.39	7.40	0.63 −7	0.61	0.72			

Table 3.2: Statistics of model comparison to total and depth-dependent transports estimated from observations for December, 1988 – February, 1989. Both maximum lagged (r_{max}) and 0 lagged (r_0) correlation coefficients are presented. Positive lags (in hrs) indicate the model leads the observed transports. The slope of the regression line (a) is also indicated.

wind forcing, removal of the depth-averaged cross-shelf velocity could result in an increased correlation of interior and BML transport with wind stress. This would be accompanied by a decreased correlation coefficient of SML transport with wind stress and a decrease in the regression coefficient of depth-dependent SML transport with modelled SML transport. This is not the case in winter as the correlation of depth-dependent SML transport with the wind-forced model is actually higher, and little change in the regression coefficient occurs.

Modelled and estimated cross-shelf transports agree most closely within the SML. Both the total (Fig. 3.5) and depth-dependent (Fig. 3.6) SML transports are well correlated with regression coefficients near one (Table 3.2). Estimated SML transport was relatively insensitive to removal of the depth-averaged transport. Its most noticeable effect was an improvement in model and estimate agreement in February (Fig. 3.5 and 3.6).

Comparison of modelled and total cross-shelf transport was poorest within the interior (Fig. 3.5 and Table 3.2). Correlation between observed and modelled interior transport is reduced mostly by the strong depth-averaged cross-shelf transport in February and over the entire time series was not significant at the 95% level in the 317°T reference frame. Rotation to 323°T did improve correlation to total interior transport slightly. If attention is focussed on the time period between 0400 December 6, 1988 and 2300 January 31, 1989 when U is generally weak, then correlation

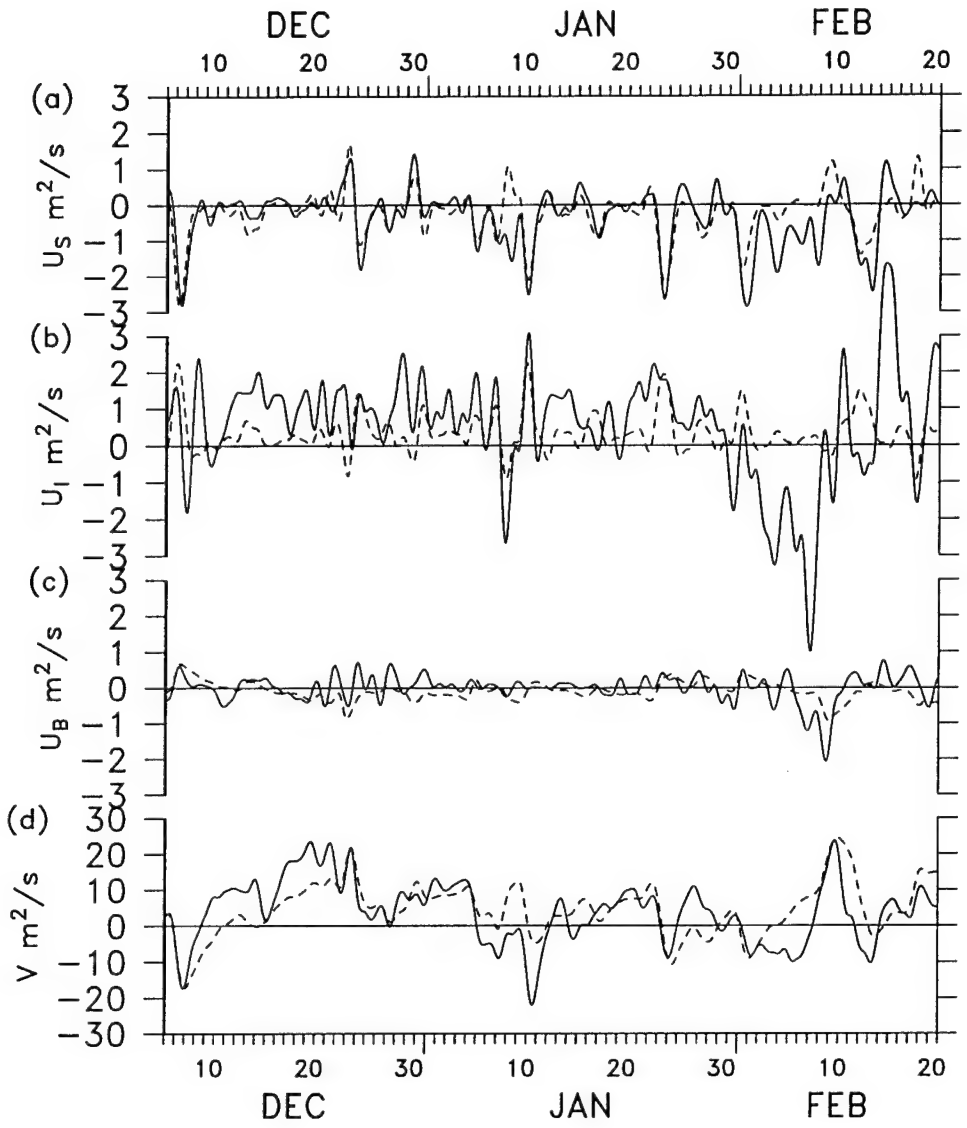

Figure 3.5. Modelled and total (including depth-averaged) estimated transports for winter 1988–1989. (a) Low-passed cross-shelf SML transport (solid) with modelled transport (dashed) in the SML. Modelled transport within the SML is given by the surface Ekman layer transport plus that portion of the modelled interior transport within the SML. (b) Low-passed cross-shelf interior transport with modelled transport in the interior. Modelled transport within the interior is given by the modelled interior transport minus that portion of the modelled interior transport within the SML and BML. (c) Low-passed cross-shelf BML transport with modelled transport in the BML. Modelled transport within the bottom boundary is given by the bottom Ekman layer transport plus that portion of the modelled interior transport within the BML. (d) Low-passed along-shelf transport and modelled along-shelf transport.

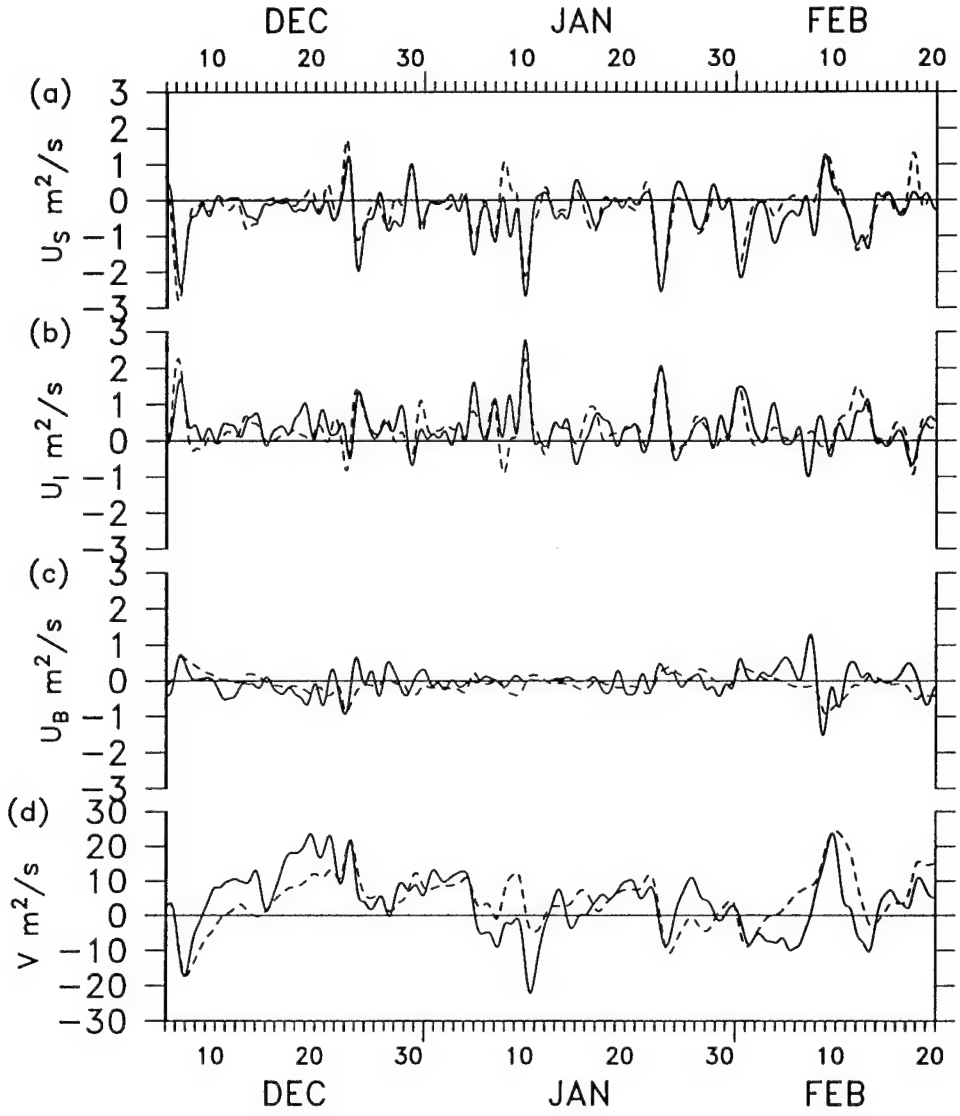

Figure 3.6. Modelled and depth-dependent estimated transports for winter 1988–1989. (a) Low-passed cross-shelf SML transport (solid) with modelled transport (dashed) in the SML. Modelled transport within the surface boundary is given by the surface Ekman layer transport plus that portion of the modelled interior transport within the SML. (b) Low-passed cross-shelf interior transport with modelled transport in the interior. Modelled transport within the interior is given by the modelled interior transport minus that portion of the modelled interior transport within the SML and BML. (c) Low-passed cross-shelf BML transport with modelled transport in the BML. Modelled transport within the bottom boundary is given by the bottom Ekman layer transport plus that portion of the modelled interior transport within the BML. (d) Low-passed along-shelf transport and modelled along-shelf transport.

coefficients between the wind forced model and total interior transport do increase, as is qualitatively indicated in Fig. 3.5. This was again particularly apparent in the 323°T reference frame. Onshore interior return flow associated with several upwelling events was most notable on December 8, January 11, and January 24.

Modelled and estimated cross-shelf transports within the BML agree fairly well. Agreement is not improved by removing the depth-averaged cross-shelf flow. Both interior and bottom Ekman flow are important to the modelled near-bottom cross-shelf transport (3.10), and even if bottom friction were modelled perfectly, the bottom Ekman transport would only be determined accurately to the extent to which the locally wind-forced transport model describes along-shelf transport.

Comparison of the modelled and estimated along-shelf transport shows a high correlation and a regression coefficient near one. Since the modelled along-shelf transport is dominated by the interior along-shelf transport, V_I, and accelerations in V_I are determined entirely by interior cross-shelf transport (3.5), the high correlation between modelled and observed along-shelf transport is taken as further evidence of the applicability of the locally forced two-dimensional model in winter. It is possible to abandon any attempt to calculate along-shelf transport and instead use the observed along-shelf transport to model the bottom Ekman transport, but agreement between the estimated and modelled bottom Ekman transport is not substantially improved, and the physical insight on the role of the interior cross-shelf transport in (3.5) is lost.

3.5.4 Comparison of observed and modelled cross-shelf transports for summer 1982

Comparison of modelled and estimated cross-shelf transports during CODE-2 (Table 3.3 and Figs. 3.7 and 3.8) shows the local wind forcing, linear dynamics and two-dimensional continuity incorporated in the model cannot account for observed cross-shelf circulation below the SML. The model response within the SML is dominated by the surface Ekman transport which is well correlated with observed SML transport [*Lentz*, 1992]. Modelled interior and bottom transports are uncorrelated with total

	mean	σ	total transport			depth-dependent transport		
	m^2/s	m^2/s	r_{max}	r_0	a	r_{max}	r_0	a
U_S:	−1.05	1.18	0.85 +3	0.84	0.73	0.87 +2	0.86	0.51
U_I:	0.84	0.76	0.35−164	−0.17	−0.50	−0.35−101	0.33	0.24
U_B:	0.21	0.91	−0.36+69	−0.07	−0.03	0.49−9	0.47	0.21
V:	−2.58	24.76	0.60−39	0.49	0.30			

Table 3.3: Statistics of model comparison to transports estimated from observations for April, 1982 – July, 1982. Both maximum lagged (r_{max}) and 0 lagged (r_0) correlation coefficients are presented. Positive lags (in hrs) indicate the model leads the observed transports. The slope of the regression line (a) is also indicated.

observed interior and bottom transports, and the modelled interior variability is much less than that of the total observed interior transport (Fig. 3.7). Observed variability in the interior transport is due largely to depth-averaged cross-shelf flow variability which, as indicated by its standard deviation (3.44 cm s^{-1}), is greater than that observed in winter (Table 3.1). Even when the model is compared to the depth-dependent transport (Fig. 3.8), correlation coefficients between observed and modelled transports below the SML remain lower than in winter. Moreover, the regression coefficient between the observed and modelled SML transport is reduced. The most noticeable improvement in agreement between modelled transports and estimated depth-dependent transports occurs in the BML which follows the predicted model behavior for long time scales. Much of the disagreement between the modelled BML transport and observed depth-dependent BML transport is explained by the imperfect ability of the model to predict interior along-shelf transport. When the observed rather than modelled along-shelf transport is used to force the bottom Ekman layer transport, the modelled and observed depth-dependent bottom transports agree much more closely. For this case the zero lag correlation is 0.75 with a regression coefficient of 0.64 compared to a correlation of 0.47 and regression coefficient of 0.21 in Table 3.3.

Some of the inability of the transport model to explain subsurface cross-shelf circulation in summer may be accounted for by inclusion of variable along-shelf pressure gradients in (3.6). Such gradients may be caused by remote (CTW) processes

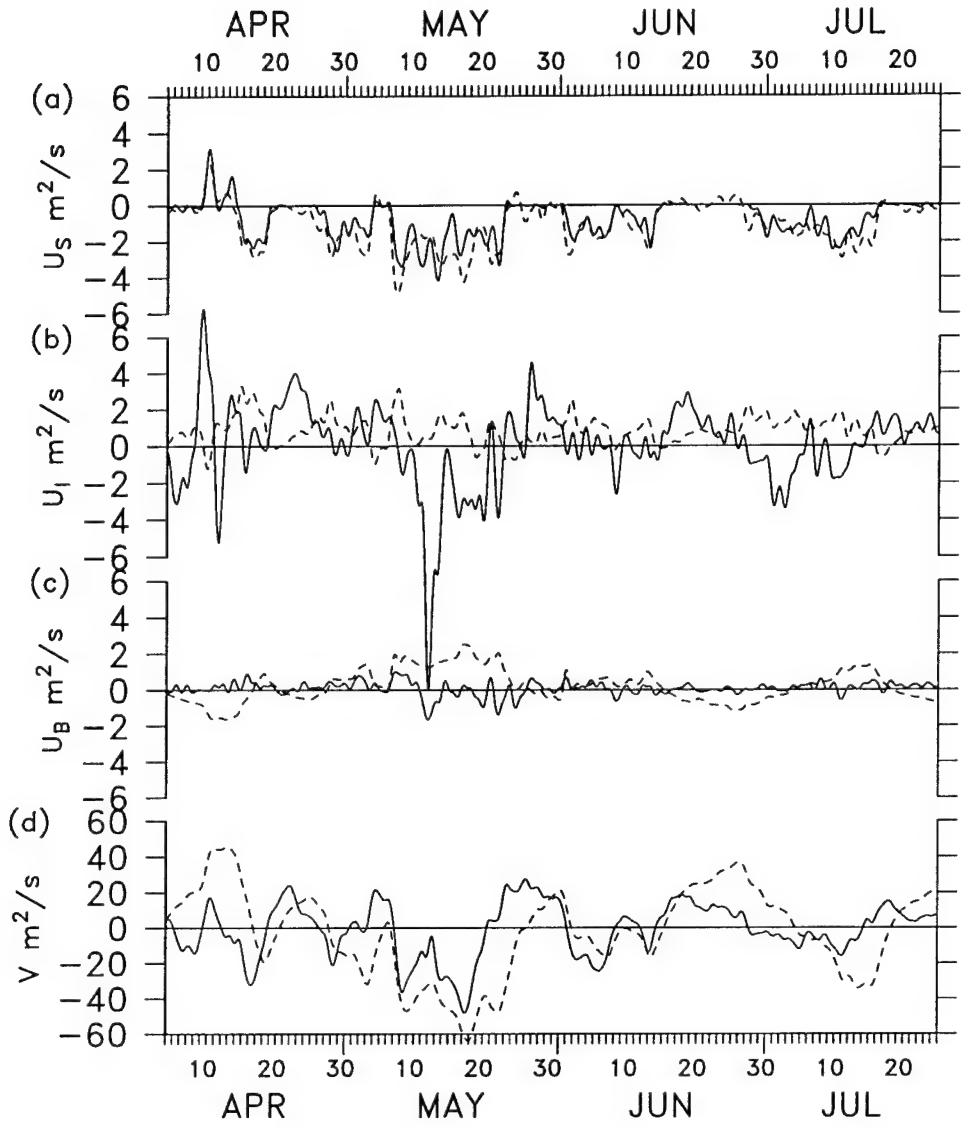

Figure 3.7. Modelled and total (including depth-averaged) estimated transports for summer 1982. Note the y-axis scales have been expanded by a factor of 2 relative to Fig. 3.5 and 3.6. (a) Low-passed cross-shelf SML transport (solid) with modelled transport (dashed) in the SML. Modelled transport within the SML is given by the surface Ekman layer transport plus that portion of the modelled interior transport within the SML. (b) Low-passed cross-shelf interior transport with modelled transport in the interior. Modelled transport within the interior is given by the modelled interior transport minus that portion of the modelled interior transport within the SML and BML. (c) Low-passed cross-shelf BML transport with modelled transport in the BML. Modelled transport within the bottom boundary is given by the bottom Ekman layer transport plus that portion of the modelled interior transport within the BML. (d) Low-passed along-shelf transport and modelled along-shelf transport.

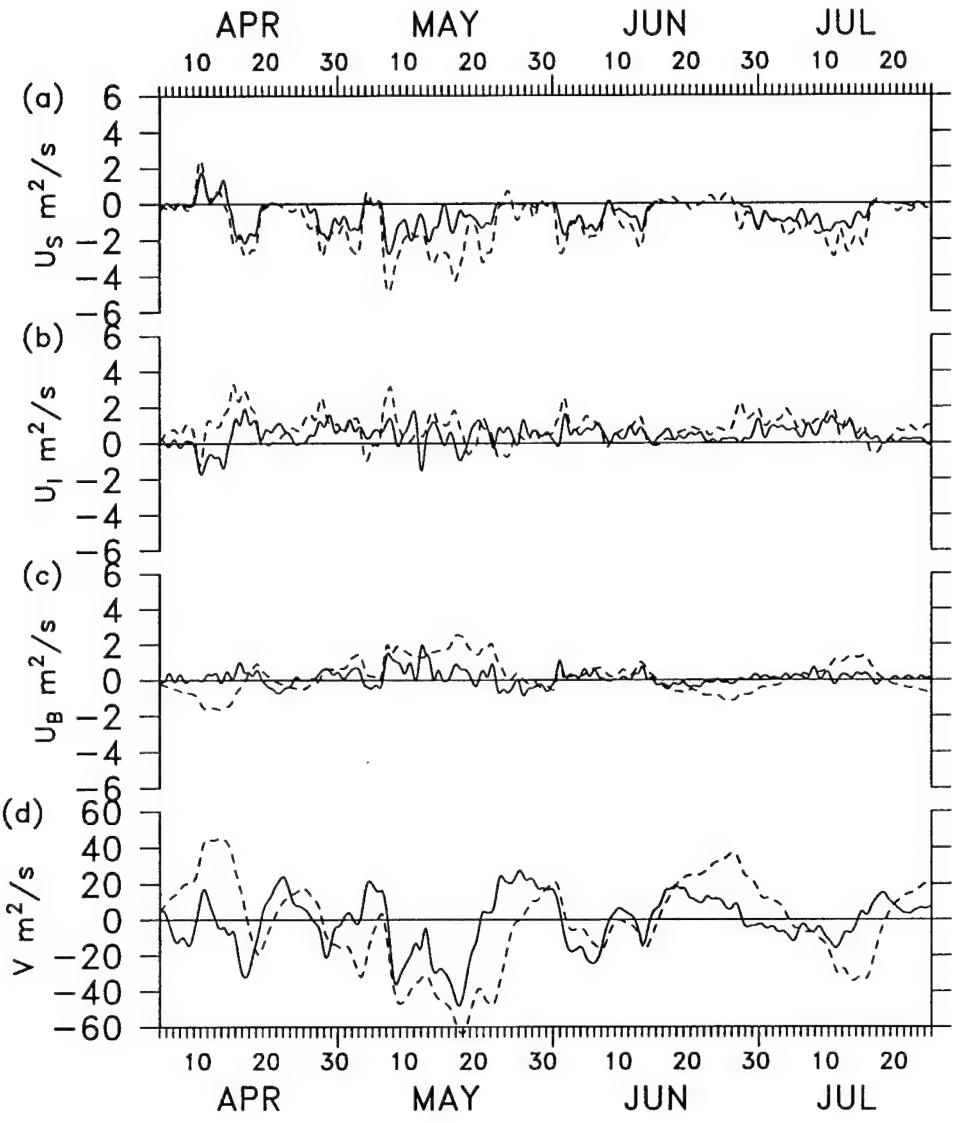

Figure 3.8. Modelled and depth-dependent estimated transports for summer 1982. Note the y-axis scales have been expanded by a factor of 2 relative to Fig. 3.5 and 3.6. (a) Low-passed cross-shelf SML transport (solid) with modelled transport (dashed) in the SML. Modelled transport within the surface boundary is given by the surface Ekman layer transport plus that portion of the modelled interior transport within the SML. (b) Low-passed cross-shelf interior transport with modelled transport in the interior. Modelled transport within the interior is given by the modelled interior transport minus that portion of the modelled interior transport within the SML and BML. (c) Low-passed cross-shelf BML transport with modelled transport in the BML. Modelled transport within the bottom boundary is given by the bottom Ekman layer transport plus that portion of the modelled interior transport within the BML. (d) Low-passed along-shelf transport and modelled along-shelf transport.

[*Lopez and Clarke*, 1989] or associated with local wind relaxation events [*Brown et al.*, 1987]. Addition of along-shelf pressure gradients estimated from observations to (3.6) slightly improves model agreement with depth-dependent quantities, but does nothing to improve agreement with total observed subsurface transport. Baroclinic pressure gradients could also affect subsurface cross-shelf transport, however the relative lack of success of a model incorporating both CTW calculated pressure gradients and baroclinic pressure gradients [*Zamudio and López*, 1994] and the large variability in depth-averaged cross-shelf transport suggest the importance of three-dimensional processes.

It is uncertain why three-dimensional processes may have greater importance in summer. Three possible reasons include offshore mesoscale variability, a non-linear response to persistent wind forcing, and a complicated ocean response to wind relaxation events. In 1987, *Kosro et al.* [1991] found mesoscale variability in a region extending from 60 to 150 km off the northern California coast to be greater in 2 cruises which occurred after the transition to strong upwelling than during 2 similar cruises in winter. Some of this variability may affect shelf circulation. *Lentz* [1987*a*] described a shallow lens of warm water which extended from over 35 km offshore onto the shelf during CODE-2. This affected strongly shelf circulation from June 27 through July 7, 1982, a period which included wind-driven offshore flow in the SML (see Figs. 3.7 and 3.8). In addition to offshore variability, it's also likely the local response to strong persistent wind forcing causes a breakdown in two-dimensional models of wind-driven circulation. In a numerical model, *Chen* [1990] found nonlinear and vertical shear stress terms in the interior along-shelf momentum balance became larger after 5 days of steady wind forcing. In a three-dimensional model, nonlinear terms in particular may induce instability and lead to a breakdown in any two-dimensional response to wind forcing. Finally, the ocean response to wind relaxation events on the northern California shelf is quite complicated. *Send et al.* [1987] found onshore flow associated with wind relaxation events occurs over the outer shelf as turbulent motions with scales less than 25 km rather than as onshore displacement of an upwelling front. However, even if wind relaxation events are excluded, the

transport model still performs poorly below the SML in summer.

3.6 Summary

Velocity time series have been used to study the mean and subinertial cross-shelf circulation on the northern California shelf under winter and summer (upwelling) conditions. The focus of this study has been to examine quantitatively the applicability of classical ideas of wind forced cross-shelf circulation to the relatively weak episodic upwelling and downwelling observed in winter and the strong upwelling observed in summer on the northern California shelf. Throughout this study an along-shelf direction of 317°T based on historical estimates of the local isobath direction has been adopted. Comparison to a reference frame defined by the principal axis of the low-passed depth-averaged velocity shows most results are not qualitatively sensitive to small changes in cross-shelf axis definition, though some small improvement in agreement to two-dimensional theory is noted in the principal axis frame.

This study is motivated largely by cross-shelf circulation observed in winter on the northern California shelf from December, 1988 to February, 1989. The circulation during this time suggested the importance of local wind forcing. Mean cross-shelf velocities observed in winter are consistent with the weak (relative to summer on the northern California shelf) mean equatorward wind stress and poleward mean interior along-shelf velocity. Near-surface cross-shelf velocities are offshore, though weaker than observed in summer, and near-bottom velocities are also offshore. The mean interior velocity is onshore and balances the offshore boundary layer transports to within our ability to define a cross-shelf direction. A mean two-dimensional mass balance can therefore be said to hold over the northern California shelf during winter in contrast to earlier CODE measurements which indicate a mean offshore flow in the the summer of 1982.

As in summer, fluctuations in the low-passed cross-shelf velocity in winter are much larger than the mean. They retain a vertical structure consistent with a wind-forced SBL, BBL, and interior region. The SML and BML, as defined by temperature,

provide reasonable estimates of the SBL and BBL thicknesses in terms of momentum. Correlation coefficients between cross-shelf velocity and along-shelf wind stress demonstrate the importance of wind forcing throughout the water column in winter. Near-surface correlations are approximately the same as those observed in summer on the northern California shelf. Interior negative correlation coefficients, though not as large as those observed near the surface, are still significant in contrast to the correlations of interior cross-shelf velocity with wind stress observed on the northern California shelf in summer. Near-bottom correlation coefficients are larger in magnitude than interior coefficients, as is also the case in summer on the northern California shelf.

Though the vertical structure of the cross-shelf velocity in winter often agrees qualitatively with the two-dimensional conceptual model, the fluctuating conservation of mass is not two-dimensional. Variability in the depth-averaged cross-shelf velocity is especially evident during the last third of the winter study period, in February. The vertically integrated cross-shelf transport during this time is often larger in magnitude than the SBL transport. It is uncorrelated with local wind forcing and has longer time scales than winter wind stress variability. In chapter 2, the heat balance is also found to be three-dimensional during this time and was possibly a result of unresolved mesoscale features.

Because both the mean and fluctuating winter cross-shelf circulation suggested the importance of local wind forcing, a simple linear two-dimensional model of wind-forced cross-shelf transport was compared quantitatively to estimates of transport within the SML, interior, and BML. Modelled transports were compared to both winter and summer observations to examine its applicability under different wind forcing conditions. Model assumptions included two-dimensionality, linear dynamics, and purely barotropic pressure gradients.

Despite these strict assumptions, the model was capable of simulating much of the cross-shelf transport in winter. The modelled SML transport was dominated by the surface Ekman transport and highly correlated with observed SML transport. Below the SML, the model showed some skill in predicting interior and bottom cross-shelf

transports during the first two-thirds of the winter study period and did surprisingly well in describing the depth-dependent cross-shelf transport over the entire time period. For the dominant time scales of wind forcing in winter, the model predicted, and the data seemed to indicate, a subsurface response to wind forcing confined primarily to the interior.

In comparison to winter, the wind-forced model did not work well in summer. Though modelled and estimated SML transports agreed well, modelled and estimated interior and BML transports did not. Some of the model's failure can be explained by its neglect of nonlinear processes, baroclinic pressure gradients, and remote forcing, however most can probably be attributed to its assumption of two-dimensionality.

Though the simple transport model seems to describe the wind forced cross-shelf velocity in winter fairly well, it is limited in both the physical processes and the dynamics it considers. Wind is only one mechanism of forcing cross-shelf velocity. Numerous other mechanisms which can influence cross-shelf velocity probably include: mesoscale eddies, upwelling fronts, topography, and small-scale wind stress. Dynamical processes that may be important include: non-linear dynamics, interior shear stress, and baroclinic pressure gradients. All of these processes may act to make the cross-shelf flow three-dimensional. The success of the two-dimensional transport model in winter relative to summer suggests some of these processes become more important under the steadier wind forcing conditions prevalent on the northern California shelf in summer. A careful numerical modelling effort may be able to determine the circumstances under which quasi-two dimensional dynamics apply to cross-shelf velocity and study the question of seasonal variability in cross-shelf dynamics on wind-forced shelves.

Chapter 4

Subtidal Velocity Correlation Scales on the Northern California Shelf

4.1 Abstract

Along and cross-shelf correlation scales of subtidal cross-shelf (u) and along-shelf (v) velocities are estimated using moored velocity time series from several field programs over the northern California shelf. These field programs acquired time series with 4–6 month record lengths. Over these record lengths, along-shelf correlation scales of v are greater than maximum mooring separations (60 km). In the cross-shelf direction, v is generally correlated between the 60 and 130 m isobaths (10–15 km separation). Along-shelf correlation scales of u are much smaller than those of v and are often not resolved by minimum mooring separations. Time series between November, 1988 and May, 1989 do resolve along-shelf correlation scales of near-surface u and indicate they are 15–20 km. During this time, the along-shelf correlation scale of near-surface u shows variability on a monthly scale. It is generally long (30 km or more) when correlation of u with wind stress is high, and short (15 km or less) when correlation with wind stress is low. On at least one occasion, short along-shelf correlation scales

coincide with the intrusion of an offshore mesoscale feature onto the shelf. Cross-shelf correlation scales of u are marginally resolved for typical mooring separations. In general, u is correlated between the 90 and 130 m isobaths (7–13 km separation) and between the 60 and 90 m isobaths (~5 km).

4.2 Introduction

There exists a considerable body of theory concerning the dynamics which govern subtidal velocity on wind-driven (upwelling) continental shelves [*Allen*, 1980]. It includes surface and bottom boundary layer theory [*Brink*, 1983; *Lentz*, 1992; *Trowbridge and Lentz*, 1991], two-dimensional upwelling models [*Csanady*, 1982; *Janowitz and Pietrafesa*, 1980; *Mitchum and Clarke*, 1986], and coastal-trapped waves theory [*Chapman*, 1987; *Brink*, 1991]. On wind-forced shelves, topography generally changes more rapidly in the cross-shelf than along-shelf direction and along-shelf wind forcing scales are generally on the order of 100 km or more. As a consequence, wind-forced theories often assume the subtidal circulation is two-dimensional or at most slowly varying in the along-shelf direction.

Estimates of along-shelf velocity correlation length scales derived from measured time series generally agree with the theoretical assumption that along-shelf scales are much greater than cross-shelf scales. *Kundu and Allen* [1976] found interior subtidal along-shelf velocity was correlated over along-shelf distances of 80 to 200 km (the maximum along-shelf mooring separation) and cross-shelf distances of 30 km on the Oregon shelf. Similarly, *Winant et al.* [1987] used Coastal Ocean Dynamics Experiment (CODE-2) time series to show depth-averaged subtidal along-shelf velocity is correlated over distances of 60 km in the along-shelf direction and 15 km in the cross-shelf direction on the northern California shelf. The lowest mode empirical orthogonal function of the same data accounts for 70% of the variability. It is highly correlated with local wind stress, and its simple spatial structure indicates much of the subtidal along-shelf velocity varies nearly in phase over the entire CODE region.

The above analyses suggest along-shelf velocity correlation scales may be quite

long when wind stress forcing is dominant. This does not preclude shorter correlation scales for subtidal along-shelf velocity when wind stress forcing is less important. For example, [*Winant*, 1983] found relatively short correlation scales (~25 km) in summer over the southern California shelf, when wind forcing was uncorrelated to along-shelf velocity.

Though both observational and theoretical estimates of along-shelf correlation scales are in the 100–200 km range [*Kundu and Allen*, 1976; *Brink et al.*, 1994] for along-shelf velocity, along-shelf scales of subtidal cross-shelf velocity are not only shorter than those predicted by wind-forced theory, but have usually been under resolved by moored measurements [*e.g*, *Kundu and Allen*, 1976; *Winant et al.*, 1987; *Winant*, 1983]. *Brink et al.* [1994] attempted to reconcile linear wind-forced theory with short cross-shelf velocity scales by investigating the influence of estimated short-scale wind variability on subtidal cross-shelf velocity. They concluded that short-scale wind stress reduced the correlation scale of modelled cross-shelf velocity but could not account for the observed energy levels.

A major difficulty in comparing theoretical and observed spatial scales of cross-shelf velocity has been our inability to resolve the spatial scales of subtidal cross-shelf velocity. Estimates of horizontal correlation scales of cross-shelf as well as along-shelf velocity should provide insight into the processes contributing to cross-shelf velocities and how observed velocities may differ from simple wind-forced theory. Additionally, a better understanding of the spatial scales over which point measurements apply to cross-shelf velocities on wind-driven shelves should be useful to interpretation of existing measurements and to future experiment design in these locations.

The first objective of this study is to use velocity time series from several extensive field programs over the northern California shelf to estimate spatial scales of both along-shelf and cross-shelf subtidal velocity. The spatial scales will be defined here in terms of correlation length scales, the length over which subtidal velocity fluctuations are correlated at some significance level. Correlation length scales will first be estimated from velocity time series lasting several months and encompassing all seasons. A second objective is to gain insight into the processes which affect cross-shelf veloc-

ity correlation length scales. To accomplish this, measurements from November, 1988 through May, 1989 will be examined on a monthly basis in light of wind forcing and other descriptions of circulation on the northern California shelf during this time.

The remainder of this chapter is broken into four sections. In section 4.3, I give a brief overview of the general geography, meteorology, and oceanography of the northern California shelf and an introduction to the field programs used in later sections. In section 4.4, I list the procedures used to estimate correlation scales and give results for the various experiments. The correlation scales for November, 1988 through May, 1989 are further examined in section 4.5 with a particular view to identifying the processes which affect correlation scales of cross-shelf velocity on a monthly basis. In section 4.6, I compare the correlation scales found in section 4.4 and 4.5 with those expected from wind-forced theory and summarize results in section 4.7.

4.3 Background and observations

4.3.1 Background

The northern California shelf is noted for its strong wind forcing, relatively straight narrow shelf, and seasonal upwelling [*Beardsley and Lentz*, 1987]. In these respects, it is perhaps an archetype of wind-forced circulation present along much of the United States Pacific coast and elsewhere. The section of the northern California coast examined in this study extends from Pt. Reyes in the south to Pt. Arena in the north (Figs. 4.1 and 4.2), a distance of approximately 100 km. Over this distance, the coastline orientation remains approximately due northwest (315° T). The shelf break, located beyond the 130 m isobath, varies between 25 km offshore (in the south) to only 15 km offshore (in the north).

Wind stress along the northern California shelf is strongly polarized in the along-shelf direction. Though the change in coastline orientation at Pt. Arena affects the cross-shelf component of wind stress and causes a wind stress curl [*Winant et al.*,

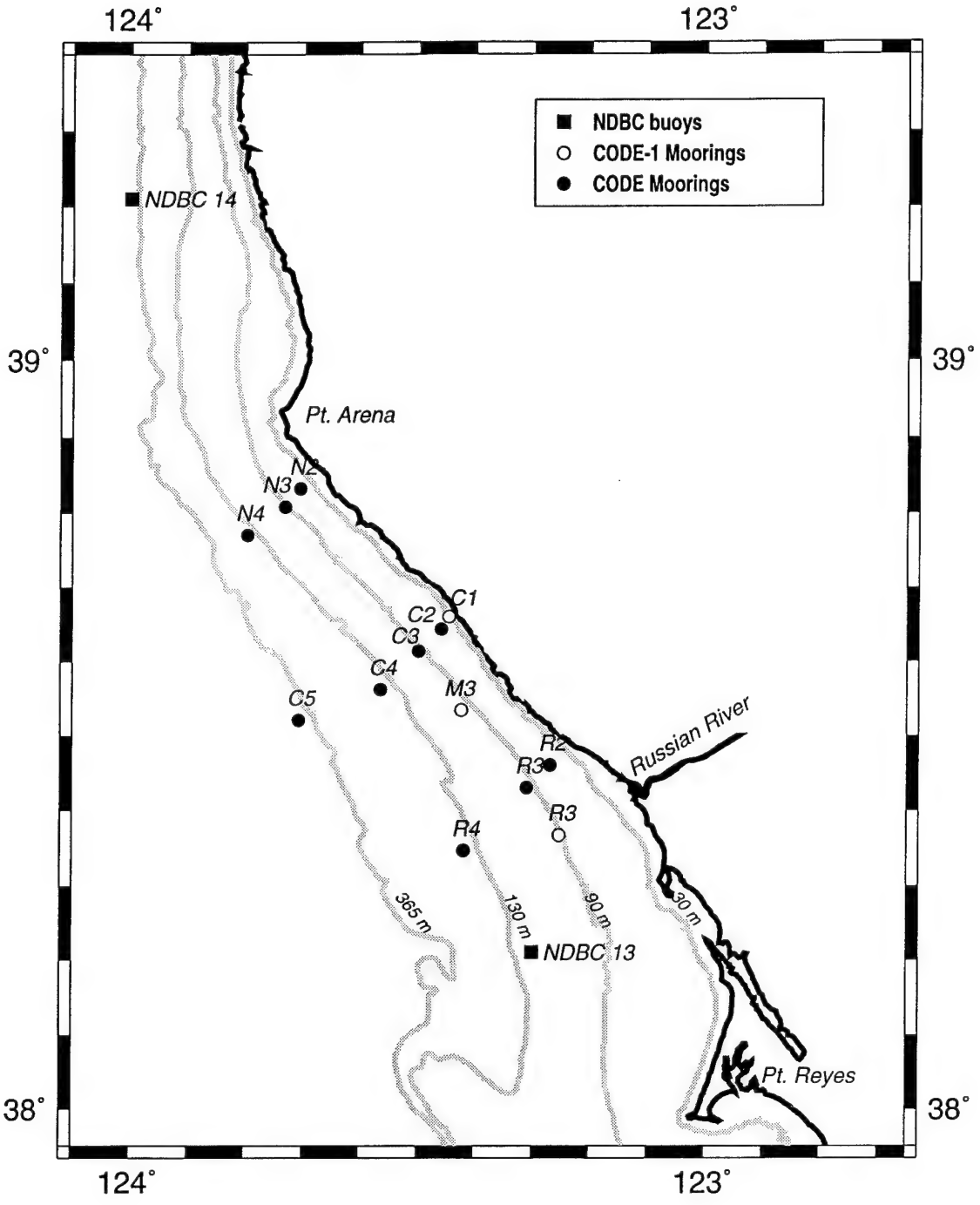

Figure 4.1. Map of northern California shelf showing nominal CODE and NDBC meteorological buoy (solid square) mooring locations. Exact locations varied slightly from deployment to deployment and most locations included nearby surface and subsurface components. Solid circles denote locations occupied during CODE-2 and open circles denote locations occupied during CODE-1. The central C-line (with the exception of C1) was present during both CODE-1 and CODE-2. The southerly R3 location was occupied during CODE-1 and fall and winter CODE deployments but was later moved north during CODE-2.

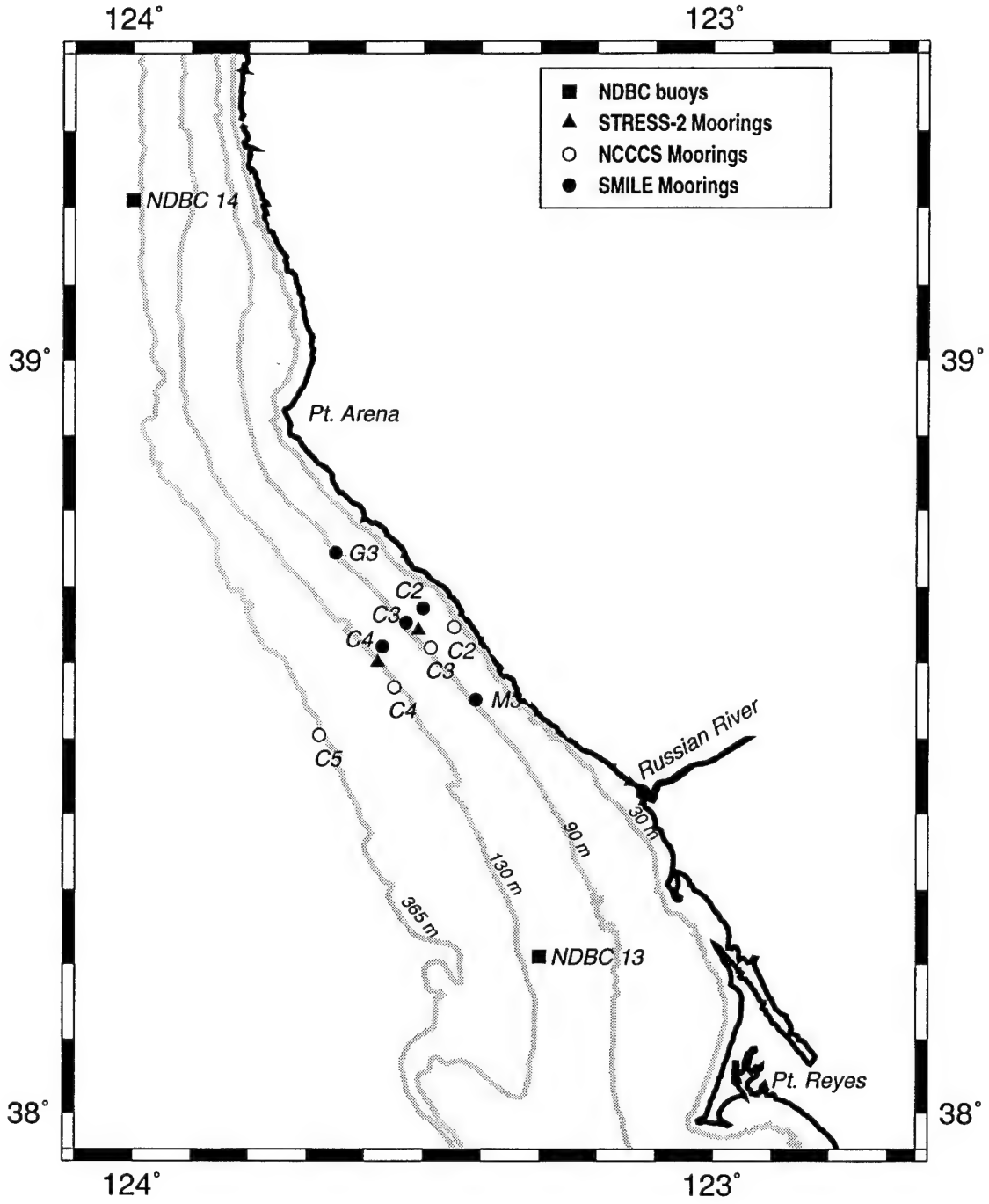

Figure 4.2. Map of northern California shelf showing nominal NCCCS (open circle), SMILE (solid circle), STRESS-2 (solid triangle), and NDBC (solid square) mooring locations. NCCCS mooring locations varied slightly from deployment to deployment.

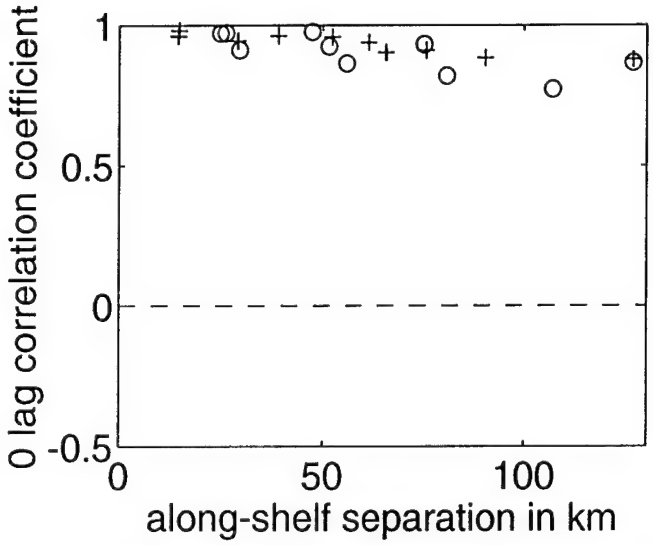

Figure 4.3. Correlations of low-passed along-shelf wind stress, τ^y, as a function of along-shelf mooring separation for summer (CODE-2) NDBC 14, N3, C3, R3, and NDBC 13 (open circles) and winter and spring (SMILE) NDBC 14, G3, C3, M3, and NDBC 13 (plus symbols). The along-shelf direction is defined as 317°T for all locations except for the NDBC 14 location where it is defined as 341°T.

1988], Fig. 4.3 shows the low frequency along-shelf wind stress is highly correlated over the shelf [see also *Beardsley et al.*, 1987]. Wind stress means (over periods of months) and variability are highly seasonal over the northern California shelf. In winter and spring, wind stress is distinguished by the passage of low pressure systems which cause weak means and poleward and equatorward fluctuations on time scales of days. In summer, it is distinguished by the establishment of the Pacific subtropical high [*Lentz*, 1987*a*] which causes strong means with periods of upwelling favorable stress which persist for several weeks, separated by periods of weak wind stress (relaxation events) which may last a week or longer [*Halliwell and Allen*, 1987; *Strub et al.*, 1987; *Beardsley et al.*, 1987].

Wind stress forcing is one factor which causes mean velocities over periods of months to be distinguished by poleward along-shelf flow and relatively weak cross-shelf circulation in winter and by equatorward along-shelf flow and strong near-surface offshelf flow in summer (see chapter 3 and *Lentz and Chapman* [1989]).

4.3.2 Field Programs

In part because of the characteristics listed above, the northern California shelf has been the site of several large field programs which acquired moored velocity time series. The first of these programs was the Coastal Ocean Dynamics Experiment (CODE) [*Beardsley and Lentz*, 1987]. CODE (Fig. 4.1) included two intensive mooring deployments referred to as CODE-1 and CODE-2 lasting approximately four months in the summers of 1981 and 1982 [*Winant et al.*, 1987]. Long term moorings at the C3, C5, and R3 locations bridged the intervening fall, winter, and spring [*Lentz and Chapman*, 1989]. Mooring locations during CODE ranged from the inner shelf to the outer shelf. Cross-shelf separations along the central C line ranged from 1 to 12 km, these distances becoming progressively larger farther offshore. The CODE mooring arrays also extended along the 90-m isobath during CODE-1 and along the 60, 90, and 130 m isobaths during CODE-2. Minimum along-shelf separations were 12 km in CODE-1 and 26 km in CODE-2. CODE velocity records exist at near-surface, interior, and near-bottom depths at most mooring locations. Further information concerning the CODE-1 and CODE-2 moored time series can be found in *Rosenfeld* [1983] and *Limeburner* [1985].

The Northern California Coastal Circulation Study (NCCCS) was designed to study large scale circulation over the northern California shelf between San Francisco and the Oregon border [*Largier et al.*, 1993]. NCCCS included one cross-shelf line of moorings approximately along the CODE C line (Fig. 4.2). Three six month deployments were used to occupy these locations continuously between March, 1988 and October, 1989. Except at the C3 and C5 sites, NCCCS moorings were instrumented only at 10 m. C3 included interior and near-bottom instruments and the C5 site included interior velocity records. Further information concerning the NCCCS field program can be found in *EG&G Inc.* [1989, 1990*a*, and 1990*b*].

The Shelf Mixed Layer Experiment (SMILE) included a field program from November, 1988 to May, 1989 designed to study the surface boundary layer on the northern California shelf (for more information see chapter 2). SMILE included moorings at

the C line (parallel to, but several km north of, the NCCCS line) and along the 90 m isobath (Fig. 4.2). Near-surface velocity measurements existed at all SMILE locations. Only at the C3 site did velocity measurements exist throughout the water column. The upper half of the water column at this site was covered by a SMILE surface mooring while the lower half was covered by a subsurface mooring deployed as part of the Sediment Transport Events over the Shelf and Slope (STRESS) study. Further information concerning SMILE and the STRESS subsurface C3 mooring can be found in *Alessi et al.* [1991].

In addition to the 1988–1989 deployment at C3, STRESS also included near-bottom velocity measurements at the C3 and C4 sites from November, 1990 to March, 1991 (Fig. 4.2). Further information concerning these deployments can be found in *Fredericks et al.* [1993].

4.4 Velocity correlation length scales

4.4.1 Procedures

Correlations were estimated from 38 h low-pass filtered velocity records. The PL64 filter used is described in *Limeburner* [1985]. Both 0 and maximum lagged correlations are listed in Tables 4.2 and 4.3. Lags at maximum correlation are generally indistinguishable from those at 0 lag so for consistency 0 lagged correlations will be plotted. Velocity record start and stop times were chosen such that complete records existed at most moorings in any given field program deployment, though some shorter records were used. To compare NCCCS and SMILE observations, the 19 month long NCCCS records were divided into three periods, the second of which was contemporaneous with SMILE. Record lengths ranged from 90 to 200 days (Table 4.1). The (one-sided) decorrelation time scale of subtidal velocity fluctuations was approximately 3 days for along-shelf velocity and 2 days for cross-shelf velocity giving 30 degrees of freedom or more for these record lengths. For 30 degrees of freedom, correlations of 0.30 (0.35) or greater are significant at the 90% (95%) level.

Velocity records were rotated into local isobath reference frames at each mooring location. *Winant et al.* [1987] list local isobath directions for CODE-2 locations. These reference frames were also used for the analogous CODE-1, NCCCS, SMILE, and STRESS locations. Isobath angles not listed in *Winant et al.* [1987] include the CODE-1 C1 location (where the angle was taken as 335° T following *Lentz* [1994]), the CODE-1 R3 location (where the local isobath angle was estimated to be 336° T), and the CODE-1 M3 and SMILE M3 and G3 locations where the local isobath angles were all estimated to be 317° T. As noted in chapter 3 and elsewhere [*e.g.*, *Smith*, 1981], the cross-shelf (u) velocity is sensitive to the reference frame. As a test of this sensitivity correlations were calculated in which all records were rotated $\pm 2°$ and $\pm 5°$ from the local isobaths defined above. The along-shelf (v) velocity correlation coefficients were nearly unaffected by these rotations and varied by only ± 0.02. Correlation coefficients for u showed more scatter (about ± 0.10). Sensitivity of u correlations to reference frame rotation was greatest for near-bottom instruments and those located at the 30 or 60 m isobath. However, qualitative results were unaffected in that u correlations which were significant in the local isobath reference frame remained significant in the rotated reference frames.

Correlations were calculated between cross-shelf and along-shelf mooring pairs for near-surface, mid-depth, and near-bottom records. These depths were chosen based on the idea that flow at all locations could be divided into a wind-forced surface boundary layer, an inviscid interior (except at the 30-m CODE-1 C1 site), and a bottom boundary layer forced by interior velocity. Near-surface records chosen were at 10 m depth, or failing that, at the shallowest available depth (always 20 m or less). Generally, these records were in the surface boundary layer, though several are probably below the surface boundary layer during weak wind stress conditions, especially in summer. Mid-depth velocity records were chosen to be as near as possible to half the total water depth at each mooring location. Near-bottom velocity records were typically 10 to 20 m above the bottom. Though 20 m is near the upper limit of bottom boundary layer thickness, it was felt that the larger number of records gained was preferable to the limited number of records within 10 m of the bottom.

mooring	position latitude	longitude	instrument depth m	water depth m	isobath angle
CODE-1					
0400 17 Apr 1981 – 1500 10 Jul 1981					
C1	38° 39.80'	123° 25.10'	4	30	335
C1	38° 39.80'	123° 25.10'	27	30	335
C2	38° 39.20'	123° 25.60'	4	63	325
C3	38° 36.38'	123° 27.71'	9	90	317
C3	38° 37.20'	123° 28.30'	39	90	317
C3	38° 37.20'	123° 28.30'	83	90	317
C4	38° 34.50'	123° 32.60'	19	133	319
C4	38° 34.50'	123° 32.60'	65	133	319
C4	38° 34.50'	123° 32.60'	123	133	319
C5	38° 31.27'	123° 40.41'	9	402	330
C5	38° 31.27'	123° 40.41'	152	402	330
M3	38° 31.60'	123° 23.20'	9	90	317
M3	38° 31.60'	123° 23.30'	55	90	317
M3	38° 31.60'	123° 23.30'	74	90	317
R3	38° 21.60'	123° 13.00'	9	90	336
R3	38° 21.65'	123° 13.00'	55	90	336
R3	38° 21.65'	123° 13.00'	75	90	336
CODEW2					
0400 07 Aug 1981 – 2100 07 Dec 1981					
C3	38° 36.11'	123° 27.18'	9	90	317
C3	38° 36.19'	123° 27.18'	55	90	317
C3	38° 36.19'	123° 27.18'	75	90	317
C5	38° 31.30'	123° 40.10'	150	400	330
R3	38° 21.80'	123° 13.00'	9	90	336
R3	38° 21.70'	123° 13.10'	55	90	336
R3	38° 21.70'	123° 13.10'	75	90	336
CODEW3					
0400 16 Dec 1981 – 2100 19 Mar 1982					
C3	38° 36.11'	123° 27.18'	9	90	317
C3	38° 36.10'	123° 27.40'	55	90	317
C3	38° 36.10'	123° 27.40'	75	90	317
C5	38° 31.30'	123° 40.60'	9	400	330
C5	38° 31.30'	123° 40.10'	150	400	330
R3	38° 21.50'	123° 13.00'	9	90	336
R3	38° 21.95'	123° 13.15'	55	90	336
R3	38° 21.95'	123° 13.15'	75	90	336

Table 4.1: Velocity data used to estimate correlation scales. Start and stop times given are those used for correlation calculations.

mooring	position latitude	longitude	instrument depth m	water depth m	isobath angle
CODE-2					
0400 05 Apr 1982 – 2100 25 Jul 1982					
C2	38° 38.16'	123° 25.32'	10	60	325
C2	38° 38.16'	123° 25.32'	35	60	325
C2	38° 38.16'	123° 25.32'	53	60	325
C3	38° 38.38'	123° 27.71'	10	93	317
C3	38° 34.30'	123° 32.70'	53	90	317
C3	38° 34.30'	123° 32.70'	83	90	317
C4	38° 33.26'	123° 31.68'	10	130	319
C4	38° 33.26'	123° 31.56'	70	130	319
C4	38° 33.26'	123° 31.56'	121	130	319
C5	38° 30.80'	123° 40.25'	20	400	330
C5	38° 30.88'	123° 40.41'	150	400	330
N2	38° 49.50'	123° 40.11'	10	60	316
N2	38° 49.50'	123° 40.11'	35	60	316
N3	38° 48.07'	123° 41.71'	10	90	319
N3	38° 48.09'	123° 41.77'	53	90	319
N3	38° 48.09'	123° 41.77'	83	90	319
N4	38° 45.79'	123° 45.60'	10	129	319
N4	38° 45.71'	123° 45.55'	70	130	319
N4	38° 45.71'	123° 45.55'	121	130	319
R2	38° 27.17'	123° 13.97'	20	60	319
R2	38° 27.14'	123° 13.94'	35	60	319
R2	38° 27.14'	123° 13.94'	53	60	319
R3	38° 25.38'	123° 16.40'	20	90	329
R3	38° 25.33'	123° 16.36'	53	90	329
R3	38° 25.38'	123° 16.40'	70	90	329
R4	38° 20.36'	123° 22.94'	10	130	339
R4	38° 20.84'	123° 22.95'	70	130	339
R4	38° 20.84'	123° 22.95'	110	130	339

Table 4.1 (continued): Velocity data used to estimate correlation scales. Start and stop times given are those used for correlation calculations.

mooring	position latitude	longitude	instrument depth m	water depth m	isobath angle
NCCCS*					
0100 23 Mar 1988 – 0000 16 Aug 1988					
C2	38° 38.33'	123° 24.60'	10	60	325
0100 23 Mar 1988 – 0600 16 Nov 1988					
C3	38° 36.77'	123° 26.93'	10	90	317
C3	38° 36.77'	123° 27.48'	45	90	317
C3	38° 36.77'	123° 26.93'	75	90	317
C4	38° 33.60'	123° 30.78'	10	130	319
C5	38° 30.00'	123° 38.55'	150	400	330
0900 04 May 1988 – 0700 17 Aug 1988					
C5	38° 30.35'	123° 39.73'	10	400	330
0700 16 Nov 1988 – 0100 12 Feb 1989					
C5	38° 30.00'	123° 38.55'	150	400	330
0700 16 Nov 1988 – 1900 13 May 1989					
C3	38° 36.77'	123° 26.93'	10	90	317
C3	38° 36.77'	123° 27.48'	45	90	317
C3	38° 36.77'	123° 26.93'	75	90	317
C4	38° 33.60'	123° 30.78'	10	130	319
0200 21 Feb 1989 – 1900 13 May 1989					
C2	38° 38.33'	123° 24.60'	10	60	325
2000 13 May 1989 – 2300 17 Oct 1989					
C2	38° 38.33'	123° 24.60'	10	60	325
C3	38° 36.77'	123° 26.93'	10	90	317
C3	38° 36.77'	123° 27.48'	45	90	317
C3	38° 36.77'	123° 26.93'	75	90	317
C4	38° 33.60'	123° 30.78'	10	130	319

Table 4.1 (continued): Velocity data used to estimate correlation scales. Start and stop times given are those used for correlation calculations.
*from overlapping multiple deployments, position given is recorded position in Scripps Data Zoo files (deployment 1)

mooring	position latitude	longitude	instrument depth m	water depth m	isobath angle
SMILE					
0700 16 Nov 1988 – 1400 21 Apr 1989					
C3	38° 38.71'	123° 29.56'	11.5	93	317
0700 16 Nov 1988 – 1900 13 May 1989					
C3	38° 38.71'	123° 29.56'	44.5	93	317
C4	38° 36.78'	123° 31.87'	10	117	319
C4	38° 36.78'	123° 31.87'	52	117	319
G3	38° 44.40'	123° 36.40'	10	93	317
M3	38° 32.67'	123° 22.97'	10	93	317
0400 28 Feb 1989 – 1900 13 May 1989					
C2	38° 39.80'	123° 27.82'	10	80	325
STRESS-1					
1800 08 Dec 1988 – 0700 25 Feb 1989					
C3	38° 38.44'	123° 29.64'	79	97	317
1200 06 Mar 1989 – 0100 05 May 1989					
C3	38° 38.14'	123° 29.97'	77	95	317
STRESS-2					
2300 20 Nov 1990 – 2200 09 Mar 1991					
C3	38° 38.14'	123° 28.31'	80	90	317
C4	38° 35.64'	123° 32.52'	120	130	319

Table 4.1 (continued): Velocity data used to estimate correlation scales. Start and stop times given are those used for correlation calculations.

4.4.2 Along-shelf correlation scales

Correlations as a function of along-shelf separation were estimated primarily along the 90 m isobath using observations from CODE-1, fall and winter CODE deployments, CODE-2, SMILE, and NCCCS. Additional estimates of along-shelf correlations along the 60 and 130 m isobaths were made using the CODE-2 data.

Along-shelf (v) velocity records (Fig. 4.4 and Table 4.2) were significantly correlated at all along-shelf mooring separations for near surface, middle, and near-bottom depths. The correlations demonstrate that along-shelf correlation scales of v are greater than 60 km for this section of the northern California shelf. Correlations as a function of separation appear to show little variation between field programs which occurred during different seasons. Though v was significantly correlated at all along-shelf separations, correlations of interior and near-bottom v were slightly larger than near-surface v (Table 4.2, Fig. 4.4). Along-shelf correlations of v are not a strong function of total water depth though CODE-2 observations indicate some decrease in correlation of near-surface v at the 130 m isobath relative to the 60 and 90 m isobath (Table 4.2).

Along-shelf correlation scales of u (Fig. 4.5 and Table 4.2) were resolved only for near-surface u during the SMILE and NCCCS observations (and possibly by CODE-1 C3 and M3) along the 90 m isobath. These observations indicate that, at least between November, 1988 and May, 1989, along-shelf correlation scales of u are from 15–20 km in the near-surface. Below the surface little information is available about u along-shelf correlation scales. There is the suggestion that mid-depth and near-bottom u may be correlated at separations of 4–10 km, but that correlation lengths are less than 25 km.

4.4.3 Cross-shelf correlation scales

Correlations as a function of cross-shelf separation were estimated primarily along the C line using observations from CODE-1, fall and winter CODE deployments, CODE-2, SMILE, NCCCS, and STRESS-2. Additional estimates of cross-shelf correlations

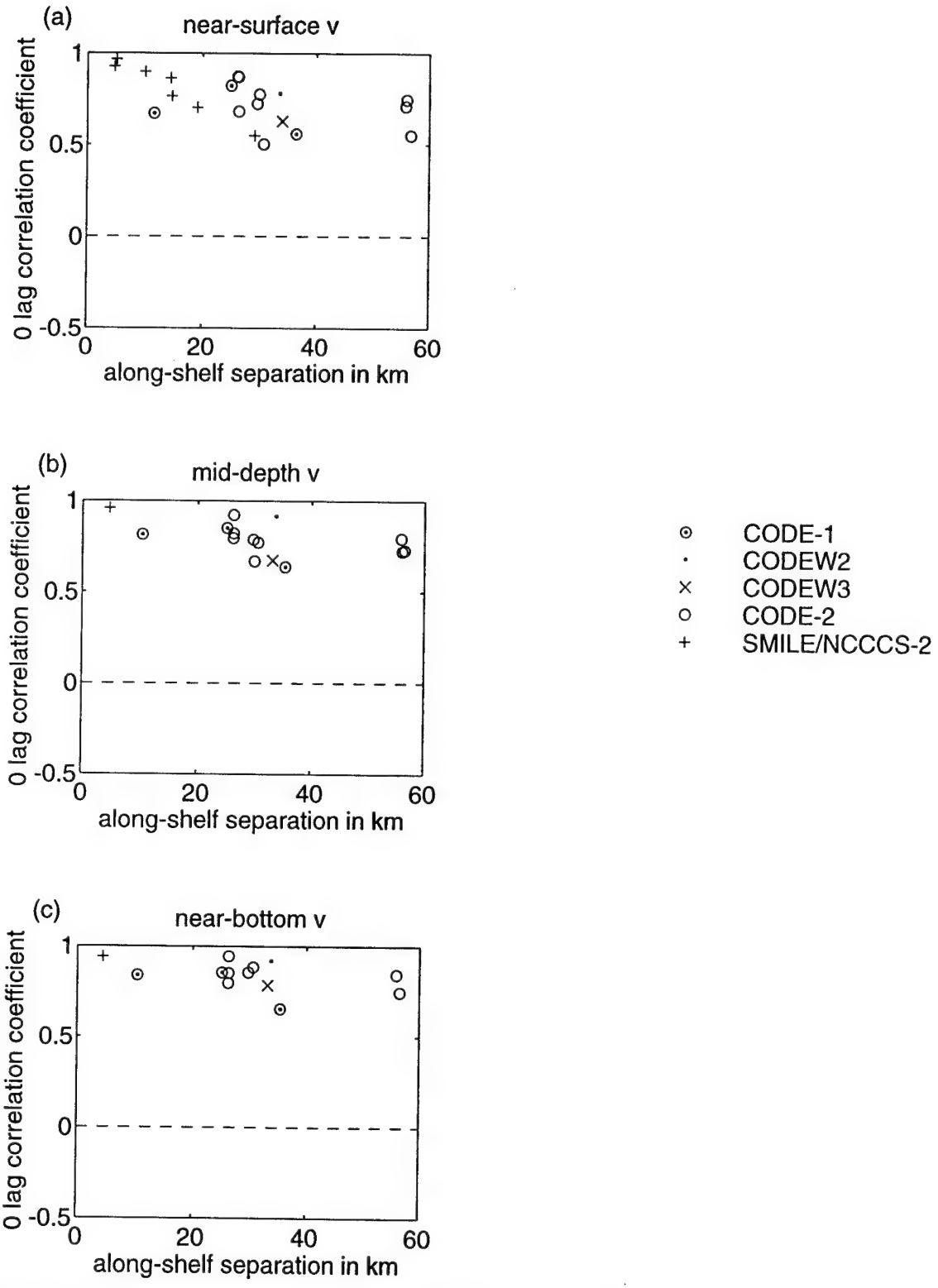

Figure 4.4. Correlations of along-shelf velocity, v, as a function of along-shelf mooring separation for near-surface (a), mid-depth (b), and near-bottom (c) instruments.

near-surface correlations

moorings	hrs	distance km	0 lag u corr	max lag u corr		0 lag v corr	max lag v corr	
CODE-1								
C3(009):M3(009)	2028	11.61	0.47	0.52	−11	0.67	0.73	−13
M3(009):R3(009)	2028	25.00	0.34	0.34	−2	0.82	0.85	−10
C3(009):R3(009)	2028	36.45	0.22	0.23	−5	0.56	0.62	−14
CODEW2								
C3(009):R3(009)	2946	33.56	0.52	0.52	−4	0.78	0.83	−14
CODEW3								
C3(009):R3(009)	2250	34.00	0.28	0.28	−2	0.63	0.64	−6
CODE-2								
C2(010):R2(020)	2682	26.18	0.03	−0.17	−89	0.87	0.87	+1
N2(010):C2(010)	2682	29.98	0.24	0.26	+100	0.78	0.78	−5
N2(010):R2(020)	2682	56.07	0.06	0.13	+100	0.75	0.75	+0
C3(010):R3(020)	2682	26.29	0.03	−0.08	−43	0.87	0.87	−3
N3(010):C3(010)	2682	29.64	0.07	−0.15	−100	0.72	0.74	−9
N3(010):R3(020)	2682	55.89	−0.01	0.19	+49	0.71	0.72	−5
C4(010):R4(010)	2682	26.42	−0.03	0.26	+56	0.68	0.68	−14
N4(010):C4(010)	2682	30.76	0.08	0.21	+55	0.50	0.50	+0
N4(010):R4(010)	2682	56.83	−0.03	−0.20	+49	0.55	0.57	−16
SMILE								
C3(010):NC(010)	3752	4.67	0.73	0.73	+0	0.93	0.93	+0
NC(010):M3(010)	4285	10.04	0.54	0.54	+2	0.90	0.90	+0
G3(010):C3(010)	3752	14.46	0.35	0.37	−4	0.86	0.86	−2
C3(010):M3(010)	3752	14.71	0.48	0.48	+0	0.77	0.77	−2
G3(010):NC(010)	4285	19.12	0.39	0.39	−2	0.70	0.71	−4
G3(010):M3(010)	4285	29.16	0.11	−0.27	−53	0.55	0.55	−4
C4(010):NC(010)	4285	5.02	0.89	0.89	−1	0.97	0.97	+0

Table 4.2: Correlations of u and v as a function of along-shelf separation. Positive lags denote the first listed series leading the second.

mid-depth correlations

moorings	hrs	distance km	0 lag u corr	max lag u corr		0 lag v corr	max lag v corr	
CODE-1								
C3(039):M3(055)	2028	10.42	0.66	0.67	−2	0.81	0.85	−9
M3(055):R3(055)	2028	25.15	−0.12	−0.28	−43	0.85	0.86	−4
C3(039):R3(055)	2028	35.36	−0.23	−0.30	−17	0.64	0.67	−9
CODEW2								
C3(055):R3(055)	2946	33.74	−0.06	−0.20	−22	0.92	0.93	−6
CODEW3								
C3(055):R3(055)	2250	33.12	−0.06	−0.22	−19	0.67	0.68	−3
CODE-2								
C2(035):R2(035)	2682	26.25	0.22	0.24	+15	0.79	0.80	+4
N2(035):C2(035)	2682	29.98	0.28	0.29	−9	0.67	0.69	−10
N2(035):R2(035)	2682	56.14	0.64	0.64	−1	0.72	0.72	−1
C3(053):R3(053)	2682	26.29	−0.12	−0.12	+7	0.92	0.92	+0
N3(053):C3(053)	2682	29.72	−0.35	−0.37	+14	0.79	0.80	−6
N3(053):R3(053)	2682	55.97	0.28	0.34	−16	0.79	0.80	−3
C4(070):R4(070)	2682	26.28	0.01	0.30	+52	0.82	0.82	+1
N4(070):C4(070)	2682	30.60	−0.08	−0.28	+88	0.77	0.77	−3
N4(070):R4(070)	2682	56.54	0.03	0.23	−57	0.73	0.73	−3
SMILE								
C3(045):NC(045)	4285	4.67	0.56	0.56	+0	0.96	0.96	+0

near-bottom correlations

moorings	hrs	distance km	0 lag u corr	max lag u corr		0 lag v corr	max lag v corr	
CODE-1								
C3(083):M3(074)	2028	10.42	0.35	0.45	−14	0.84	0.86	−6
M3(074):R3(075)	2028	25.15	0.25	0.36	+17	0.85	0.86	−5
C3(083):R3(075)	2028	35.36	0.44	0.49	+10	0.65	0.68	−8
CODEW2								
C3(075):R3(075)	2946	33.74	0.16	−0.31	−40	0.92	0.93	−5
CODEW3								
C3(075):R3(075)	2250	33.12	0.10	0.26	+15	0.78	0.78	+0
CODE-2								
C2(053):R2(053)	2682	26.25	0.41	0.41	−2	0.80	0.80	+2
C3(083):R3(070)	2682	26.29	0.44	0.44	−1	0.95	0.95	+1
N3(083):C3(083)	2682	29.72	0.31	0.32	−6	0.86	0.86	−3
N3(083):R3(070)	2682	55.97	0.73	0.75	−8	0.84	0.84	−1
C4(121):R4(110)	2682	26.28	0.03	0.16	+56	0.85	0.85	−2
N4(121):C4(121)	2682	30.60	0.34	0.38	−14	0.88	0.88	+0
N4(121):R4(110)	2682	56.54	0.26	0.39	−24	0.75	0.75	−3
SMILE								
C3(079):NC(075)	3268	4.38	0.51	0.51	+2	0.94	0.94	+1

Table 4.2 (continued): Correlations of u and v as a function of along-shelf separation. Positive lags denote the first listed series leading the second.

near-surface correlations

moorings	hrs	distance km	0 lag u corr	max lag u corr		0 lag v corr	max lag v corr	
CODE-1								
C1(004):C2(004)	2028	1.18	0.73	0.73	+1	0.82	0.86	+8
C2(004):C3(009)	2028	5.52	0.42	0.50	+10	0.70	0.79	+13
C1(004):C3(009)	2028	6.68	0.36	0.46	+12	0.50	0.71	+22
C3(009):C4(019)	2028	7.99	0.38	0.39	+8	0.61	0.68	+20
C4(019):C5(009)	2028	11.46	0.15	−0.42	−76	−0.02	0.36	+100
C2(004):C4(019)	2028	13.49	−0.08	−0.21	−29	0.22	0.39	+44
C1(004):C4(019)	2028	14.64	0.09	0.17	+35	0.13	0.41	+53
C3(009):C5(009)	2028	18.53	−0.03	−0.21	−38	−0.06	0.15	+94
C2(004):C5(009)	2028	23.56	0.13	0.17	−74	0.02	−0.14	+43
C1(004):C5(009)	2028	24.60	0.33	0.33	+3	0.07	0.14	−81
CODEW3								
C3(009):C5(009)	2250	21.39	0.49	0.49	−3	0.13	0.22	+89
CODE-2								
N2(010):N3(010)	2682	3.52	0.57	0.57	+2	0.88	0.89	+6
C2(010):C3(010)	2682	4.74	0.30	0.30	+2	0.86	0.87	+8
R2(020):R3(020)	2682	4.86	0.51	0.51	−2	0.87	0.87	+4
N3(010):N4(010)	2682	7.03	0.75	0.75	+2	0.45	0.54	+30
C3(010):C4(010)	2682	8.06	0.66	0.66	+2	0.53	0.58	+23
R3(020):R4(010)	2682	12.77	0.02	0.17	+100	0.57	0.57	+4
N2(010):N4(010)	2682	10.50	0.31	0.35	+12	0.21	0.32	+33
C2(010):C4(010)	2682	12.80	0.04	0.14	+86	0.36	0.42	+24
C4(010):C5(020)	2682	13.37	0.11	−0.23	−78	0.46	0.53	+94
C3(010):C5(020)	2682	20.94	0.00	0.18	+95	0.13	0.18	+68
C2(010):C5(020)	2682	25.57	0.07	0.23	+83	0.01	−0.21	−99
R2(020):R4(010)	2682	17.63	−0.20	−0.20	+3	0.47	0.47	+5
NCCCS-1								
C2(010):C3(010)	3504	4.52	0.38	0.39	−4	0.76	0.77	+8
C3(010):C4(010)	5718	8.06	0.55	0.55	+0	0.75	0.76	+9
C2(010):C4(010)	3504	12.57	0.05	0.11	−53	0.40	0.46	+60
C4(010):C5(010)	2519	13.21	0.44	0.45	+6	0.47	0.57	+100
C3(010):C5(010)	2519	21.11	0.48	0.49	+5	0.34	0.36	−100
C2(010):C5(010)	2488	25.63	0.35	0.35	−3	0.14	0.21	−100
NCCCS-2								
C2(010):C3(010)	1962	4.36	0.44	0.48	−6	0.83	0.83	+2
C3(010):C4(010)	4285	7.37	0.69	0.69	−1	0.58	0.58	+3
C2(010):C4(010)	1962	11.73	0.00	−0.30	+34	0.20	0.21	+9
NCCCS-3								
C2(010):C3(010)	3772	4.57	0.47	0.48	−5	0.75	0.76	+8
C3(010):C4(010)	3772	7.47	0.64	0.65	−1	0.80	0.81	+12
C2(010):C4(010)	3772	12.03	0.24	0.29	−16	0.54	0.57	+27
SMILE								
C2(010):C3(010)	1259	3.23	0.81	0.81	+0	0.90	0.90	+0
C3(010):C4(010)	3752	4.90	0.85	0.85	+1	0.82	0.82	+3
C2(010):C4(010)	1792	8.11	0.75	0.75	+0	0.39	0.39	+6

Table 4.3: Correlations of u and v as a function of cross-shelf separation. Positive lags denote the first listed series leading the second.

mid-depth correlations

moorings	hrs	distance km	0 lag u corr	max lag u corr		0 lag v corr	max lag v corr	
CODE-1								
C3(039):C4(065)	2028	8.13	0.02	−0.30	−72	0.74	0.76	+8
C4(065):C5(152)	2028	12.64	0.06	−0.41	−56	0.32	0.45	+86
C3(039):C5(152)	2028	20.75	−0.36	−0.40	+31	0.05	0.27	−100
CODEW2								
C3(055):C5(150)	2946	20.80	0.13	0.14	−78	0.17	0.17	−3
CODEW3								
C3(055):C5(150)	2250	20.83	0.03	0.16	+75	0.25	0.25	+3
CODE-2								
N2(035):N3(053)	2682	3.55	0.63	0.63	+0	0.91	0.92	+5
C2(035):C3(053)	2682	4.74	0.02	−0.04	−62	0.86	0.87	+6
R2(035):R3(053)	2682	4.86	0.67	0.68	−3	0.88	0.88	+3
N3(053):N4(070)	2682	7.02	0.65	0.65	+1	0.73	0.74	+6
C3(053):C4(070)	2682	8.06	0.29	−0.29	−60	0.66	0.67	+7
R3(053):R4(070)	2682	12.68	0.37	0.44	−13	0.65	0.65	+2
N2(035):N4(070)	2682	10.54	0.41	0.41	+0	0.51	0.53	+10
C2(035):C4(070)	2682	12.80	0.11	0.14	−22	0.38	0.44	+84
C4(070):C5(150)	2682	13.37	0.06	−0.24	−97	0.33	0.34	−8
C3(053):C5(150)	2682	20.94	−0.19	−0.22	−14	0.24	0.24	+1
C2(035):C5(150)	2682	25.57	0.03	−0.12	+100	0.15	0.27	+94
R2(035):R4(070)	2682	17.54	0.23	0.24	−4	0.54	0.54	+4
NCCCS-1								
C3(045):C5(150)	5718	21.11	−0.25	−0.38	−36	0.23	0.24	+100
NCCCS-2								
C3(045):C5(150)	2107	21.44	0.19	0.19	+2	−0.02	−0.14	+26
SMILE								
C3(045):C4(052)	4285	4.90	0.50	0.52	−4	0.83	0.83	+0
STRESS−2								
C3(059):C4(059)	2487	7.66	0.47	0.48	+3	0.78	0.78	+0

near-bottom correlations

moorings	hrs	distance km	0 lag u corr	max lag u corr		0 lag v corr	max lag v corr	
CODE-1								
C1(027):C3(083)	2028	7.12	0.14	0.23	−12	0.49	0.66	+19
C3(083):C4(123)	2028	8.13	0.67	0.68	+3	0.81	0.81	+1
C1(027):C4(123)	2028	15.00	0.17	0.18	−6	0.30	0.44	+18
CODE-2								
C2(053):C3(083)	2682	4.74	0.36	0.37	−3	0.77	0.79	+6
R2(053):R3(070)	2682	4.86	0.70	0.70	+1	0.84	0.85	+6
N3(083):N4(121)	2682	7.02	0.76	0.76	+1	0.85	0.86	+1
C3(083):C4(121)	2682	8.06	0.70	0.70	−1	0.76	0.76	+2
R3(070):R4(110)	2682	12.68	0.50	0.53	−7	0.66	0.66	−3
C2(053):C4(121)	2682	12.80	0.35	0.35	−4	0.44	0.46	+9
R2(053):R4(110)	2682	17.54	0.31	0.34	−7	0.54	0.54	+3
STRESS−2								
C3(080):C4(120)	2489	7.66	0.58	0.58	+0	0.86	0.86	−1

Table 4.3 (continued): Correlations of u and v as a function of cross-shelf separation. Positive lags denote the first listed series leading the second.

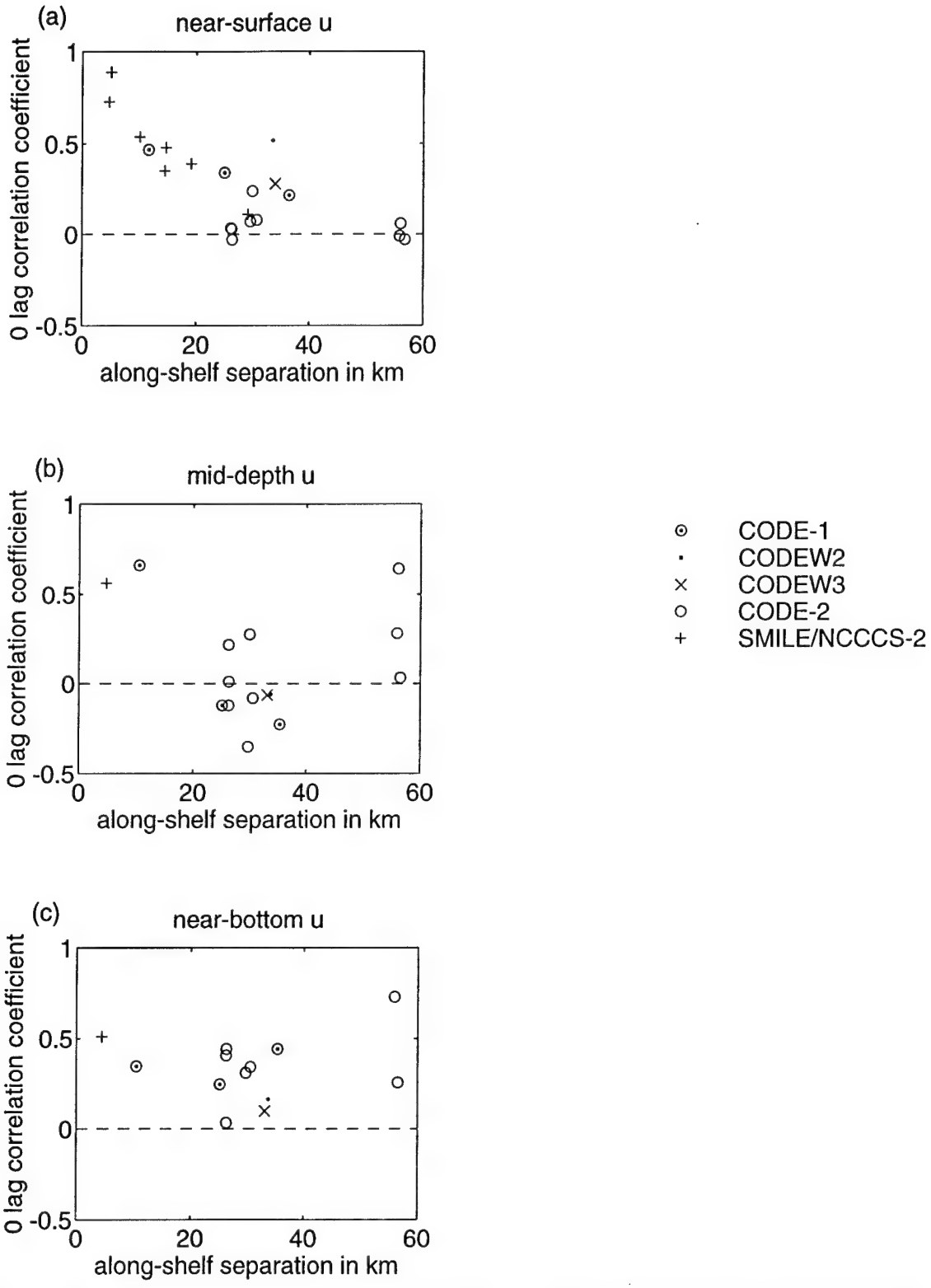

Figure 4.5. Correlations of cross-shelf velocity, u, as a function of along-shelf mooring separation for near-surface (a), mid-depth (b), and near-bottom (c) instruments.

along the N and R lines were made using the CODE-2 data.

Cross-shelf scales in general are more difficult to interpret than along-shelf correlation scales. For a straight shelf with large-scale wind forcing, interpretation of along-shelf correlation scales is fairly straightforward in that we expect along-shelf correlations to be primarily a function of separation and not along-shelf position. In contrast, there is no reason to expect cross-shelf correlation scales to be independent of cross-shelf position. Coastal oceanographers often divide shelves into three regions (see *e.g.*, *Lentz* [1995] and *Allen et al.* [1983]): an inner-shelf where near-shore processes such as relaxation from upwelling may be important [*Send et al.*, 1987] and surface and bottom boundary layers interact, a mid-shelf where surface and bottom boundary layers are thin but the shelf is generally isolated from off-shelf variability, and an outer-shelf where oceanic variability is important. Because the processes which govern the velocity field on the shelf are themselves often a strong function of cross-shelf position, cross-shelf correlations estimated here will be discussed in light of cross-shelf position as well as separation, though summary plots showing cross-shelf correlation as a function of cross-shelf distance will also be presented.

Cross-shelf correlation scales of v (Fig. 4.6, Table 4.3) are 10–15 km. Despite showing more scatter than v correlations as a function of along-shelf separation, they are well resolved in the sense that observations are significantly correlated to their nearest neighbors in the cross-shelf direction. Scatter between experiments again shows no seasonal variability. Most moored observations are over the 60 m, 90 m, and 130 m isobaths. Within this region, v correlations are not a strong function of position, *i.e.*, correlations between v at 60 m and 90 m (a distance of about 5 km) appear to be about the same as correlations between v at 90 m and 130 m (a distance of about 8 km). Similarly, cross-shelf correlations of v exhibit little systematic variability with instrument depth (near-surface, interior, or near-bottom).

Like the along-shelf u correlations, the cross-shelf u correlations were best resolved in the near-surface observations where the cross-shelf correlation scale is about 10 km. In contrast to along-shelf correlations of u, cross-shelf correlations of u (Fig. 4.7, Table 4.3) were resolved by typical mooring separations. Comparison of u correlations

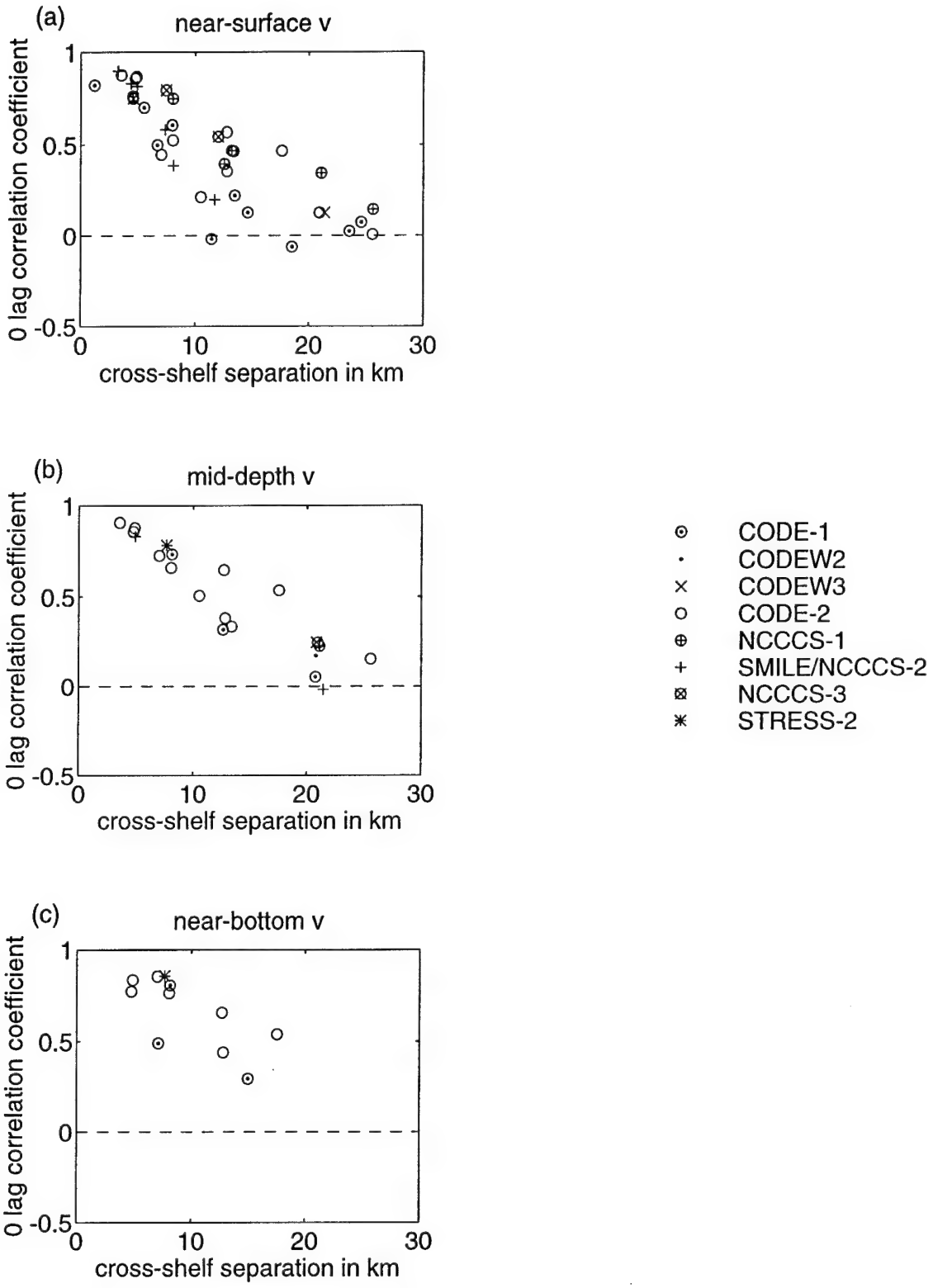

Figure 4.6. Correlations of along-shelf velocity, v, as a function of cross-shelf mooring separation for near-surface (a), mid-depth (b), and near-bottom (c) instruments.

between 60 and 90 m locations with those between 90 to 130 m (mostly from summer observations) gives some suggestion that near-surface u is more highly correlated between the outer shelf pair despite the greater mooring separation. Though the CODE-2 observations give some indication that u correlations are higher for near-surface and near-bottom instruments than for interior instruments, the large scatter and limited number of time series make definitive statements about depth dependence impossible.

4.5 Interpreting u along-shelf correlation length scales during the winter and spring 1988–1989

Both along-shelf and cross-shelf correlation scales of v and cross-shelf correlation scales of u were resolved adequately by most field programs examined in section 4.4. Along-shelf correlation scales of v were over 60 km, reflecting the long correlation scales of along-shelf wind stress on the northern California shelf (Fig. 4.3). Cross-shelf correlation scales of u and v were 10–15 km; about half the shelf width and explained readily in terms of the different physical processes which are important over the inner, mid, and outer-shelf (see section 4.4.3). However, along-shelf u correlations were not resolved by typical along-shelf mooring separations of 30 km, and short mooring separations (5–15 km) are required. Between November, 1988 and May, 1989, the along-shelf scale of near-surface u was 15-20 km. This is much shorter than the scale of the along-shelf wind stress (see Fig. 4.3) which is generally acknowledged to be a dominant driving force of near-surface cross-shelf circulation [*e.g.*, chapter 3 and *Lentz*, 1992] and warrants a closer examination.

To gain insight into the processes which reduce along-shelf correlation scales of u, observations from the combined, SMILE, STRESS, and NCCCS moorings (Fig. 4.2) are examined here in further detail. These moorings come closest to meeting the requirements for resolving along-shelf scales of u, though spatial coverage is only

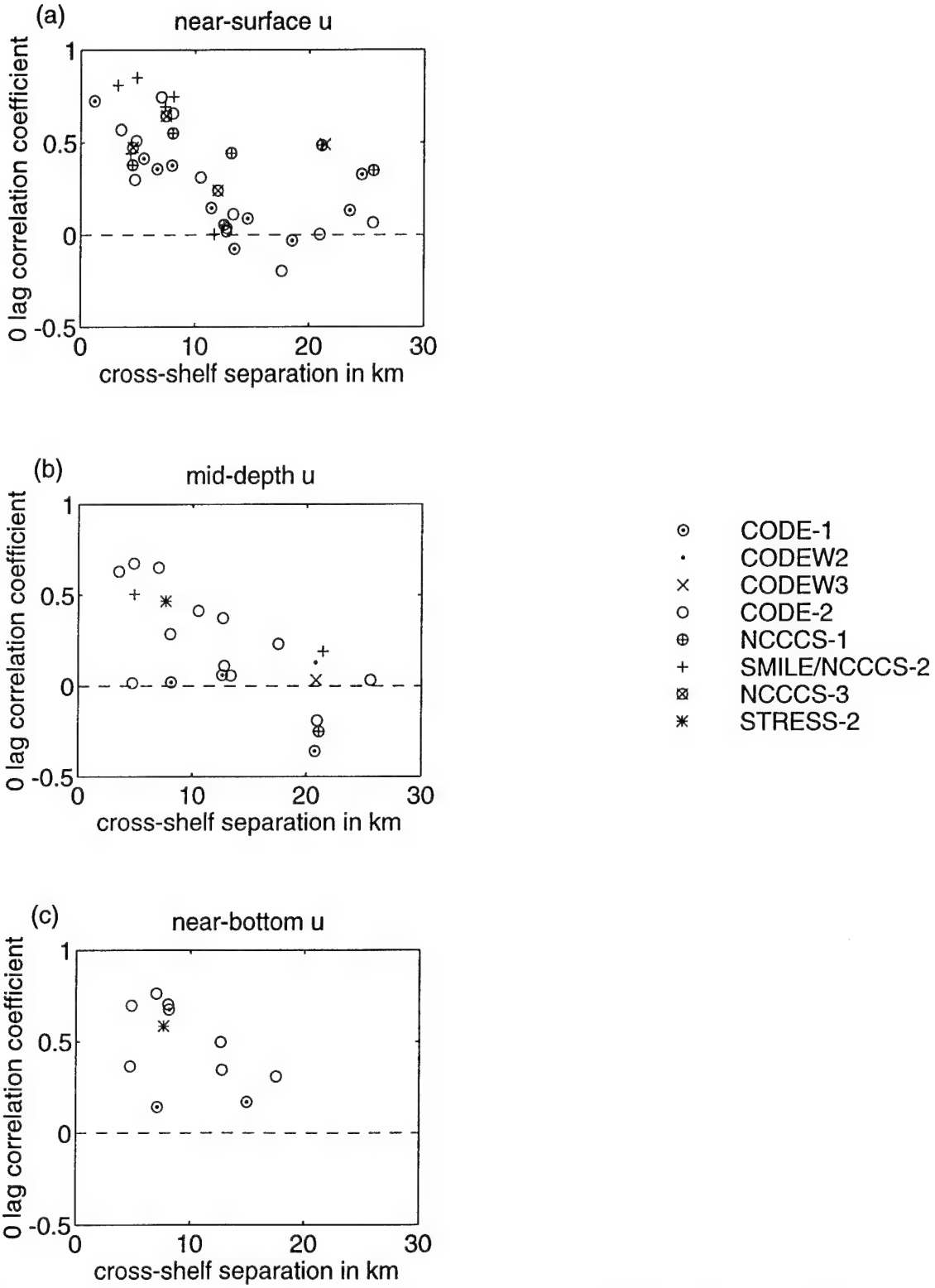

Figure 4.7. Correlations of cross-shelf velocity, u, as a function of cross-shelf mooring separation for near-surface (a), mid-depth (b), and near-bottom (c) instruments.

extensive near the surface. They provide correlation scale estimates for near-surface u from 4 to 30 km along the 90 m isobath between November, 1988 and May, 1989.

Time series of low-pass filtered along-shelf wind stress (τ^y) and u (Fig. 4.8) show visually that wind forcing is observed at all mooring sites along the 90 m isobath for both poleward and equatorward wind fluctuations. Numerous wind forcing events (*e.g.*, December 6–7, December 22–24, March 1, April 10) are reflected to some extent at all mooring sites, however there is additional u variability which is not evident at all mooring sites. For example, from early to mid-February offshore flow at 10 m is observed at C3, NCCCS C3, and M3, but is absent at G3. Similarly, in late April offshore flow is observed at M3, while onshore flow is observed at G3. What then are the processes which reduce correlation lengths of near-surface u? To understand these processes better, 28 day subsets of the six month time period are here considered. Twenty-eight days was chosen in order to give approximately 10 degrees of freedom per subset. Correlations of 0.50 (0.58) are significant at the 90% (95%) level for 10 degrees of freedom.

4.5.1 Monthly variation in correlation scales of near-surface cross-shelf velocity

Monthly plots of near-surface u correlation as a function of along-shelf separation (Fig. 4.9) show a great deal of variability. From mid-November to mid-January, and again from mid-February to early April, along-shelf correlations show little drop-off as a function of separation. However from mid-January to early February and again from early April to early May shorter along-shelf correlation scales exist. Correlation scales are always greater than or equal to 4 km as the SMILE C3 and NCCCS C3 moorings remain well correlated over all months.

Monthly variability in along-shelf correlation scales of near-surface u appears to be related to the importance of along-shelf wind stress forcing relative to other processes. Table 4.4 lists the correlations of moorings with along-shelf wind stress (measured at SMILE C3) and along-shelf wind stress standard deviation for each of the 28 day

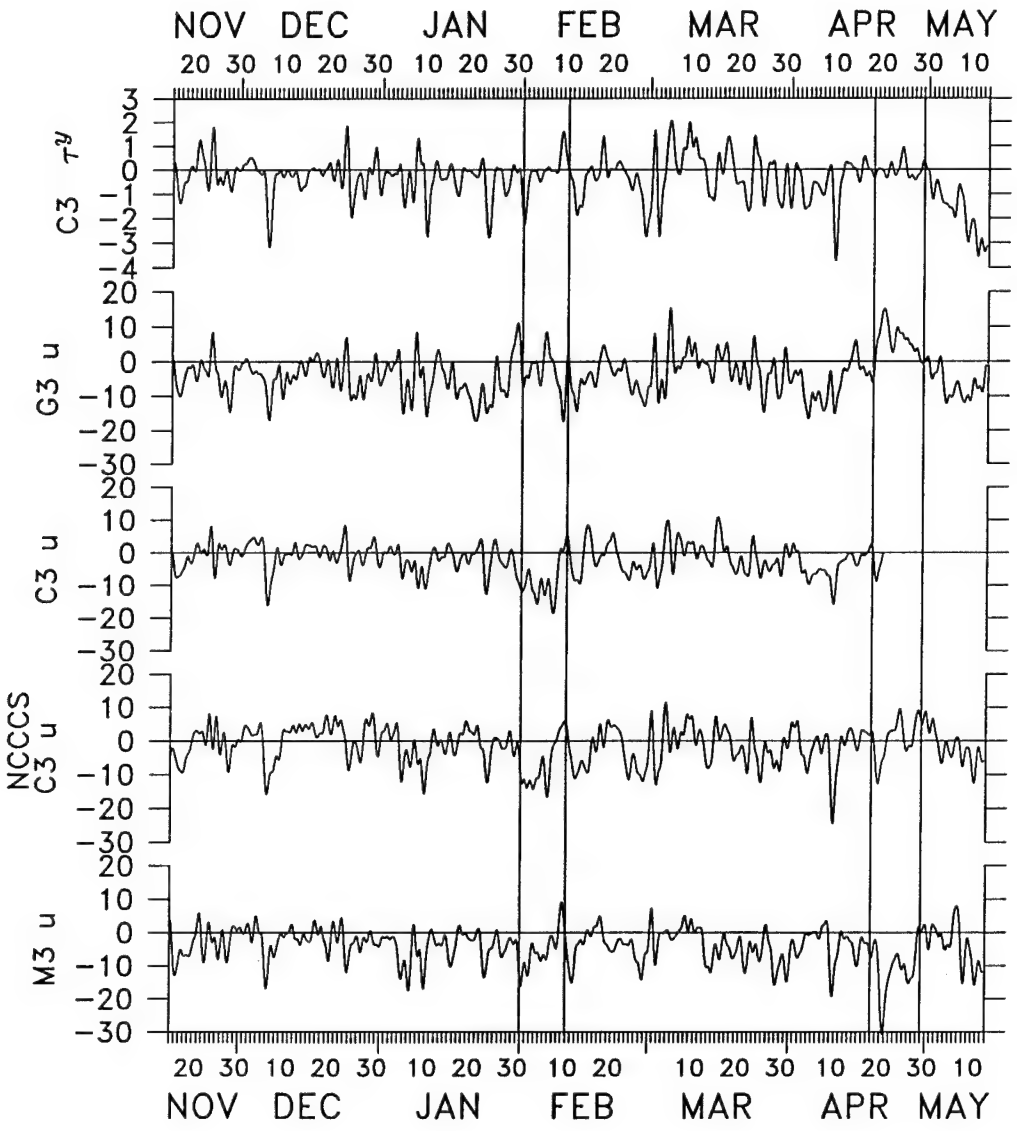

Figure 4.8. Time series of low-pass filtered τ^y (dyn/cm^2), and u (cm/s) at 10 m. Mooring locations are as denoted in Fig. 4.2. Correlations of u with τ^y range from 0.5–0.6. Periods of along-shelf variability in early February and late April are bracketed by solid lines.

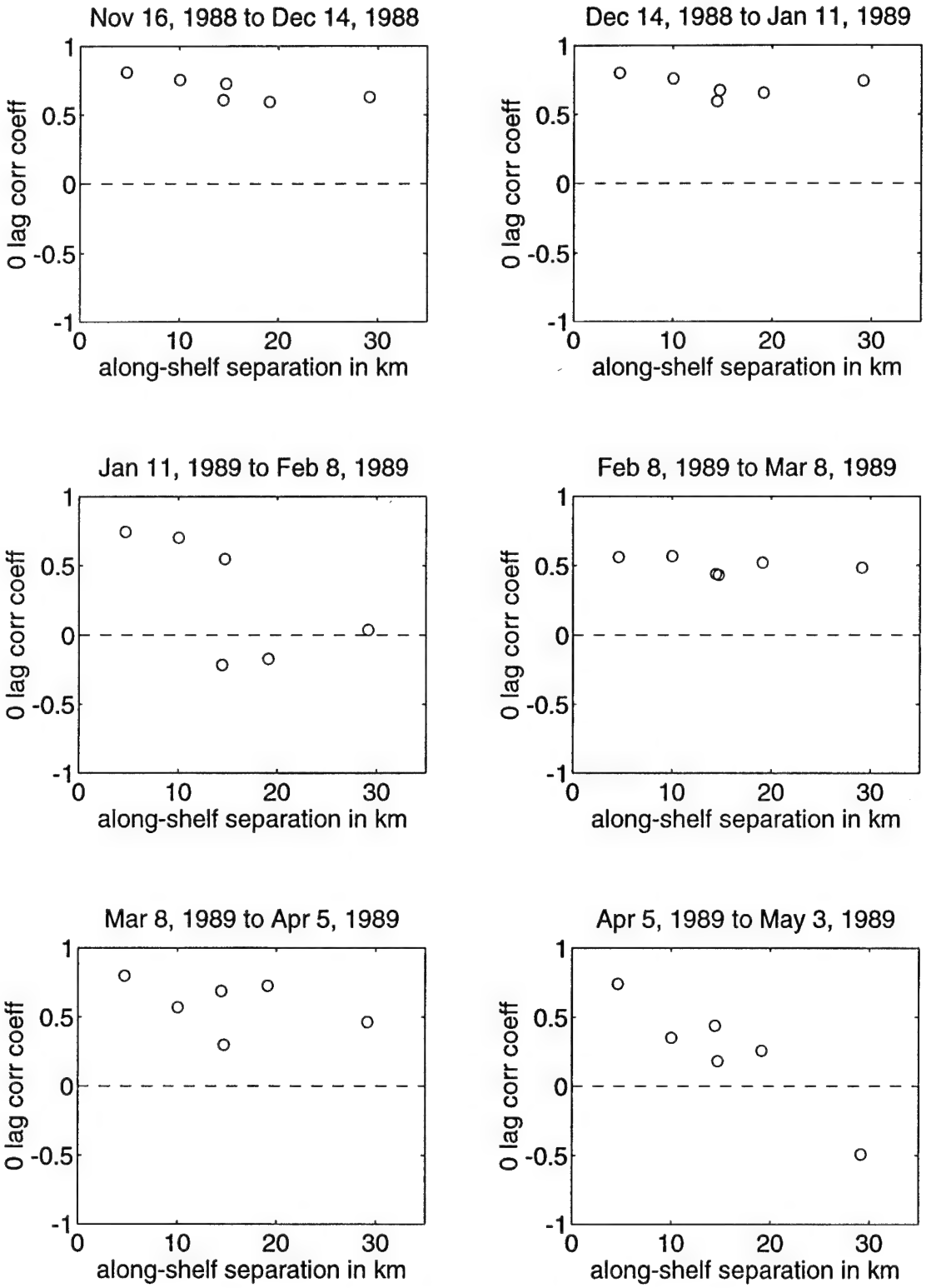

Figure 4.9. Correlations of near-surface cross-shelf velocity, u, as a function of along-shelf mooring separation for 6 one month periods between November, 1988 and May, 1989.

start:	11/16/88	12/14/88	1/11/89	2/8/89	3/8/89	4/5/89
stop:	12/14/88	1/11/89	2/8/89	3/8/89	4/5/89	5/3/89
wind σ, dyn/cm^2:	0.74	0.72	0.65	1.02	0.95	0.71
u scale, km:	30	30	15	30	30	15
mooring						
G3	0.77	0.82	0.44	0.61	0.81	0.56
C3	0.78	0.63	0.41	0.60	0.63	0.76*
NCCCS C3	0.68	0.67	0.38	0.79	0.79	0.70
M3	0.71	0.73	0.69	0.75	0.73	0.18

Table 4.4: Correlations of near-surface u with along-shelf wind stress over one month periods for the along-shelf moorings used in Fig. 4.9. Short records are indicated by asterisks. Also shown are rough estimates of u correlation scales and the standard deviations, σ, of τ^y for each month.

periods examined. During months in which correlation length scales are long, all moorings tend to be highly correlated with local wind stress (Table 4.4). Conversely during months when correlation length scales are short some or most moorings are less well correlated with along-shelf wind stress. Because wind stress variability, as indicated by its standard deviation, remains similar through most of the experiment, lower correlations of near-surface u with along-shelf wind stress are attributed not to a weakening of wind stress, but to the greater importance of other processes in mid-January through early February and April.

Between mid-January and early February, near-surface u is well correlated between moorings NCCCS C3 and SMILE C3 and M3 but not between G3 and the other moorings. This suggests a break in cross-shelf circulation between the northern and southern parts of the study area rather than a general increase in short scale u fluctuations. This along-shelf variability is marked by a three-dimensional heat balance between January 30 and February 12 (chapter 2, Fig. 2.9) and by a strongly three-dimensional mass balance as indicated by depth-averaged cross-shelf flow at C3 between January 30 and February 20 (chapter 3, Fig. 3.3 and 3.5). This depth-averaged cross-shelf flow, which is uncorrelated with the wind (chapter 3, Table 3.1), also probably reduces along-shelf correlations of near-surface u between early February and early March (Fig. 4.9) as shifting the start and stop times of the 28 day

periods shows reduced along-shelf correlation scales (and correlations with along-shelf wind stress) are most evident from from late January to mid-February and increase again in late February.

During April, correlation scales are reduced probably by the presence of a mesoscale feature over much of the shelf. This feature, described by *Largier et al.* [1993], originates from offshore as indicated by its high temperature and low salinity [*Alessi et al.*, 1991]. It is responsible for strong equatorward flow over the study area despite the absence of strong wind forcing (Fig. 4.8), and it affects both the near-surface circulation and the heat and salt balances (chapter 2, Fig. 2.10). Similar features have been observed at different times in previous years [*e.g. Lentz*, 1987*b*].

Largier et al. [1993] postulate oceanic mesoscale features may commonly occur over the northern California shelf and that they are a significant source of forcing for shelf circulation at periods longer than 10 days for which wind stress variance is low. During the winter 1988–1989, along-shelf wind stress variance is concentrated at periods between 2.5 and 10 days (see Fig. 3.4 in chapter 3). If wind stress forcing constitutes the predominant source of forcing at these periods and oceanic mesoscale variability constitutes the source of forcing for longer periods, then spatial coherence of near-surface u should be highest in the wind band as there is no reason to expect oceanic mesoscale forcing to be two-dimensional. Fig. 4.10 lends support to this idea. Both coherence with the wind stress and along-shelf coherence are largest in the wind-forced band and decline for longer periods where oceanic mesoscale forcing may be important.

The idea that the longest spatial scales of near-surface u are associated with wind stress forcing is also supported by Empirical Orthogonal Functions (EOF's) of near-surface u during SMILE and NCCCS. The along-shelf structures and time series of the near-surface u EOF's are shown in Figs. 4.11 and 4.12. The lowest mode, which accounts for 57% of the variance, is highly correlated (0.76) with along-shelf wind stress and is important throughout the November to May time period. Higher modes have more complex spatial structures and are uncorrelated with the wind stress. They become important on time scales of weeks when correlation scales are reduced.

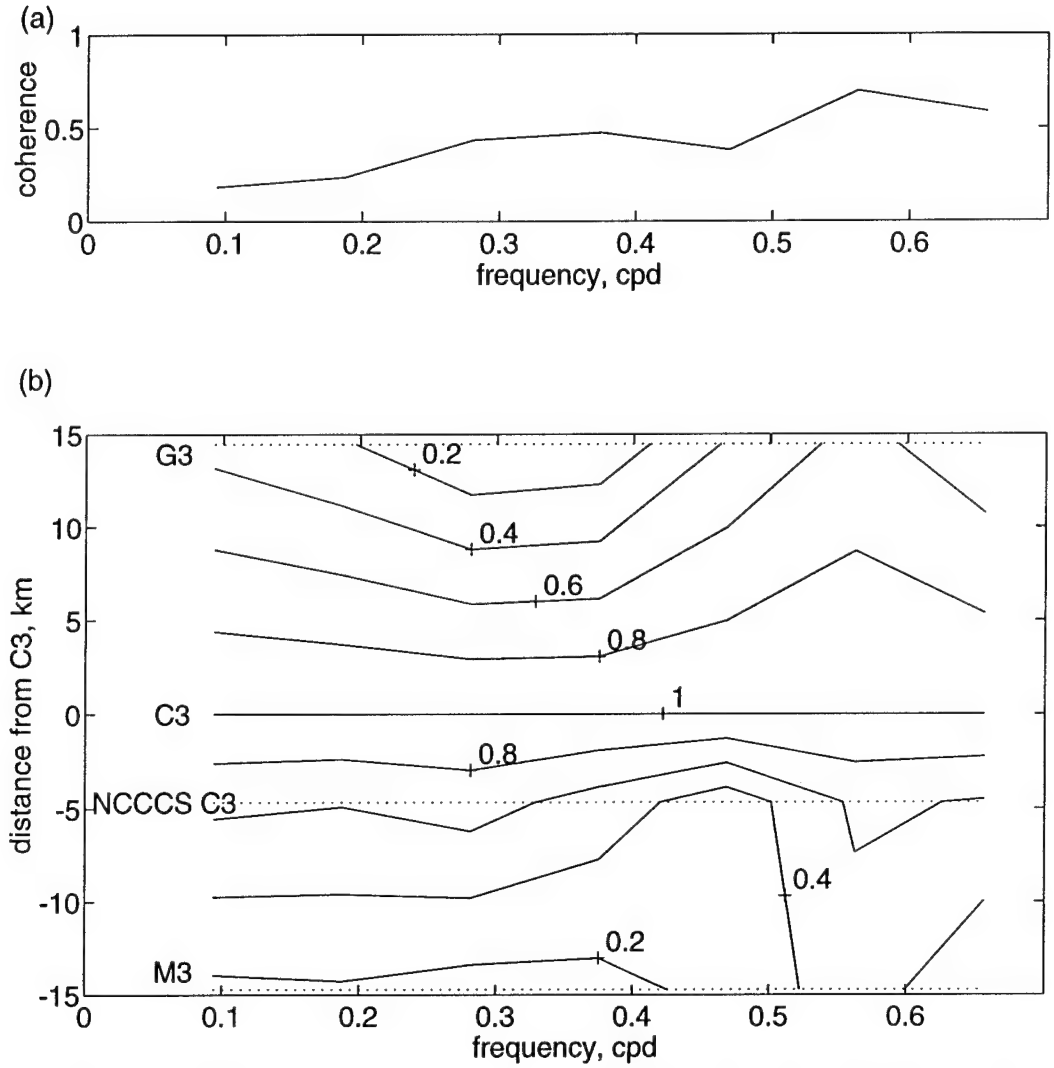

Figure 4.10. (a) Coherence of near-surface u at C3 with τ^y. Coherence of other near-surface u records with τ^y also decline with decreasing frequency. (b) coherence of near-surface u with distance from C3. The 90% confidence level is 0.45 and the 95% confidence level is 0.50.

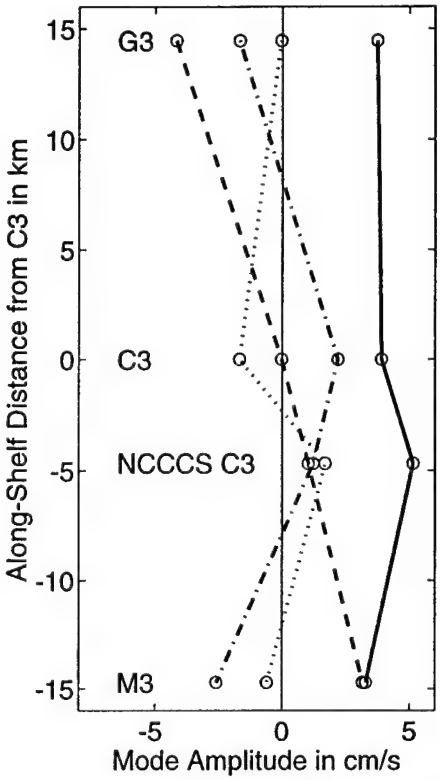

Figure 4.11. Along-shelf structure of near-surface u EOF's. The solid line indicates mode 1 which accounts for 57% of the total variance. Modes 2, 3, and 4, indicated by the dashed, dash-dotted, and dotted lines, account for 24%, 13% and 5% of the total variance respectively.

Modes 2 and 3 become important during January and early February. Together they represent u fluctuations at G3 (in January) and C3 and NCCCS C3 (in February). Mode 2 again becomes important in late April when it represents offshore flow at M3 at onshore flow at G3. The time scales of the higher modes, their intermittent nature, and lack of correlation with wind stress all suggest they are not associated with wind forcing.

4.5.2 Monthly variation in cross-shelf velocity correlation between SMILE C3 and NCCCS C3

Velocity measurement at most SMILE and NCCCS moorings was limited to the near-surface (10 m). However the central C3 site was instrumented at near-surface, mid-depth, and near-bottom depths during NCCCS and was instrumented in the

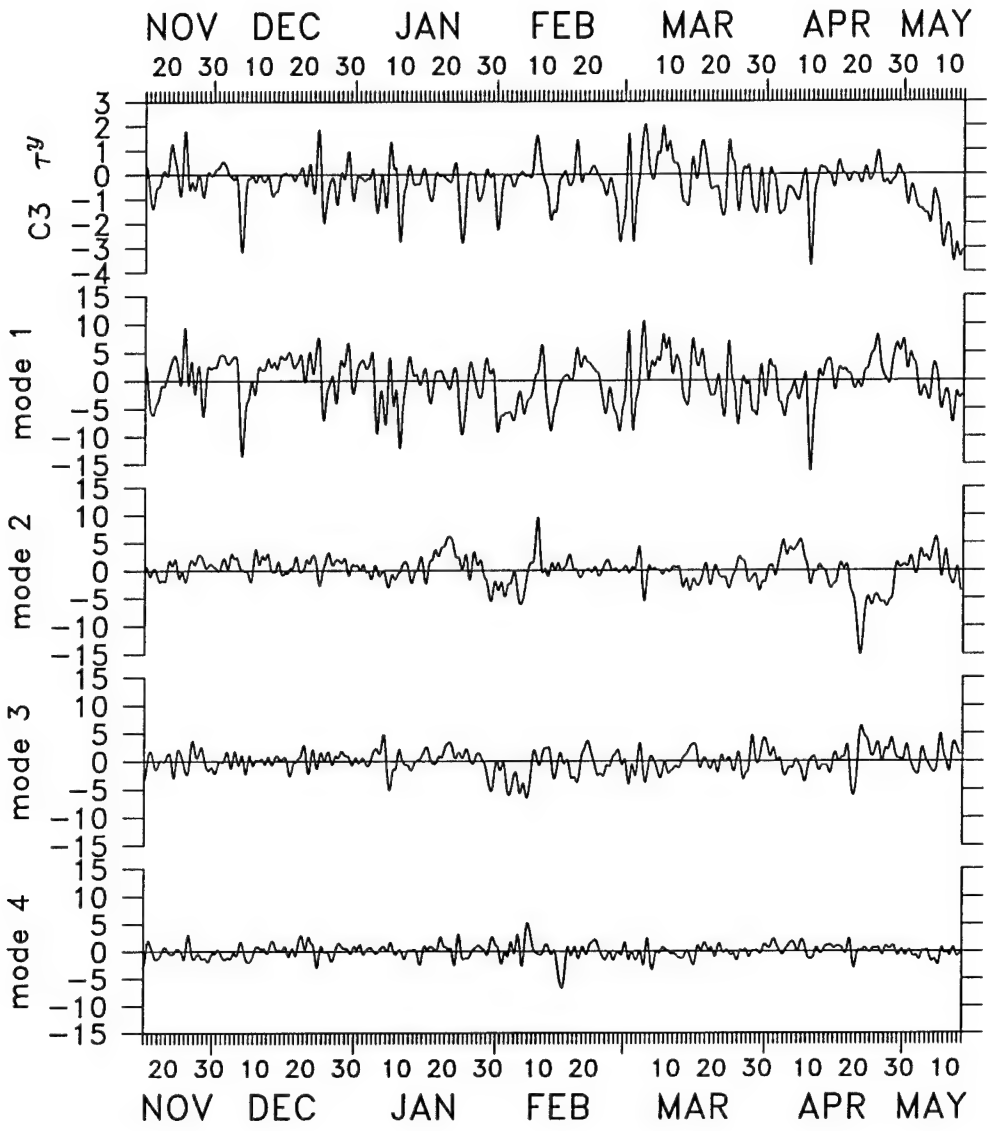

Figure 4.12. Time series of τ^y (dyn/cm^2) and near-surface u (cm/s) EOF modes. To lengthen the EOF time series into late April, the time series at C3 has been extended by patching the 7 and 10 m time series together. The correlation coefficient of mode 1 with τ^y at C3 is 0.76. Higher modes are uncorrelated with τ^y.

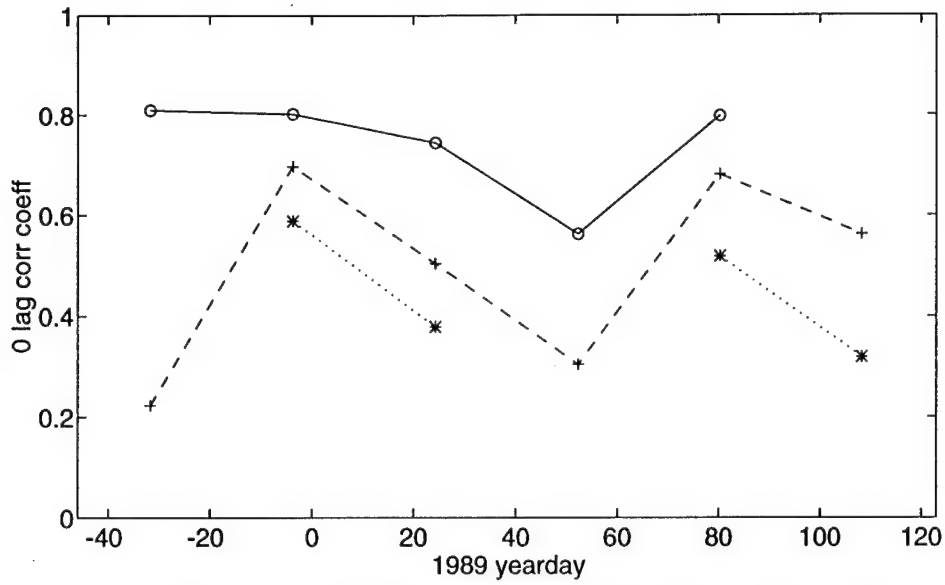

Figure 4.13. Correlations of cross-shelf velocity, u, for near surface, mid-depth, and near-bottom measurements for 6 one month periods between November, 1988 and May, 1989.

near-surface and mid-depths during SMILE and near-bottom during STRESS. The C3 sites of NCCCS and SMILE and STRESS were located approximately 4 km apart in the along-shelf direction. These moorings provide an opportunity to examine correlation in the along-shelf direction for near-surface, mid-depth and near-bottom depths. Correlations between these two sites (Fig. 4.13) showed near-surface correlations were the highest and that monthly trends in correlations were the same at all depths. This indicates that the discussion concerning correlation scales of near-surface u may also be applicable to interior and near-bottom u.

4.6 Discussion

On wind-forced shelves, CTW's and Ekman theory have been compared quantitatively with observed interior [*e.g.*, *Chapman*, 1987] and boundary layer flows [*e.g.*, chapter 3 and *Lentz*, 1992]. Both CTW's and Ekman theory imply definite correlation scales for u and v. *Brink et al.* [1987] and more recently *Brink et al.* [1994] have examined the scales of motion implied by full (*i.e.*, no long-wave assumption) CTW's for interior u and v. They found v is resonant for low wavenumber along-shelf wind

stress variability implying correlation scales of 100–200 km. The physics of CTW's lead to interior v velocities which are much larger than v velocities forced directly by surface and bottom stresses so that the wind-forced v is dominated by the CTW response throughout the water column. Though interior u exhibits a similar resonance for low wave numbers, it is more sensitive to high wave number (non-resonant) along-shelf wind stress with scales of 15 km or less, implying similarly short correlation scales for interior u. However, unlike v, the character of the total u is not determined by interior flow. Cross-shelf boundary transports are the same magnitude as interior cross-shelf transports and, because they are confined to relatively thin boundary layers, the velocities associated with them are greater than interior u's (see chapter 3). Therefore, in the absence of other processes, theoretical u correlation scales within the surface and bottom boundary layers should reflect those of surface along-shelf wind stress, and interior v. Over the northern California shelf, these have along-shelf correlation scales of 100 km or more and over 60 km respectively (Figs. 4.3 and 4.4).

Correlations of v estimated in this study and previously [*Winant et al.*, 1987] over the northern California shelf and elsewhere [*Kundu and Allen*, 1976] are in many ways consistent with those expected from CTW's. The correlation scale of v estimated here, though almost certainly less than the limits implied by CTW's, is greater than 60 km. Maximum lagged v along-shelf correlation coefficients, though often very near 0 lagged correlation coefficients, tend to exhibit behavior consistent with CTW's in that southern velocity records generally lead northern velocity records by about 3 to 12 hours (Table 4.2). Application of CTW's is limited to the mid and outer shelf where surface and bottom boundary layers can be considered thin. The increasing importance of mesoscale processes offshore and the cross-shelf structure of CTW modes on the northern California shelf [*Chapman*, 1987] would suggest along-shelf correlation scales decrease offshore. In this study, examination of along-shelf correlation scales of v was limited to CODE-2 observations between 60 and 130 m. Within this region, little cross-shelf variation in along-shelf v correlations is evident except for near-surface observations where along-shelf v correlations at the 130 m isobath are reduced slightly relative to those at the 60 and 90 m isobaths. This is a possible

indication that mesoscale processes are more important near the surface.

In the cross-shelf direction, v is generally correlated from 60 to 130 m. Despite its smaller magnitude and possible effects of local bathymetry, inner shelf v (30 m) is also significantly correlated out to the mid-shelf (90 m), arguing for a similar response in v to wind-forcing over much of the shelf. Maximum lagged v cross-shelf correlations tend to exhibit behavior consistent with two-dimensional upwelling models in that inshore velocity records generally lead offshore velocity records (Table 4.3), suggesting a more rapid response to wind forcing in shallow water.

Along-shelf correlation scales of u are much shorter than those of v and were best resolved by near-surface measurements during SMILE and NCCCS. Along the 90 m isobath, near-surface u correlation scales are 15–20 km, and along-shelf interior and near-bottom u correlation scales are greater than 4 km but less than 25 km. Near-surface and near-bottom along-shelf scales of u are substantially less than those of along-shelf wind stress and interior along-shelf velocity which set the scales of u in models of surface and bottom boundary layers. Figs. 4.8, 4.9, 4.10, and 4.12 and Table 4.4 all suggest wind forcing is associated with the longest scales of near-surface u in winter and spring and that other processes act to reduce correlation scales on periods of several weeks to one month (Figs. 4.8 and 4.9 and Table 4.4). The time scales and spatial structures of variability in short-scale u are consistent with those of mesoscale features which compete with wind forcing as a driving mechanism for u. The similar time variation of correlations between two nearby moorings at near-surface, middle, and near-bottom locations (Fig. 4.13) suggests the processes which act to reduce near-surface u correlation are also important throughout the water column. The importance of short-scale wind stress in reducing correlation scales of interior u remains uncertain. Though interior u scales are similar to the predicted scales for interior u in *Brink et al.'s* [1994] stochastic model which includes the effects of an estimated short-scale (down to 10 km) wind stress, *Brink et al.* [1994] point out that observed interior u fluctuations are more energetic than predictions of their linear model, and that the true energy present in short-scale wind stress is unknown.

Examination of u along-shelf correlation scales was limited to the period between

November, 1988 and May, 1989. This period covered the winter and spring storm season and ended days after the spring transition to upwelling; hence the applicability of the above observations to u correlation scales in the summer (upwelling) season is uncertain. Section 4.4 showed that for some periods of one month or more, along-shelf correlation scales were at least 30 km, the maximum along-shelf mooring separation in SMILE. Though 30 km is the minimum along-shelf mooring separation during CODE-2, making it difficult to compare spatial scales, a similar treatment of summer CODE-2 data revealed no time when correlation scales were as great as 30 km. This suggests the possibility of seasonal (or interannual) variation in along-shelf scales of near-surface u. Seasonal variability could be due to greater offshore mesoscale activity in the summer [*Kosro et al.*, 1991] which would tend to shorten correlation length scales in summer. Offshore mesoscale variability in summer may or may not be related to instability of an upwelling front. *Barth* [1994] examined the development of frontal instabilities and found the time scale for development of a short wavelength (20 km) baroclinic instability was about 1.5 days. In winter, wind forcing events tend to be relatively brief and do not lead to the development of an upwelling front. After the spring transition to upwelling, a front develops and moves offshore. Instabilities associated with this front, and with later fronts caused by wind stress relaxation and subsequent upwelling, could be a source of three-dimensional variability in summer. In this way, persistent upwelling favorable winds may be an indirect source of short correlation length scales. Seasonal or interannual variation in the spatial scales of wind stress could also lead to variation in u correlation scales as the work of *Brink et al.* [1994] suggests. Examination of Fig. 4.3 shows along-shelf wind stress is highly correlated over distances of up to 130 km for both SMILE and CODE-2, however the different along-shelf positions of the SMILE and CODE-2 moorings make a detailed comparison of wind stress correlations inconclusive.

Cross-shelf correlation scales of u are about 10 km. These correlation scales extend over a substantial portion of the northern California shelf and are only about 5 km less than the cross-shelf correlation scales of v. There is some indication that u is more weakly correlated from the inner to the mid-shelf (60 to 90 m, a distance of

$\sim$ 5 km) than from the mid-shelf to the outer shelf (90 to 130 m, a distance of $\sim$ 8 km). Because we expect offshore mesoscale features to reduce correlation scales over the outer rather than inner-shelf, it's likely some other process is responsible for this. As most of the observations used in Table 4.3 come from summer, one reasonable explanation is near-shore variability caused by relaxation from upwelling [*Send et al.*, 1987]. Relaxation from upwelling occurs in summer when the normally persistent equatorward winds weaken or even cease for periods of 7–10 days. During these times, northward advection of warm saline water from Pt. Reyes occurs in a wedge along the coast. This wedge is confined primarily to the inner-shelf and mid-shelf locations and could cause a break in the character of the flow field between the 60 and 90 m isobaths. Three-dimensional variability caused by relaxation from upwelling could overwhelm the wind-driven signal especially over the inner-shelf where two-dimensional wind-driven models suggest the magnitude of wind-driven u is reduced relative to deeper water by the overlap of surface and bottom stresses [*Mitchum and Clarke*, 1986; *Lentz*, 1994].

4.7 Summary

Correlations of subtidal cross-shelf (u) and along-shelf (v) velocities are estimated as a function of along-shelf and cross-shelf distance using moored velocity time series from several field programs over the northern California shelf. Distances over which velocities are significantly correlated are termed correlation scales.

Over periods of 4–6 months, correlation scales of v are resolved in both the along-shelf and cross-shelf directions. In the along-shelf direction, v is significantly correlated for distances greater than 60 km, the maximum mooring separation. In the cross-shelf direction, v is generally correlated between the 60 and 130 m isobaths (10–15 km). Correlations of v show little dependence on instrument depth; subsurface v is perhaps more highly correlated than surface v.

Correlation scales of u over periods of 4–6 months are much smaller than those of v and are often not resolved by minimum mooring separations. Moorings deployed

in SMILE and NCCCS do resolve along-shelf correlation scales of near-surface u and indicate they are 15–20 km. Along-shelf correlation scales of subsurface u are not well resolved by available data, but are less than 25 km. In the cross-shelf direction, u correlation scales are approximately 10 km. There is some indication that u is more highly correlated between the 90 and 130 m isobaths than between the 60 and 90 m isobaths.

To investigate further the processes which determine along-shelf correlation scales of u, SMILE and NCCCS records from November, 1988 to May, 1989 were examined in greater detail. Monthly variation of correlation scales was compared to correlation with along-shelf wind stress, the heat balance, and other descriptive information about shelf circulation. During several months, the along-shelf correlation scale of near-surface u was at least 30 km, the maximum mooring separation, and it was always greater than 4 km, the minimum mooring separation. Along-shelf correlation scales were generally long when correlation of velocity with wind stress was high and short when correlation with wind stress was low. Short correlation scales coincided with three-dimensional heat balances. During April, 1989, short correlation scales coincided with the intrusion of an offshore mesoscale feature onto the shelf. Along-shelf correlations of near-surface, mid-depth, and near-bottom u between two nearby (4 km) sites showed near-surface correlations were highest but that monthly trends in correlations were similar at all depths.

Chapter 5

Conclusions

The goals of this thesis were to examine the applicability of the two-dimensional conceptual model of wind-driven upwelling to observed subtidal u and to gain insight into seasonal variability on the northern California shelf. To accomplish these goals, I estimated the heat and salt balances in winter and spring (chapter 2), compared a simple analytic model of cross-shelf transport to observed cross-shelf transport at a mid-shelf mooring site (chapter 3), and estimated the correlation scales of subtidal velocity with a focus on the u component (chapter 4). Detailed conclusions for each of these studies are presented in chapters 2, 3, and 4. The purpose here is to interpret the results of previous chapters in terms of the broader goals laid out in chapter 1. I will comment on the seasonal variability of wind forcing and u, the effects of mesoscale features on u, and the general applicability of a two-dimensional wind-forced conceptual model for u. I will end chapter 5 by discussing implications for future work.

5.1 Seasonal variability

Cross-shelf circulation was examined using data from several field programs on the northern California shelf. The two time periods which were examined most closely were the winter and spring of 1988–1989 and the summer of 1982. Data from the Shelf Mixed Layer Experiment (SMILE), Sediment Transport Events over the Shelf and

Slope (STRESS) study, and Northern California Coastal Circulation Study (NCCCS) were used to examine the heat and salt balances in the winter and spring of 1988–1989 and the cross-shelf circulation in the winter 1988–1989. Data from the Coastal Ocean Dynamics Experiment (CODE-2) were also used to examine cross-shelf circulation in the summer of 1982. The winter/spring and summer periods give an opportunity to explore seasonal variability in cross-shelf circulation over the northern California shelf.

One obvious source of seasonal variability is the wind stress (Fig. 3.4). In winter and spring, wind stress over the northern California shelf is distinguished by the passage of low pressure systems which cause poleward and equatorward fluctuating winds on time scales of days. In summer, it is distinguished by the establishment of strong upwelling favorable winds which persist for several weeks, separated by periods of weak wind stress (relaxation events) which may last a week or longer [*Halliwell and Allen*, 1987 ; *Strub et al.*, 1987; *Beardsley et al.*, 1987].

The effect of wind stress forcing is especially clear on the near-surface u which is primarily due to the wind-forced surface Ekman transport [*Lentz*, 1992]. In winter, near-surface u is distinguished by weak mean offshore flow and fluctuations on time scales of days (Figs. 3.2 and 3.3). In summer, it is distinguished by strong mean offshore flow and fluctuations on time scales of weeks [*Winant et al.*, 1987]. These seasonal differences are also present in the cross-shelf heat fluxes (Figs. 2.7, 2.8, 2.9, and 2.10 and *Lentz* [1987*b*]) and the modelled surface mixed layer transports (Figs. 3.5 and 3.7).

The effects of seasonal variability of wind stress forcing on interior u are less certain. The simple wind-forced model adopted in chapter 3 offers some insight. This model has a frictional time scale of about four days and predicts that for winter wind forcing, which has time scales shorter than this, the subsurface response should be strongest in the interior rather than bottom boundary layer. Winter observations seem to confirm this, and an interior onshore flow occurs on several occasions in response to wind-driven near-surface offshore flow (Figs. 3.5 and 3.6). In contrast, little evidence of a wind-forced interior cross-shelf transport is seen in summer (Figs 3.7

and 3.8). The dominant time scales of summer wind forcing are longer than the model friction time scale and lead to a subsurface model response which is primarily in the bottom boundary layer rather than interior. Though model agreement with subsurface observations is poorer in summer than in winter, the observed depth-dependent near-bottom flow in summer is more energetic than in winter and is correlated with the modelled near-bottom transport (Figs. 3.6 and 3.8 and Table 3.3).

Seasonal variability in wind stress almost certainly has effects on the cross-shelf velocity beyond those represented by the locally wind-forced model adopted in chapter 3. Coastal-trapped waves (CTW's) forced by remote winds determine a large portion of the along-shelf velocity, particularly in summer [*Chapman*, 1987]. Along-shelf velocity affects near-bottom cross-shelf velocity which, in the context of a two-dimensional volume balance, influences interior and near-surface velocities. CTW's can be accounted for in a two-dimensional model by adopting a local plus remote approach as *Lopez and Clarke* [1989] and *Zamudio and López* [1994] do. A more sophisticated two-dimensional model could also account for baroclinic pressure gradients which affect the vertical structure of velocity and frictional coupling between interior and near-bottom transports. However, other effects of seasonal wind stress variability cannot be accounted for by a two-dimensional linear model. For example, persistent upwelling favorable wind stress may increase the importance of non-linear dynamics and interior shear stress. Through such processes as development of an upwelling front [*de Szoeke and Richman*, 1984] and subsequent instability [*Barth*, 1994], persistent wind stress forcing may lead to a fundamentally three-dimensional cross-shelf circulation in summer. If this is the case, then more complicated numerical models which retain the assumption of two-dimensionality are unlikely to offer much improvement in agreement with u observations over the simple model applied in chapter 3.

One especially intriguing difference between winter SMILE and STRESS observations and summer CODE-2 observations is the character of the depth-averaged u. In winter, the mean depth-averaged u (Fig. 3.2) is zero to within our ability to define a cross-shelf direction, and fluctuations in depth-averaged u are smaller than the

interior return flow over much of the winter (Fig 3.5). In summer, the mean depth-averaged u is non-zero, and fluctuations in depth-averaged u overwhelm any onshore return flow associated with offshore surface Ekman transport (Fig. 3.7). The relationship of depth-averaged u to wind forcing is unclear. In winter, it is uncorrelated with local wind forcing (Table 3.1), but it's interesting to note that during several strong upwelling events in summer, the depth-averaged u is offshore (Fig. 3.7). This may be coincidence, the influence of local topography, or some other as yet unknown process.

5.2 The role of mesoscale variability

Though much of the variability in u is consistent with wind forcing, mesoscale variability cannot be neglected. The exact spatial structure and causes of mesoscale variability cannot be resolved with the available observations, but it does display a number of characteristics which distinguish it from wind-driven variability. Mesoscale variability is episodic rather than continuous at the mid-shelf C3 location. It contributes to three-dimensional variability in the winter and spring heat and salt balances (Figs. 2.7, 2.8, 2.9, and 2.10) and the summer heat balance [*Lentz*, 1987*b*] during several periods which last one to two weeks rather than continuously. When mesoscale variability becomes important, it reduces along-shelf correlation scales of near-surface u from greater than 30 km to 5–10 km (Fig. 4.9). Mesoscale variability is most important at frequencies less than 0.3 cpd where wind forcing is relatively weak and is not coherent with near-surface cross-shelf velocity (Fig. 4.10). This may account for the greater low-frequency energy in observed cross-shelf transports relative to those in the wind-driven model.

Largier et al. [1993] identify low frequency variability with offshore mesoscale forcing and contour low frequency variability as a function of cross-shelf position for several locations along the northern California shelf. They show it is greatest from the outer-shelf to about the 90 m isobath. The same plot shows it is also surface intensified, and hence has a strong baroclinic component. Seasonal variability may

also play a role in mesoscale forcing as *Kosro et al.* [1991] find mesoscale variability within the Coastal Transition Zone (CTZ) to be greatest in summer. This may help to explain the greater success of the two-dimensional cross-shelf transport model in winter relative to summer.

5.3 Applicability of a two-dimensional model of u

Chapter 3 contains one of the principal thesis results; during periods in winter, a simple two-dimensional locally wind-forced model can describe the most basic vertical structure of cross-shelf transport on the northern California shelf. This result is supported by the fluctuating heat and salt balances and by the along-shelf correlation scales of near-surface u during this time. Comparison between winter and summer clearly demonstrates this model is most appropriately applied under the conditions which prevail in winter when the depth-averaged u is generally weak and the dominant wind forcing occurs on time scales of days rather than weeks, however other questions as to the model's applicability also arise.

The cross-shelf transport model was applied in both summer and winter to a mid-shelf site approximately 6 km from the coast in a water depth of $\sim$90 m. This site satisfied the model assumption that separate surface and bottom boundary layers exist and was close enough to the coast that a two-dimensional volume balances could be applied in winter. Over how great a region of the shelf can such a model be expected to apply? The outer and inner-shelf limits over which this model is applicable are probably set by offshore mesoscale processes and the merging of surface and bottom boundary layers respectively. Over the northern California shelf, cross-shelf correlation scales suggest the processes which describe cross-shelf flow over the 90 m isobath are also important between the 130 m and 60 m isobaths, a cross-shelf distance of approximately 10 km.

Extension of the locally wind-forced cross-shelf transport model to areas beyond

the northern California shelf is another natural question. The wind forcing and narrow, straight shelf off the northern California coast are fairly typical of much of the North American Pacific coast, and I expect the model has a similar applicability over this region. Moreover, nearly all shelves are subject to wind forcing, so the model may give some insight into u caused by brief, strong wind-forced events such as those from storms. For example, *Janowitz and Pietrafesa* [1980] applied essentially the same model over the North Carolina shelf with some success. One limitation on the geographic applicability of the model is its assumption of Ekman transport within boundary layers. This restricts its use at low latitudes where the inertial period may be longer than much of the wind forcing. For example, along the Peruvian shelf at 15°S, the inertial period is approximately 46 hrs. If, as along the northern California coast, only periods longer than twice the inertial period are considered, the model forcing would be restricted to periods longer than 92 hrs and preclude much of the wind-forced variability.

5.4 Future work

This work has focussed on the two-dimensional linear response of u to local wind-forcing. Winter observations indicate there are time periods when this response is an important part of the observed cross-shelf circulation, but spring and summer observations demonstrate the complicated nature of u. Two useful areas of further theoretical investigation may be the non-linear response of u to wind forcing and the response of u to other processes such as remotely generated mesoscale features. These investigations could include numerical studies of the response of u to the different types of wind forcing which characterize winter and summer on the northern California shelf, as well as further studies of eddy interaction with the continental shelf.

This work also raises a number of observational questions. Chapter 4 has shown that along-shelf correlation scales of subtidal u over six months in winter and spring are in the 15–20 km range. These correlation scales vary on time periods of one

month, depending on the presence or absence of mesoscale variability. At times, u is significantly correlated to separations of 30 km (the maximum mooring separation distance in SMILE and NCCCS) and shows little evidence of decrease with separation. This implies correlation scales are greater than 30 km during periods in winter and spring and the maximum along-shelf correlation scales for near-surface u are unknown. However, summer observations indicate u along-shelf correlation scales are always under 30 km (the minimum mooring separation distance in CODE-2). The apparent difference in u along-shelf correlation scales raises the question of seasonal variability, but the mismatch in summer and winter mooring separations means the results in chapter 4 could not resolve the issue. Additionally, the study of monthly variability in along-shelf correlation scales in SMILE and NCCCS was limited mostly to the near-surface u by mooring coverage. Questions regarding seasonal variability in along-shelf correlation scales of u in the near-surface and below could be addressed on the northern California shelf using a mooring array similar to that designed by *Winant* [1983] with along-shelf separations near 5 km and modest vertical coverage. Such an array would allow us to further examine the processes which determine three-dimensional variability in u.

References

Alessi, C. A., S. J. Lentz, and R. C. Beardsley, The Shelf MIxed Layer Experiment (SMILE): Program overview and moored and coastal array data report. *WHOI Tech. Rep. 91-39*, 211 pp., Woods Hole Oceanogr. Inst., Woods Hole, Mass., 1991.

Allen, J. S., Models of wind-driven currents on the continental shelf. *Annu. Rev. Fluid Mech.*, *12*, 389–433, 1980.

Allen, J. S., and P. K. Kundu, On the momentum, vorticity and mass balance on the Oregon shelf. *J. Phys. Oceanogr.*, *8*, 13–27, 1978.

Allen, J. S., R. C. Beardsley, J. O. Blanton, W. C. Boicourt, B. Butman, L. K. Coachman, A. Huyer, T. H. Kinder, T. C. Royer, J. D. Schumacher, R. L. Smith, W. Sturges, and C. D. Winant, Physical oceanography of continental shelves. *Rev. Geophys. and Space Phys.*, *21*, 1149–1181, 1983.

Badan-Dangon, A., On the dynamics of subinertial currents off northwest Africa. Ph.D. dissertation, Oregon State University, Corvallis, Ore., 1981.

Badan-Dangon, A., K. H. Brink, and R. L. Smith, On the dynamical structure of the mid-shelf water column off northwest Africa. *Cont. Shelf Res.*, *5*, 629–644, 1986.

Barth, J. A., Short-wavelength instabilities on coastal jets and fronts. *J. Geophys. Res.*, *99*, 16095–16115, 1994.

Beardsley, R. C., and S. J. Lentz, The Coastal Ocean Dynamics Experiment collection: An introduction. *J. Geophys. Res.*, *92*, 1455–1464, 1987.

Brink, K. H., The near-surface dynamics of coastal upwelling. *Prog. Oceanog.*, *12*, 223–257, 1983.

Brink, K. H., Coastal-trapped waves and wind-driven currents over the continental shelf. *Annu. Rev. Fluid Mech.*, *23*, 389–412, 1991.

Brink, K. H., D. Halpern, and R. L. Smith, Circulation in the Peruvian upwelling system near 15°S. *J. Geophys. Res.*, *85*, 4036–4048, 1980.

Brink, K. H., D. C. Chapman, and G. R. Halliwell, Jr., A stochastic model for wind-driven currents over the continental shelf. *J. Geophys. Res.*, *92*, 1783–1797, 1987.

Brink, K. H., J. H. LaCasce, and J. D. Irish, The effect of short-scale wind variations on shelf currents. *J. Geophys. Res.*, *99*, 3305–3314, 1994.

Brown, W. S., J. D. Irish, and C. D. Winant, A description of subtidal pressure field observations on the northern California continental shelf during the coastal ocean dynamics experiment. *J. Geophys. Res.*, *92*, 1605–1635, 1987.

Bryden, H. L., D. Halpern, and R. D. Pillsbury, Importance of eddy heat flux in a heat budget for Oregon coastal waters. *J. Geophys. Res.*, *85*, 6649–6653, 1980.

Chapman, D. C., Application of wind-forced, long, coastal-trapped wave theory along the California coast. *J. Geophys. Res.*, *92*, 1798–1816, 1987.

Chen, D., Dynamics of time-variable coastal upwelling. Ph.D. thesis, 83 pp., State Univ. of New York at Stony Brook, 1990.

Chen, D., and D-P. Wang, Simulating the time-variable coastal upwelling during CODE-2. *J. Marine Res.*, *48*, 335–338, 1990.

Csanady, G. T., *Circulation in the Coastal Ocean*, 279 pp., D. Reidel Publishing Company, Dordrecht, 1982.

Davis, R. E., and P. S. Bogden, Variability on the California shelf forced by local and remote winds during the coastal ocean dynamics experiment. *J. Geophys. Res.*, *94*, 4673–4783, 1989.

de Szoeke, R. A., and J. G. Richman, On wind-driven mixed layers with strong horizontal gradients– a theory with application to coastal upwelling. *J. Phys. Oceanogr.*, *14*, 364–377, 1984.

Dever, E. P., and S. J. Lentz, Heat and salt balances over the northern California shelf in winter and spring. *J. Geophys. Res.*, *99*, 16001–16017, 1994.

Dickey, T. D., and J. C. Van Leer, Observations and simulation of a bottom Ekman layer on a continental shelf. *J. Geophys. Res.*, *89*, 1983–1988, 1984.

EG&G, Inc., Northern California Coastal Circulation Study data report no. 2: Main measurement program, March–August 1988, *Oceanogr. Serv. Rep. NCCCS-89-17*, 2 vol., 442 pp., Washington Anal. Serv. Cent., Waltham, Mass., Sept. 1989.

EG&G, Inc., Northern California Coastal Circulation Study data report no. 3: Main measurement program, August 1988–March 1989, *Oceanogr. Serv. Rep. NCCCS-90-4*, 2 vol., 344 pp., Washington Anal. Serv. Cent., Waltham, Mass., March 1990*a*.

EG&G, Inc., Northern California Coastal Circulation Study data report no. 4: Main measurement program, March–October 1989, *Oceanogr. Serv. Rep. NCCCS-90-5*, 2 vol., 326 pp., Washington Anal. Serv. Cent., Waltham, Mass., Aug. 1990*b*.

Fredericks, J. J., J. H. Trowbridge, A. J. Williams III, S. J. Lentz, B. Butman, and T. F. Gross, Fluid mechanical measurements within the bottom boundary layer over the northern California continental shelf during STRESS. *WHOI Tech. Rep. 93-32*, 116 pp., Woods Hole Oceanogr. Inst., Woods Hole Mass., 1993.

Friehe, C. A., and K. F. Schmitt, Parameterization of air-sea heat fluxes of sensible heat and moisture by bulk aerodynamical formulas. *J. Phys. Oceanogr.*, *6*, 801–809, 1976.

Grant, W. D., A. J. Williams, and S. M. Glenn, Bottom stress estimates and their prediction on the northern California continental shelf during CODE-1: the importance of wave-current interaction. *J. Phys. Oceanogr.*, *14*, 506–527, 1984.

Gross, T. F., A. E. Isley, and C. R. Sherwood, Estimation of stress and bed roughness during storms on the northern California shelf. *Cont. Shelf Res.*, *12*, 389–413, 1992.

Halliwell, G. R. and J. S. Allen, The large scale coastal wind field along the west coast of North America, 1981–1982. *J. Geophys. Res.*, *92*, 1861–1884, 1987.

Halpern, D., R. L. Smith and E. Mittelstaedt, Cross-shelf circulation on the continental shelf off northwest Africa during upwelling. *J. Marine Res.*, *35*, 787–796, 1977.

Hickey, B. M. and N. E. Pola, The seasonal alongshore pressure gradient on the west coast of the United States. *J. Geophys. Res.*, *88*, 7623–7633, 1983

Huyer, A., Hydrographic observations along the CODE central line off northern California, 1981. *J. Phys. Oceanogr.*, *14*, 1647–1658, 1984.

Janowitz, G. S., and L. J. Pietrafesa, A model and observations of time-dependent upwelling over the mid-shelf and slope. *J. Phys. Oceanogr.*, *10*, 1574–1583, 1980.

Jenter, H. L., and O. S. Madsen, Bottom stress in wind-driven depth-averaged coastal flows. *J. Phys. Oceanogr.*, *19*, 962–974, 1989.

Kosro, P. M., Structure of the coastal current field off northern California during the coastal ocean dynamics experiment. *J. Geophys. Res.*, *92*, 1637–1654, 1987.

Kosro, P. M., A. Huyer, S. R. Ramp, R. L. Smith, F. P. Chavez, T. J. Cowles, M. R. Abbott, P. T. Strub, R. T. Barber, P. Jessen, and L. F. Small, The structure of the transition zone between coastal waters and the open ocean off northern California, winter and spring 1987. *J. Geophys. Res.*, *96*, 14707–14730, 1991.

Kundu, P. K., Ekman veering observed near the ocean bottom. *J. Phys. Oceanogr.*, *6*, 238–242, 1976.

Kundu, P. K., and J. S. Allen, Some three-dimensional characteristics of low-frequency current fluctuations near the Oregon coast. *J. Phys. Oceanogr.*, *6*, 181–199, 1976.

Kundu, P. K., and R. C. Beardsley, Evidence of a critical Richardson number in moored measurements during the upwelling season off northern California. *J. Geophys. Res.*, *96*, 4855–4868, 1991.

Large, W. G., and S. Pond, Open ocean momentum flux measurements in moderate to strong winds. *J. Phys. Oceanogr.*, *11*, 324–336, 1981.

Largier, J. L., B. A. Magnell, and C. D. Winant, Subtidal circulation over the northern California shelf. *J. Geophys. Res.*, *98*, 18147–18179, 1993.

Lentz, S. J., A description of the 1981 and 1982 spring transitions over the northern California shelf. *J. Geophys. Res.*, *92*, 1545–1567, 1987*a*.

Lentz, S. J., A heat budget for the northern California shelf during CODE 2. *J. Geophys. Res.*, *92*, 14491–14509, 1987*b*.

Lentz, S. J., The surface boundary layer in coastal upwelling regions. *J. Phys. Oceanogr.*, *22*, 1517–1539, 1992.

Lentz, S. J., Current dynamics over the northern California inner shelf. *J. Phys. Oceanogr.*, *24*, 2461–2478, 1994.

Lentz, S. J., Sensitivity of the inner-shelf circulation to the form of the eddy viscosity profile. *J. Phys. Oceanogr.*, *25*, 19–28, 1995.

Lentz, S. J., and D. C. Chapman, Seasonal differences in the current and temperature variability over the northern California shelf during the Coastal Ocean Dynamics Experiment. *J. Geophys. Res.*, *94*, 12571–12592, 1989.

Lentz, S. J. and J. H. Trowbridge, The bottom boundary layer over the northern California shelf. *J. Phys. Oceanogr.*, *21*, 1186–1201, 1991.

Limeburner, R. (Ed.), CODE-2: Moored array and large-scale data report, *WHOI Tech. Rep. 85-35*, 234 pp., Woods Hole Oceanogr. Inst., Woods Hole Mass., 1985.

Limeburner, R. and R. C. Beardsley, CTD observations off northern California during The Shelf MIxed Layer Experiment, SMILE, November 1988. *WHOI Tech. Rep. 91-25*, 272 pp., Woods Hole Oceanogr. Inst., Woods Hole, Mass., 1989*a*.

Limeburner, R. and R. C. Beardsley, CTD observations off northern California during The Shelf MIxed Layer Experiment, SMILE, February/March 1989. *WHOI Tech. Rep. 91-41*, 218 pp., Woods Hole Oceanogr. Inst., Woods Hole, Mass., 1989*b*.

Limeburner, R. and R. C. Beardsley, CTD observations off northern California during The Shelf MIxed Layer Experiment, SMILE, May 1989. *WHOI Tech. Rep. 91-42*, 239 pp., Woods Hole Oceanogr. Inst., Woods Hole, Mass., 1989*c*.

Lopez, M., and A. J. Clarke, The wind-driven shelf and slope water flow in terms of a local and remote response. *J. Phys. Oceanogr.*, *19*, 1092–1101, 1989.

Mitchum, G. T, and A. J. Clarke, The frictional nearshore response to forcing by synoptic scale winds. *J. Phys. Oceanogr.*, *16*, 934–946, 1986.

Nelson, C. S., Wind stress and wind stress curl over the California Current. *NOAA Tech. Rep. NMFS SSRF-714*, 87 pp., 1977.

Nelson, C. S., and D. M. Husby, Climatology of surface heat fluxes over the California Current region. *NOAA Tech. Rep. NMFS SSRF-763*, 155 pp., 1983

Payne, R. E., Albedo of the sea surface. *J. Atmos. Sci.*, *29*, 959–970, 1972.

Pedlosky, J., *Geophysical Fluid Dynamics*, 624 pp., Springer-Verlag, New York, 1979.

Richman, J. G., and A. Badan-Dangon, Mean heat and momentum budgets during upwelling for the coastal waters off northwest Africa. *J. Geophys. Res.*, *88*, 2626–2632, 1983.

Rosenfeld, L. (Ed.), CODE-1 moored array and large-scale data report, *WHOI Tech. Rep. 83-23*, 186 pp., Woods Hole Oceanogr. Inst., Woods Hole Mass., 1983.

Rudnick, D. L., and R. E. Davis, Mass and heat budgets on the northern California shelf. *J. Geophys. Res.*, *93*, 14013–14024, 1988.

Santala, M. J., Surface-referenced current meter measurements, Ph.D. thesis, Mass. Inst. of Technol./Woods Hole Oceanogr. Inst., Woods Hole, Mass., 1991.

Send, U., R. C. Beardsley, and C. D. Winant, Relaxation from upwelling in the Coastal Ocean Dynamics Experiment. *J. Geophys. Res.*, *92*, 1683–1698, 1987.

Send, U., The origin of eddy heat fluxes in the northern California upwelling regime. *J. Geophys. Res.*, *94*, 871-876, 1989.

Smith, R. L., A comparison of the structure and variability of the flow field in three coastal upwelling regions: Oregon, northwest Africa, and Peru. *Coastal Upwelling*, F. A. Richards Ed., Amer. Geophys. Union, pp. 107–118, 1981.

Simpson, J. J. , and C. A. Paulson, Mid-ocean observations of atmospheric radiation. *Q. J. R. Meteorolo. Soc.*, *105*, 487–502, 1979.

Strub, P. T. and C. James, Atmospheric conditions during the spring and fall transitions in the coastal ocean off western United States. *J. Geophys. Res.*, *93*, 15561–15584, 1988.

Strub, P. T., J. S. Allen, A. Huyer, R. L. Smith, and R. C. Beardsley, Seasonal cycles of currents, temperatures, winds, and sea level over the northeast Pacific continental shelf: 35°N to 48°N. *J. Geophys. Res.*, *92*, 1507–1526, 1987*a*.

Strub, P. T., J. S. Allen, A. Huyer, and R. L. Smith, Large scale structure of the spring transition in the coastal ocean off North America. *J. Geophys. Res.*, *92*, 1527–1544, 1987*b*.

Trowbridge, J. H., and S. J. Lentz, Asymmetric behavior of an oceanic boundary layer above a sloping bottom. *J. Phys. Oceanogr.*, *21*, 1171–1185, 1991.

Weatherly, G. L., and P. L. Martin, On the structure and dynamics of the oceanic bottom boundary layer. *J. Phys. Oceanogr.*, *8*, 557–570, 1978.

Weller, R. A., D. L. Rudnick, R. E. Payne, J. P. Dean, N. J. Pennington, and R. P. Trask, Measuring near-surface meteorology over the ocean from an array of surface moorings in the subtropical convergence zone. *J. Atmos. Ocean. Tech.*, *7*, 85–103, 1990.

Winant, C. D, Longshore coherence of currents on the southern California shelf during the summer. *J. Phys. Oceanogr.*, *13*, 54–64, 1983.

Winant, C. D., R. C. Beardsley, and R. E. Davis, Moored wind, temperature, and current observations made during Coastal Ocean Dynamics Experiments 1 and 2 over the northern California shelf and upper slope. *J. Geophys. Res.*, *92*, 1569–1604, 1987.

Winant, C. D., C. E. Dorman, C. A. Friehe, and R. C. Beardsley, The marine layer off northern California: an example of supercritical channel flow. *J. Atmos. Sci.*, *45*, 3588–3605, 1988.

Zamudio, L., and M. López, On the effect of the alongshore pressure gradient on numerical simulations over the northern California shelf. *J. Geophys. Res.*, *99*, 16117–16129, 1994.

DOCUMENT LIBRARY

Distribution List for Technical Report Exchange – May 1995

University of California, San Diego
SIO Library 0175C
9500 Gilman Drive
La Jolla, CA 92093-0175

Hancock Library of Biology & Oceanography
Alan Hancock Laboratory
University of Southern California
University Park
Los Angeles, CA 90089-0371

Gifts & Exchanges
Library
Bedford Institute of Oceanography
P.O. Box 1006
Dartmouth, NS, B2Y 4A2, CANADA

Commander
International Ice Patrol
1082 Shennecossett Road
Groton, CT 06340-6095

NOAA/EDIS Miami Library Center
4301 Rickenbacker Causeway
Miami, FL 33149

Research Library
U.S. Army Corps of Engineers
Waterways Experiment Station
3909 Halls Ferry Road
Vicksburg, MS 39180-6199

Institute of Geophysics
University of Hawaii
Library Room 252
2525 Correa Road
Honolulu, HI 96822

Marine Resources Information Center
Building E38-320
MIT
Cambridge, MA 02139

Library
Lamont-Doherty Geological Observatory
Columbia University
Palisades, NY z10964

Library
Serials Department
Oregon State University
Corvallis, OR 97331

Pell Marine Science Library
University of Rhode Island
Narragansett Bay Campus
Narragansett, RI 02882

Working Collection
Texas A&M University
Dept. of Oceanography
College Station, TX 77843

Fisheries-Oceanography Library
151 Oceanography Teaching Bldg.
University of Washington
Seattle, WA 98195

Library
R.S.M.A.S.
University of Miami
4600 Rickenbacker Causeway
Miami, FL 33149

Maury Oceanographic Library
Naval Oceanographic Office
Building 1003 South
1002 Balch Blvd.
Stennis Space Center, MS, 39522-5001

Library
Institute of Ocean Sciences
P.O. Box 6000
Sidney, B.C. V8L 4B2
CANADA

Library
Institute of Oceanographic Sciences
Deacon Laboratory
Wormley, Godalming
Surrey GU8 5UB
UNITED KINGDOM

The Librarian
CSIRO Marine Laboratories
G.P.O. Box 1538
Hobart, Tasmania
AUSTRALIA 7001

Library
Proudman Oceanographic Laboratory
Bidston Observatory
Birkenhead
Merseyside L43 7 RA
UNITED KINGDOM

IFREMER
Centre de Brest
Service Documentation - Publications
BP 70 29280 PLOUZANE
FRANCE

50272-101

REPORT DOCUMENTATION PAGE	1. REPORT NO. MIT/WHOI 95-16	2.	3. Recipient's Accession No.

4. Title and Subtitle
Subtidal Cross-Shelf Circulation on the Northern California Shelf

5. Report Date
June 1995

6.

7. Author(s)
Edward Paul Dever

8. Performing Organization Rept. No.

9. Performing Organization Name and Address
MIT/WHOI Joint Program in Oceanography/Applied Ocean Science & Engineering

10. Project/Task/Work Unit No.
MIT/WHOI 95-16

11. Contract(C) or Grant(G) No.
(C) OCE-91-15713
(G)

12. Sponsoring Organization Name and Address
the National Science Foundation

13. Type of Report & Period Covered
Ph.D. Thesis

14.

15. Supplementary Notes
This thesis should be cited as: Edward Paul Dever, 1995. Subtidal Cross-Shelf Circulation on the Northern California Shelf. Ph.D. Thesis. MIT/WHOI, 95-16.

16. Abstract (Limit: 200 words)

Moored time series are used to study the subtidal cross-shelf circulation over the northern California shelf and to examine the applicability of a two-dimensional model of cross-shelf circulation. In this model, surface and bottom cross-shelf flows are forced by along-shelf wind stress and bottom stress, and interior cross-shelf flow compensated such that the depth-averaged flow is zero. Between December, 1988 and May, 1989, cross-shelf heat and salt fluxes are consistent with this model. Comparison of the model to observed surface, interior, and bottom transports suggests it is better suited to transient rather than steady wind forcing. For 2-3 day wind events between December, 1988 and February, 1989, the model is well correlated with observed depth-dependent (total minus depth-averaged) transports throughout the water column and with total surface mixed layer transports. For 2-3 week wind events between April and July, 1982, the model does not work nearly as well. Success of this model would imply wind stress sets the along-shelf scales of near-surface cross-shelf velocity. However, between November, 1988 and May, 1989, scales vary from month to month are often shorter. Intrusion of offshore mesoscale features onto the shelf is one process which reduces spatial scales of cross-shelf flow.

17. Document Analysis a. Descriptors
coastal circulation
wind-forcing
observations

b. Identifiers/Open-Ended Terms

c. COSATI Field/Group

18. Availability Statement
Approved for publication; distribution unlimited.

19. Security Class (This Report)
UNCLASSIFIED

20. Security Class (This Page)

21. No. of Pages
162

22. Price

(See ANSI-Z39.18) *See Instructions on Reverse*

OPTIONAL FORM 272 (4-77)
(Formerly NTIS-35)
Department of Commerce